FLUCTUATION-DRIVEN PHASE RECONSTRUCTION AT ITINERANT FERROMAGNETIC QUANTUM CRITICAL POINTS

Una Karahasanovic

A Thesis Submitted for the Degree of PhD
at the
University of St. Andrews

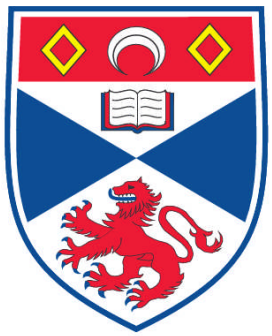

2012

FLUCTUATION-DRIVEN PHASE RECONSTRUCTION AT ITINERANT FERROMAGNETIC QUANTUM CRITICAL POINTS

Una Karahasanovic

A Thesis Submitted for the Degree of PhD
at the
University of St. Andrews

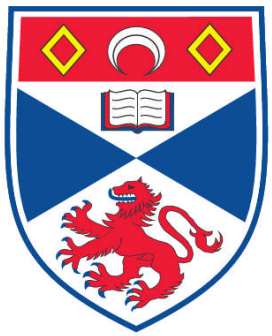

2012

Fluctuation-driven phase reconstruction at itinerant ferromagnetic quantum critical points

Una Karahasanovic

This thesis is submitted in partial fulfilment for the degree of
PhD
at the
University of St Andrews

July, 23rd, 2012

Abstract

The formation of new phases close to itinerant electron quantum critical points has been observed experimentally in many compounds. We present a unified analytical model that explains the emergence of new types of phases around itinerant ferromagnetic quantum critical points. The central idea of our analysis is that certain deformations of the Fermi surface enhance the phase-space available for low-energy quantum fluctuations and so self-consistently lower the free energy. Using this quantum order-by-disorder mechanism, we find instabilities towards the formation of a spiral ferromagnet and spin-nematic phase close to an itinerant ferromagnetic quantum critical point.

Further, we employ the quantum order-by-disorder mechanism to describe the partially ordered phase of MnSi. Using the simplest model of a Stoner-like helimagnetic transition, we show that quantum fluctuations naturally lead to the formation of an unusual phase near to the putative quantum critical point that shares many of the observed features of the partially ordered phase in MnSi. In particular, we predict an angular dependence of neutron scattering that is in good agreement with neutron-scattering data.

1. Candidate's declarations:

I, Una Karahasanovic, hereby certify that this thesis, which is approximately 31 000 words in length, has been written by me, that it is the record of work carried out by me and that it has not been submitted in any previous application for a higher degree.

I was admitted as a research student in October 2008 and as a candidate for the degree of Doctor of Philosophy in October 2008; the higher study for which this is a record was carried out in the University of St Andrews between 2008 and 2012.

Date 23/07/2012 Signature of candidate

2. Supervisor's declaration:

I hereby certify that the candidate has fulfilled the conditions of the Resolution and Regulations appropriate for the degree of Doctor of Philosophy in the University of St Andrews and that the candidate is qualified to submit this thesis in application for that degree.

Date: 23/07/2012 Signature of supervisor

3. Permission for electronic publication: (to be signed by both candidate and supervisor)

In submitting this thesis to the University of St Andrews I understand that I am giving permission for it to be made available for use in accordance with the regulations of the University Library for the time being in force, subject to any copyright vested in the work not being affected thereby. I also understand that the title and the abstract will be published, and that a copy of the work may be made and supplied to any bona fide library or research worker, that my thesis will be electronically accessible for personal or research use unless exempt by award of an embargo as requested below, and that the library has the right to migrate my thesis into new electronic forms as required to ensure continued access to the thesis. I have obtained any third-party copyright permissions that may be required in order to allow such access and migration.

The following is an agreed request by candidate and supervisor regarding the electronic publication of this thesis:

Acknowledgements

First of all, I would like to thank my supervisor Andrew Green for his guidance, support, constant optimism and for always being there when I needed his help. He taught me to think about physical insights first, before embarking on rigorous mathematical journeys and I will always be grateful to him for that. Big thanks to Frank Krüger, my collaborator in this work and the best office-mate ever. I appreciate his patience and willingness to answer numerous (sometimes very stupid) questions that I have had throughout my PhD. I would also like to thank Andrew Berridge and Chris Pedder, who it has been pleasure to discuss with and 'hang out' with. I am also grateful to Gareth Conduit for stimulating discussions throughout the course of this work. Finally, I would like to thank Fabian Essler, who introduced me to the beauty of research and without whose little 'push' I would not be doing condensed matter theory today.

Last but not least, I wish to thank my family – Mirjana, Namik, Jovanka, Semsa and Vesna for their constant love and support. I am very lucky to have amazing people around me and friends who I can always rely on, and whom I would like to thank here: Daniela Castellanos Montes, Suada Dervisbegovic, Jerome Fontane, Jan Grill, Amna Hadziabdic (a very special thanks!), Tanja Jackel, Goran Nisic, Andrzej Nowojewski, Gordana Savic and Richard Tatham.

Original work

The majority of Chapters 3, 4 and 6 of this thesis are the original work, in collaboration with Prof. A. G. Green and Dr. F. Krüger. Chapters 3 and 4 form the basis for the following publication:

Quantum order-by-disorder driven phase reconstruction in the vicinity of itinerant ferromagnetic quantum critical points.
U. Karahasanovic, F. Krüger, A. G. Green, Phys. Rev. B **85**, 165111 (2012).

Chapter 6 (and a part of Chapter 7) forms the basis for the following publication:

Quantum order-by-disorder near quantum criticality and the secret of partial order in MnSi.
F. Krüger, U. Karahasanovic, A. G. Green, Phys. Rev. Lett. **108**, 067003 (2012)

Contents

Contents vi

List of Figures x

Nomenclature xi

1 Introduction 1
- 1.1 Classical Phase Transitions . . . 3
  - 1.1.1 Scale invariance . . . 4
- 1.2 Quantum Phase Transitions . . . 5
  - 1.2.1 Introduction . . . 5
  - 1.2.2 Quantum-to-classical mapping . . . 6
  - 1.2.3 Finite T phase diagram . . . 6
  - 1.2.4 Quantum critical region . . . 7
- 1.3 Ferromagnetism . . . 8
  - 1.3.1 Stoner Model . . . 8
    - 1.3.1.1 Stoner criterion . . . 8
    - 1.3.1.2 Mean-field theory of the Stoner model . . . 9
    - 1.3.1.3 Quantum criticality . . . 10
  - 1.3.2 Hertz-Millis theory . . . 11
- 1.4 The Breakdown of Itinerant Quantum Criticality . . . 14
  - 1.4.1 Experimental evidence . . . 14
    - 1.4.1.1 First order transition . . . 14
    - 1.4.1.2 Formation of new phases around itinerant electron quantum critical points . . . 14
  - 1.4.2 Theoretical approaches to the breakdown of the itinerant electron quantum criticality . . . 16
    - 1.4.2.1 Non-analytic extensions of Hertz-Millis theory . . . 16
    - 1.4.2.2 Why did Hertz-Millis theory fail? . . . 17
    - 1.4.2.3 Coleman-Weinberg mechanism . . . 18
    - 1.4.2.4 Quantum order-by-disorder . . . 19

1.5 Summary . . . 20
1.6 Thesis Outline . . . 20

2 Quantum Order-by-Disorder **22**
2.1 Order-by-Disorder Mechanism . . . 23
2.1.1 Classical order-by-disorder . . . 23
2.1.2 Quantum order-by-disorder . . . 24
2.2 Quantum Order-by Disorder for an Itinerant Ferromagnet . . . 26
2.2.1 Heuristic picture . . . 26
2.2.2 Self-consistent perturbation theory . . . 26
2.2.2.1 Free energy . . . 28
2.2.3 Equivalent field-theoretical derivation . . . 29
2.2.3.1 Free energy . . . 30
2.2.4 Explicit calculation of fluctuation corrections . . . 32
2.2.4.1 Free energy in terms of particle-hole densities of states . . . 33

3 Ginzburg-Landau Theory **35**
3.1 Introduction . . . 36
3.2 Uniform Ferromagnet . . . 37
3.2.1 Mean-field Ginzburg-Landau coefficients . . . 37
3.2.2 Fluctuation contributions to the Ginzburg-Landau coefficients . . . 38
3.2.2.1 Quadratic coefficient α_{fl} . . . 39
3.2.2.2 Quartic coefficient β_{fl} . . . 40
3.3 Spiral . . . 42
3.3.1 Mean-field electron dispersion in the presence of spiral magnetic order . . . 42
3.3.2 Mean-field Ginzburg-Landau coefficients . . . 43
3.3.3 Fluctuation contributions to the Ginzburg-Landau coefficients . . . 43
3.4 d-wave Spin Nematic . . . 44
3.4.1 In search of new phases of matter: electron nematic states 44
3.4.2 Generating function . . . 46
3.4.2.1 Mean-field coefficients of the generating function 47
3.4.2.2 Fluctuation contributions to the coefficients . . . 47
3.4.3 Ginzburg-Landau expansion of the d-wave spin nematic . . 48
3.5 Deviations from the Isotropic Free-Electron Dispersion . . . 48
3.5.1 Free energy of the uniform ferromagnet . . . 49
3.5.2 Spiral free energy . . . 49
3.5.3 d-wave spin-nematic free energy . . . 50

4 Phase Diagram of the Itinerant Ferromagnet **52**
4.1 Isotropic Free-Electron Dispersion 54
4.1.1 Uniform ferromagnet 54
4.1.1.1 Line of second order transitions 54
4.1.1.2 Line of first order transitions 54
4.1.2 Fluctuation-driven spiral phase 55
4.1.2.1 Spiral-to-paramagnet transition 56
4.1.2.2 Spiral-to-uniform ferromagnet transition 57
4.1.2.3 Evolution of the order parameters 58
4.1.2.4 Comparison to previous work 58
4.1.3 d-wave spin nematic 59
4.1.3.1 d-wave spin nematic-to-paramagnet boundary . . 59
4.1.3.2 d-wave spin nematic-to-spiral boundary 59
4.2 Small Deviations from the Isotropic Free-Electron Dispersion . . . 61
4.2.1 Uniform ferromagnet 61
4.2.1.1 Line of second order transitions 61
4.2.1.2 Line of first order transitions 62
4.2.2 Spiral phase 62
4.2.2.1 Spiral-to-paramagnet boundary 62
4.2.2.2 Uniform ferromagnet-to-spiral transition 64
4.2.3 d-wave spin nematic 64
4.2.3.1 d-wave spin nematic-to-paramagnet boundary . . 65
4.2.3.2 d-wave spin nematic-to-spiral boundary 65

5 Experimental Phase Diagram of MnSi **67**
5.1 Helical phase 68
5.1.1 Role of the spin-orbit coupling in MnSi 68
5.2 Partially ordered phase 69
5.2.1 MnSi under hydrostatic pressure - a world of mysteries . . 69
5.2.2 Signatures of the partially ordered phase in thermo-power measurements 71
5.3 Open questions and problems 72

6 Quantum Order-by-Disorder in MnSi **74**
6.1 Central Idea of Our Approach 75
6.1.1 Recap of Chapter 4 75
6.1.2 Connection to Chapter 4 75
6.1.3 Directional dependence of the wave vector 76
6.2 Mean-field theory 76
6.2.1 Ginzburg - Landau phenomenology 77
6.2.2 Microscopic mean-field theory 78

6.2.2.1 Spin-orbit coupling in MnSi 79
6.2.2.2 Mean-field dispersion 79
6.2.2.3 Directional dependence of Q 82
6.3 Quantum Order-by-Disorder in MnSi 83
6.3.1 Phase diagram 83
6.3.2 Directional dependence of the wave vector 84
6.3.2.1 Mean-field like directional dependent term δF_1 . 85
6.3.2.2 Fluctuation-driven directional dependent term δF_2 85
6.3.2.3 Change of the directional dependence 86

7 Comparison with Experiment and Other Related Theories 88
7.1 Phase diagram 89
7.1.1 Distribution of magnetic moments in the partially ordered phase: comparison to experiment 89
7.1.1.1 Calculation of the correlation volume 91
7.2 Other related theories 93
7.2.1 Magnetic analogue of blue phases and skyrmion structures in MnSi 94

8 Conclusions 98
8.1 Summary 98
8.2 Suggestions for Further Work 99
8.2.1 Quantum order-by-disorder at an itinerant ferromagnetic quantum critical point in two spatial dimensions 99
8.2.2 Interplay between quantum fluctuations and lattice effects 100
8.2.3 Fluctuation-driven spiral state with multiple wave vectors 100
8.2.4 Fluctuating spiral phase 100
8.2.5 Superconductivity 101

Appendix A: Modified Particle-Hole Densities of States and Their Derivatives 103

Appendix 2: Leading temperature dependence of $\alpha_{\mathbf{fl}}$ and $\beta_{\mathbf{fl}}$ 107

References 111

List of Figures

1.1 Finite temperature phase diagram in the vicinity of a quantum critical point 7
1.2 Phase diagram of an itinerant ferromagnet in mean-field theory . 11
1.3 Landau damping due to the particle-hole continuum 13
1.4 Formation of new phases in the vicinity of quantum critical points 15

2.1 $J_1 - J_2$ next nearest neighbours model on a diamond lattice . . . 24
2.2 $J_1 - J_2$ next nearest neighbours model on a square lattice – linear spin-wave theory. 25
2.3 $J_1 - J_2$ next nearest neighbours model on a square lattice – phase diagram beyond the linear spin-wave theory 26
2.4 Distortions of the Fermi surface enhance the phase-space for quantum fluctuations. 27
2.5 Diagrammatic contributions to the partition function in the quantum order-by-disorder approach 32

3.1 Free energy profiles for first and second order phase transitions . . 37
3.2 Fluctuation contributions to the quadratic coefficient α 40
3.3 Fluctuation contributions to the quartic coefficient β 41

4.1 Phase diagram of the uniform ferromagnet, including quantum fluctuations 55
4.2 Phase diagram of the itinerant ferromagnet allowing for the possibility of spatially modulated ferromagnetism 57
4.3 The evolution of the order parameters M and Q in the spiral phase 58
4.4 Phase diagram of the itinerant ferromagnet, allowing for the possibility for the formation of spiral and spin-nematic phases 60
4.5 Modification to the phase diagram of the spiral state with a weakly anisotropic dispersion 63

5.1 Temperature versus pressure phase diagram of MnSi 70
5.2 Resistivity as a function of temperature for MnSi 71

5.3 Thermo-power mapped out over the phase diagram in temperature-pressure plane 72

6.1 Two coordinate frames: the crystal axes frame and the spiral frame 78
6.2 Phase diagram of MnSi, determined using the quantum order-by-disorder approach 83

7.1 Formation of domains in MnSi 90
7.2 Principal directions in MnSi 92
7.3 Theoretically predicted neutron scattering pattern 93
7.4 Double-twist structure in liquid crystals 94
7.5 Blue fog phase diagram of MnSi 95
7.6 The magnetization pattern of a skyrmion 96

Chapter 1

Introduction

This chapter discusses some basic notions of classical and quantum phase transitions, with the particular emphasis on ferromagnetic transitions in itinerant systems. The failure of the standard theory of metallic quantum criticality – Hertz-Millis theory – to predict first order transitions and the emergence of new exotic quantum phases in the vicinity of putative quantum critical points is discussed. This question will be the subject of this thesis. We will aim to develop a unified theoretical model that describes the formation of new phases near to an itinerant ferromagnetic quantum critical point.

We begin the chapter by discussing classical phase transitions. In classical phase transitions, a subtle balance between thermal fluctuations and inter-particle interactions determines the phase that a system will adopt. We will introduce some basic concepts of critical phenomena, such as scale invariance, universality and critical exponents. One of the circumstances that makes classical phase transitions relatively straightforward to study is the fact that the statics and dynamics of a system decouple.

Quantum phase transitions take place at zero temperature. Here, quantum fluctuations compete with inter-particle interactions. The balance between the two can be altered by a variation of a non-thermal control parameter (like pressure or doping), which then drives a phase transition. The statics and dynamics in a quantum phase transition are coupled. This requires the introduction of an additional critical exponent – the dynamical exponent z. Here, the imaginary time acts as an extra dimension(s). This leads us to an attempt to map a quantum system in d dimensions onto a classical system in $d + z$ dimensions. Although this quantum-to-classical mapping is a powerful tool, it has its limitations. First, because of negative Boltzmann weights it does not work for fermions; secondly there are problems even in bosonic theories, related to analytical continuation. This makes quantum phase transitions difficult and interesting to study.

Although quantum phase transitions strictly happen at zero temperature,

where two phases are separated by a quantum critical point, the signatures of quantum criticality are noticeable at surprisingly high temperatures. In this quantum critical region there is a rich interplay between quantum and thermal effects and interactions. This leads to unusual temperature dependencies of various experimentally measurable quantities, that cannot be described within the concept of the Fermi-liquid theory. Particularly satisfying is the fact that there exist a large amount of experimental data that provides guidance on essential ingredients for a successful theoretical model and that enables one to test predictions quickly.

In this thesis, we will concentrate on a particular class of quantum phase transitions – those that occur in itinerant ferromagnetic systems. Ferromagnetism arises when the potential energy gain of magnetizing the system overcomes the kinetic energy cost of moving electrons between the two different Fermi-surface bands (those of spin-up and spin-down electrons). A simple model that captures the physics of this process is the Stoner model, where electrons interact via a point-like Colomb repulsion. The Stoner model displays quantum criticality – at zero temperature there is a paramagnet-to-ferromagnet quantum phase transition, tuned by changing the strength of the electron-electron interaction.

In their pioneering work, Hertz and Millis developed a theory of itinerant quantum criticality. They constructed an effective low-energy theory for fluctuations of the bosonic order parameter, that successfully explained some experimentally observed scaling relations. Recently, a growing number of experimental examples that suggest the failure of Hertz-Millis theory have emerged. Hertz-Millis theory predicts a second order paramagnet-to-ferromagnet transition, failing to account for a number of experimentally observed first order transitions. Secondly, it cannot explain the emergence of new phases in the vicinity of itinerant quantum critical points, which has been seen in a variety of systems. It looks as though a system is trying to avoid a singularity – the quantum critical point – by forming new phases in its vicinity. This is a familiar concept in high-energy physics where naked singularities are prevented from happening due to other kinds of instabilities. One might ask: Is this instability of quantum critical points a generic principle?

The theory of non-analytic corrections to Hertz-Millis theory is one of the approaches that ultimately addresses this problem. There, it is argued that Hertz-Millis theory neglected the coupling of order parameter fluctuations to other soft modes present in an itinerant system – those of low-energy particle-hole pairs. Their inclusion leads to a non-analytic dependence of the free energy (and equivalently the static spin susceptibility). It is essential to include them on equal footing if one wants to construct a reliable low-energy theory. The instabilities close to itinerant ferromagnetic quantum critical points found using this method include first order transitions, spiral and p-wave spin-nematic states.

The quantum-order-by disorder formalism, which we will follow throughout this work, represents an alternative unified approach. It leads to easily accessible calculations, that can be understood by a broad audience. We present an intuitive physical picture of the formation of new phases in the vicinity of an itinerant ferromagnetic quantum critical point. Certain deformations of the Fermi surface associated with the onset of a new type of order enhance quantum fluctuations. Enhanced quantum fluctuations lower the free energy of those phases and make them stable. The instabilities that we find in the vicinity of the putative quantum critical point include a spiral ferromagnet and a d-wave spin nematic.

1.1 Classical Phase Transitions

Classical phase transitions are governed by the competition between inter-particle interactions that try to order a system and thermal fluctuations. The system will adopt a certain ground state, in such a way that its free energy $\mathcal{F} = E - TS$ minimized. Here E represents the energy and S is the entropy of the system at temperature T. A phase transition is characterized by the discontinuity of some derivative of the free energy.

Perhaps the simplest example of a classical phase transition is that of melting ice to form water. The energy E is minimized in the crystalline structure of ice, while the entropy S is maximized in the the liquid phase. At low temperatures, where the TS term in the free energy does not play a significant role, the system will form ice. As we increase the temperature, the entropy term in the free energy will win over the energy term and ice will melt into water. At 0^oC, where the phase transition takes place, the free energies of water and ice are the same. The phase transition is however, characterized by a discontinous change in density.

In classical phase transitions, statics and dynamics decouple. The partition function factorizes into kinetic and potential parts

$$\begin{aligned} \mathcal{H}(p_i, q_i) &= \mathcal{H}_{kin}(p_i) + \mathcal{H}_{pot}(q_i) \\ \mathcal{Z} &= \int \Pi dp_i e^{-\frac{\mathcal{H}_{kin}(p_i)}{kT}} \int \Pi dq_i e^{-\frac{\mathcal{H}_{pot}(q_i)}{kT}} = \mathcal{Z}_{kin}\mathcal{Z}_{pot}, \end{aligned} \tag{1.1}$$

since, in a classical phase transition, the kinetic and potential part of the Hamiltonian commute. We can therefore study classical phase transitions using effective time-independent theories, such as the Ginzburg-Landau theory. The order parameter is time-independent, but can vary in space.

Every phase transition can be described by an order parameter – a quantity characterized by a zero thermodynamic average in the disordered phase and a finite value average in the ordered phase. Near to a phase transition, the value of the order parameter is small. We can therefore expand the free energy in

powers of the order parameter. This is known as the Ginzburg-Landau expansion [1]. It enables us to determine phase boundaries and analyse the nature of the phase transition. In a second order transition, the order parameter increases continously from zero. If the order parameter jumps from zero to a finite value, the transition is of first order. A first order transition is associated with the release of latent heat. In general, an nth order phase transition is characterized by the discontinuity of the nth derivative of the free energy.

1.1.1 Scale invariance

Close to a critical point, spatial correlations of the order parameter fluctuations become long-ranged [2]. That is to say, the correlation length ξ diverges, according to

$$\xi \propto |\delta|^{-\nu}, \tag{1.2}$$

where $\delta = \frac{T-Tc}{T_c}$ represents the distance from the transition. T_c is the critical temperature and ν the critical exponent of the correlation length. Hence, near to a phase transition, the correlation length is the only relevant length scale. This is known as **scale invariance**.

Due to scale invariance, the nature of a transition is independent of microscopic details. It solely depends on dimensionality and symmetries of the order parameter. This concept of **universality** is very important in the study of phase transitions.

The behaviour of a system in the vicinity of a phase transition can be described by a set of **critical exponents** [2]. Critical exponents describe power-law dependencies of various quantities, such as specific heat or susceptibility, with the distance from the transition δ. Critical exponents are listed in Table 1.1. They are not independent from each other but are related by scaling relations. For example, the Rushbroke scaling law shows that

$$\alpha + 2\beta + \gamma = 2. \tag{1.3}$$

Table 1.1: Critical exponents

Quantity	Exponent	Definition
specific heat	α	$c \sim \|\delta\|^{-\alpha}$
order parameter	β	$M \sim \|\delta\|^{\beta}$
susceptibility	γ	$\chi \sim \|\delta\|^{-\gamma}$
correlation length	ν	$\xi \sim \|\delta\|^{-\nu}$

1.2 Quantum Phase Transitions

1.2.1 Introduction

Quantum phase transitions happen at zero temperature. Quantum fluctuations, associated with the Heisenberg uncertainty principle, compete with inter-particle interactions to drive a phase transition. The application of pressure, doping or any other non-thermal control parameter can change the relative size of the interactions and quantum fluctuations and drive the system from one phase into another.

A simple experimental example is that of $LiHoF_4$ [3]. This compound can be described by the transverse-field Ising model. The Hamiltonian is given by

$$\mathcal{H} = -J \sum_{\langle ij \rangle} \sigma_i^z \sigma_j^z - Jg \sum_i \sigma_i^x, \tag{1.4}$$

where $J > 0$ is the exchange coupling between the z components of nearest neighbour spins, and gJ denotes the strength of the external magnetic field applied along the transverse x direction. In the limit $g \to 0$ the ground state is ferromagnetic: $|0\rangle = \Pi_i |\uparrow\rangle_i$ (or $|0\rangle = \Pi_i |\downarrow\rangle_i$) and breaks the Z_2 symmetry. In the opposite limit, $g \to \infty$, the ground state is $|0\rangle = \Pi_i |\rightarrow\rangle_i$, where $|\rightarrow\rangle = \frac{1}{\sqrt{2}}(|\uparrow\rangle + |\downarrow\rangle)$, i.e. all spins point along the field direction. We now imagine increasing the interaction strength g continously from zero. Eventually, the transverse field will induce spin flips and destabilize the magnetic order. There will be a quantum phase transition from the ferromagnetic into the paramagnetic state.

In a quantum phase transition, statics and dynamics are intrinsically coupled to each-other. There is a simple way to see this. In quantum mechanics the kinetic part of the Hamiltonian $\mathcal{H}_{kin}$ and the potential part $\mathcal{H}_{pot}$ do not commute i.e $[\mathcal{H}_{kin}, \mathcal{H}_{pot}] \neq 0$. As a result of this, the partition function (1.1) does not factorize, as it did in the classical case.

We note that the operator $e^{-\frac{\mathcal{H}}{kT}}$ entering the partition function looks like the time-evolution operator if we change $\frac{1}{kT} = \tau = -\frac{it}{\hbar}$. The imaginary time τ acts as an extra dimension. The order parameter now fluctuates in both space and time.

In addition to long-range spatial correlations (1.2), there also exist long-range correlations of order parameter fluctuations in time. Near to a quantum critical point, the correlation time diverges as

$$\tau_C \propto |\delta|^{-\nu z}, \tag{1.5}$$

where now $\delta = \frac{g - g_c}{g_c}$ represents the distance from the quantum phase transition and g_c the critical interaction strength (or any other non-thermal control parameter). The dynamical exponent z measures how time enters the system. Close

to a phase transition, there is no other characteristic time scale than τ_C. This mixing of statics and dynamics leads to a different set of critical exponents than those predicted by the corresponding classical theory.

1.2.2 Quantum-to-classical mapping

There is a very useful analogy between quantum systems and higher dimensional classical systems. We have seen how the time enters like the zth power of space; this leads us to believe that the classical phase transition in $D = d+z$ dimensions is equivalent to the quantum phase transition in d dimensions.

In principle, the quantum-to-classical mapping works well for bosonic theories. For example, the Ising model can be mapped onto a classical ϕ^4 theory. Similarly, the model for the Mott-insulator-to-superfluid transition can be mapped to ϕ^4 theory with a complex order parameter. Sometimes $z \neq 1$ leads to an anisotropic classical theory, but this is not a problem.

Although quantum-to-classical mapping is a powerful concept we cannot always apply it and use the results for classical phase transitions. There are certain problems that arise even in bosonic theories – issues with non-analytic continuation and Berry phases [2]. Berry phases, that arise in spin systems, lead to complex valued Boltzmann weights in the classical theory. They are a consequence of underlying quantum mechanics and have no classical analogues. The issue of non-analytic continuation is a subtle one. The quantum-to-classical mapping leads to correlation functions in imaginary time. In order to obtain the real time correlations we need to perform an analytical continuation. Of course, it is possible to analytically continue **exact** imaginary time results to real time without encountering any problems. In practice, we always use an approximation scheme. The problem is that approximations schemes that work in imaginary time usually fail after analytic continuation.

For fermions, the quantum-to-classical mapping leads to negative Boltzmann weights. This is known as the fermion sign problem.

1.2.3 Finite T phase diagram

In principle, at low but finite temperature, there is an interplay between both quantum and thermal fluctuations and interactions. We want to explore what happens there. Strictly speaking, quantum phase transitions happen at $T = 0$, which can never be approached experimentally. The question is: Can we somehow see the presence of a quantum critical point at finite temperatures? The answer is: Yes, we can, in a special region of the finite-temperature phase diagram – the quantum critical region, which we will describe shortly. Let us first investigate the general setting for the interplay of thermal and quantum fluctuations.

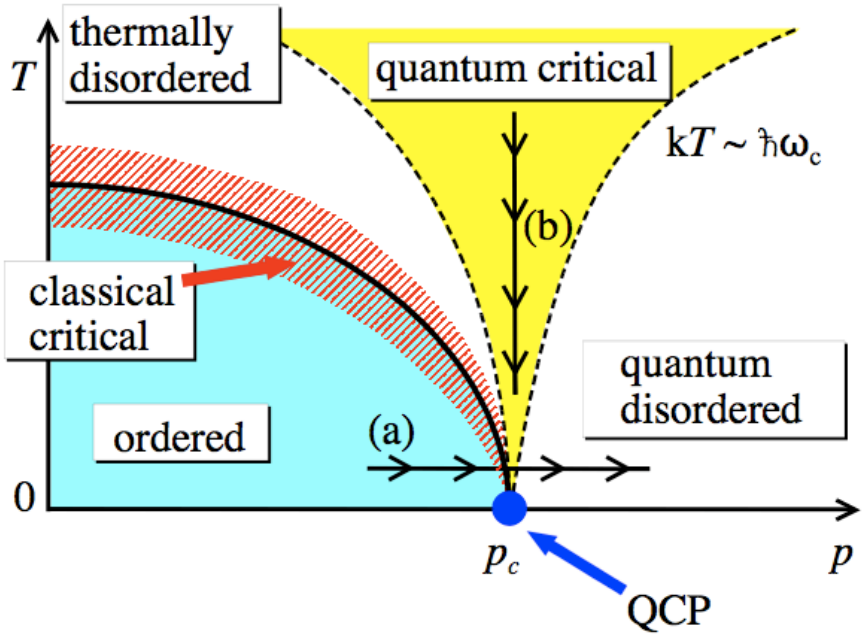

Figure 1.1: **Finite temperature phase diagram in the vicinity of a quantum critical point:** Taken from [4]. The classical critical region is denoted red. The quantum critical region (yellow) is denoted by (b), and extend as a cone from the quantum critical point (QCP). Its boundaries are determined by $\hbar\omega_c \sim kT$.

We first consider typical energy scales. The typical energy scales of thermal fluctuations are of order kT, while those of quantum fluctuations are of order $\hbar\omega_c$, where $\omega_c = \tau_c^{-1}$. Quantum mechanics will play no important role in the phase transition, if the condition $kT \gg \hbar\omega_C$ is satisfied. At a finite temperature transition T_C, $kT \approx kT_c$, while $\hbar\omega_C \to 0$. Hence in the region sufficiently close to a finite temperature phase transition a classical description holds, see Fig 1.1. This region gets narrower as we lower the temperature.

1.2.4 Quantum critical region

In the quantum critical region (region (b) in Fig 1.1), thermal and quantum fluctuations are equally important. The boundaries of this region are given by the condition $\hbar\omega_C \approx kT$, and the region extends like a cone from a quantum critical point. Within this region, experimentally measurable quantities display unusual temperature dependencies that cannot be described by the standard framework of the Fermi liquid theory. The presence of the zero-temperature quantum critical point, can therefore be seen at reasonably high temperatures!

The Fermi liquid concept, developed by Landau, provides a standard description of metals. The main idea is that in the Fermi liquid, electrons behave like almost non-interacting quasi-particles, just with renormalized parameters. The Fermi liquid theory predicts a specific heat that is linear in temperature and resistivity that scales as T^2. As seen in many recent experiments, Fermi liquid behaviour breaks down in the vicinity of a quantum critical point [5]. As electrons get scattered by diverging magnetic fluctuations this results in different temperature dependence of the resistivity from the Fermi liquid one.

Finally, we address the role of fluctuations on critical behaviour. It is well-known that fluctuations become stronger for lower-dimensional systems. Above the upper critical dimension, $d > d_c^+$ fluctuations become irrelevant and the system is well described by a mean-field theory. For, $d_c^+ > d > d_c^-$, where d_c^- represents the lower critical dimension, a phase transition exists, but the critical behaviour differs from the mean-field one. If $d < d_c^-$ there is no long-range order.

1.3 Ferromagnetism

This section provides an introduction to ferromagnetism. It outlines the physical picture behind it and presents a simple mathematical model that we will employ in our calculations - the Stoner model. We also discuss Hertz-Millis theory of an itinerant ferromagnetic quantum critical point.

1.3.1 Stoner Model

Our starting point is the free electron system in three spatial dimensions interacting through Hubbard point repulsion

$$\mathcal{H} = \sum_{\mathbf{k},\sigma=\pm} (\epsilon_{\mathbf{k}} - \mu)\, \hat{n}_{\mathbf{k},\sigma} + g \int \mathrm{d}^3\mathbf{r}\; \hat{n}_+(\mathbf{r})\hat{n}_-(\mathbf{r}). \tag{1.6}$$

Here $\epsilon_{\mathbf{k}} = \frac{k^2}{2}$ is the isotropic free-electron dispersion, μ denotes the chemical potential and $\hat{n}_\pm(\mathbf{r})$ are the density operators of spin up/down electrons. The strength of the contact interaction is given by g.

1.3.1.1 Stoner criterion

Ferromagnetism occurs because there is an imbalance in the number of spin up and spin down electrons. In momentum space this corresponds to spin-up and spin-down Fermi surfaces being shifted up and down with respect to the Fermi surface of an un-magnetised state, and having different volumes. There is a competition between the kinetic energy required to take the electrons from one band and

to place them into another, which penalizes the magnetization, and the interaction that favors it. The ratio between the terms depends on the density of states at the Fermi surface. Let the spin band splitting be $\Delta\epsilon$, and the density of states at the Fermi surface $\rho(\epsilon_F)$. The cost of taking $n \approx \rho(\epsilon_F)\Delta\epsilon$ electrons from one band and placing them in another, which is $\Delta\epsilon$ higher in energy, is $E_{kin} \approx \rho(\epsilon_f)(\Delta\epsilon)^2$. The interaction energy gain of the system is $E_{int} = gn_+n_- \approx -g(\rho(\epsilon_f)\Delta\epsilon)^2$. By comparing E_{kin} and E_{int}, we find that the magnetized state is favored when $g\rho(\epsilon_f) > 1$. This is known as the Stoner criterion [6]. Changing external parameters, such as pressure or doping, affects the density of states at the Fermi level. When it moves the Fermi level to the region where the density of states is high, it becomes favorable for the system to magnetize. We will now derive the Stoner criterion quantitatively, and explicitly show that it leads to a second order transition.

1.3.1.2 Mean-field theory of the Stoner model

We discuss the mean-field theory of the Stoner model, derive the mean-field Ginzburg-Landau expansion of the free energy and from there rigorously re-derive the Stoner criterion.

Mean-field Hamiltonian. In order to obtain the mean-field Hamiltonian we perform a mean-field decoupling in the spin channel

$$g \int \mathrm{d}^3\mathbf{r}\ \hat{n}_+(\mathbf{r})\hat{n}_-(\mathbf{r}) \approx g \sum_{\mathbf{r},\nu,\nu'} \mathbf{M}(\mathbf{r}) \cdot \boldsymbol{\sigma}_{\nu,\nu'} c^\dagger_{\mathbf{r}\nu} c_{\mathbf{r}\nu'} \tag{1.7}$$

where the magnetization is given $\mathbf{M}(\mathbf{r}) = \langle \boldsymbol{\sigma}_{\nu,\nu'} c^\dagger_{\mathbf{r}\nu} c_{\mathbf{r}\nu'} \rangle$. We first consider a uniform magnetization $\mathbf{M}(\mathbf{r}) = \mathbf{M}$ and for simplicity assume that the magnetization vector points along the z axis. This results in the following mean-field Hamiltonian:

$$\mathcal{H} = \sum_{\mathbf{k}} \tilde{\psi}^\dagger_{\mathbf{k}} \begin{pmatrix} \epsilon_{\mathbf{k}} - gM & 0 \\ 0 & \epsilon_{\mathbf{k}} + gM \end{pmatrix} \tilde{\psi}_{\mathbf{k}} + gM^2, \tag{1.8}$$

where

$$\tilde{\psi}^\dagger_{\mathbf{k}} \ = \ \left(\psi^\dagger_{\mathbf{k},+},\ \psi^\dagger_{\mathbf{k},-} \right). \tag{1.9}$$

From here, we can read-off the mean field dispersion in the presence of the uniform ferromagnetic order

$$\epsilon^\sigma_{\mathbf{k}} = \epsilon_{\mathbf{k}} - \sigma g M. \tag{1.10}$$

Ginzburg-Landau expansion. The mean-field free energy is given by

$$\mathcal{F}_{MF} = -\frac{1}{\beta}\sum_{\mathbf{k},\sigma}\ln\left(1+e^{-\beta(\epsilon^{\sigma}_{\mathbf{k}}-\mu)}\right)+g\int \mathrm{d}^3\mathbf{r}\,\mathbf{M}^2(\mathbf{r}), \tag{1.11}$$

where $\beta = T^{-1}$ represents the inverse temperature. Expanding the expression (1.11) in powers of magnetization M, assumed small, we obtain the following Ginzburg-Landau expansion:

$$\mathcal{F}[M] = \alpha M^2 + \beta M^4 + \gamma M^6 + ..., \tag{1.12}$$

where the Ginzburg-Landau coefficients α, β, γ are functions of the interaction strength g and temperature T:

$$\begin{aligned}
\alpha_{MF} &= g + g^2\sum_{\mathbf{k}} n^{(1)}(\epsilon_{\mathbf{k}}),\\
\beta_{MF} &= \frac{2}{4!}g^4\sum_{\mathbf{k}} n^{(3)}(\epsilon_{\mathbf{k}}),\\
\gamma_{MF} &= \frac{2}{6!}g^6\sum_{\mathbf{k}} n^{(5)}(\epsilon_{\mathbf{k}}).
\end{aligned} \tag{1.13}$$

Here $n^{(j)}(\epsilon) = \partial^j_\epsilon n(\epsilon)$ denotes the jth derivative of the Fermi function with respect to its energy argument. In the limit $T \to 0$ we obtain the analytic results for the mean field coefficients $\alpha_{MF} = g - \frac{2\sqrt{2}}{(2\pi)^2}g^2$, $\beta_{MF} = \frac{\sqrt{2}}{4!(2\pi)^2}g^4$ and $\gamma_{MF} = \frac{15\sqrt{2}}{4\cdot 6!(2\pi)^2}g^6$. At finite temperature, the above integrals are straightforward to calculate numerically for the present k^2 dispersion.

Phase diagram. We can now construct the mean-field phase diagram. In the limit $T \to 0$, the quartic coefficient β_{MF} is positive. Therefore, only a second order paramagnet-to-ferromagnet phase transition is possible. This happens when the quadratic coefficient α_{MF} changes sign: the minimum in the free energy at $M = 0$ turns into a local maximum, and minima adjacent to $M = 0$ (from both sides) start developing (see free energy profiles in paramagnetic and ferromagnetic phases in Fig. 1.2). The condition for ferromagnetism, $\alpha_{MF} < 0$, corresponds to $g\rho(\epsilon_f) > 1$, where $\rho(\epsilon_f)$ represents the density of states at the Fermi surface. We have recovered the Stoner criterion.

1.3.1.3 Quantum criticality

We have seen how the Stoner model predicts a paramagnet-to-ferromagnet quantum phase transition for some critical value of the interaction strength g. Hertz realized that, due to the coupling of statics and dynamics, different scaling laws will be realised than those predicted by the classical theory. We now briefly discuss the Hertz-Millis theory.

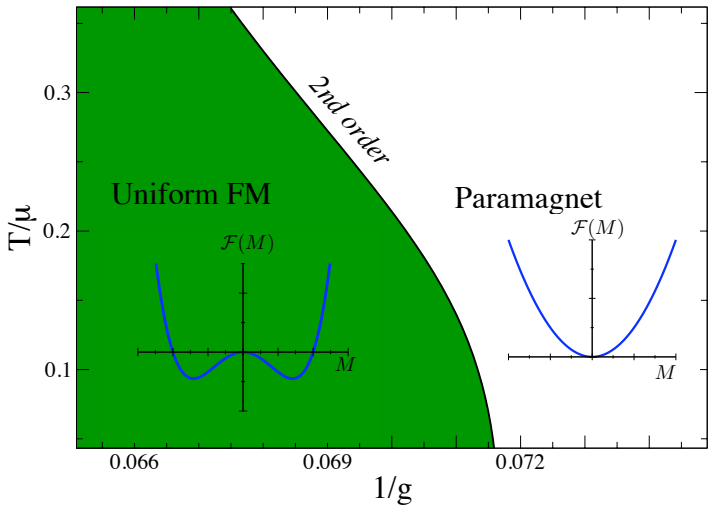

Figure 1.2: **Phase diagram of an itinerant ferromagnet in mean-field theory:** The transition between the uniform ferromagnet and the paramagnet is always second order in mean-field theory.

1.3.2 Hertz-Millis theory

In his pioneering work, Hertz [7] studied the paramagnet-to-ferromagnet quantum phase transition of itinerant fermions that occurs by varying the strength of the Coulomb repulsion between electrons. He derived an effective action for dynamical fluctuations of the bosonic order parameter. Later, Millis [8] used this approach to calculate temperature dependencies of the correlation length, susceptibility and specific heat.

Outline of the calculation. We present a brief outline of Hertz's calculation. We start from the fermionic partition function,

$$\begin{aligned} \mathcal{Z} &= \int \mathcal{D}(\bar{\psi},\psi) e^{-S[\bar{\psi},\psi]}, \\ S[\bar{\psi},\psi] &= \int_0^\beta \mathrm{d}\tau \int \mathrm{d}^3\mathbf{r} \left[\bar{\psi}\partial_\tau \psi + \mathcal{H}(\bar{\psi},\psi)\right], \end{aligned} \tag{1.14}$$

where $\psi = (\psi_+, \psi_-)^T$ and $\bar{\psi} = (\bar{\psi}_+, \bar{\psi}_-)$ denote Grassman fields which vary throughout space and imaginary time, and the Hamiltonian is given by Eq. (1.6). After performing a Hubbard-Stratonovich decoupling of the interaction in the

spin channel $\boldsymbol{\phi}$ we obtain

$$\begin{aligned} \mathcal{Z} &= \int \mathcal{D}(\bar{\psi},\psi)\mathcal{D}\boldsymbol{\phi}\; e^{-S[\bar{\psi},\psi,\boldsymbol{\phi}]}, \\ S[\bar{\psi},\psi,\boldsymbol{\phi}] &= \int \bar{\psi}(\hat{G}_0^{-1} - g\boldsymbol{\phi}\cdot\boldsymbol{\sigma}))\psi + g\int \boldsymbol{\phi}^2, \end{aligned} \tag{1.15}$$

where $\hat{G}_0^{-1}$ is the free-electron Green function and $\boldsymbol{\sigma}$ denotes the vector of Pauli matrices. After integrating out the fermions, we obtain an effective theory in terms of fluctuations of the bosonic order parameter

$$\begin{aligned} \mathcal{Z} &= \int \mathcal{D}\boldsymbol{\phi}\; e^{-S[\boldsymbol{\phi}]}, \\ S[\boldsymbol{\phi}] &= -\mathrm{Tr}\ln\left[\hat{G}_0^{-1} - g\boldsymbol{\sigma}\cdot\boldsymbol{\phi})\right] + g\int \boldsymbol{\phi}^2. \end{aligned} \tag{1.16}$$

Expanding the $Tr\ln$ we obtain the free energy:

$$\begin{aligned} \mathcal{F} \approx \quad & \sum_{q,\omega} v_2(q,\omega)|\phi(q,\omega)|^2 + \sum_{q_i,\omega_i}{}' v_4(q_i,\omega_i)\phi(q_1,\omega_1)\phi(q_2,\omega_2)\phi(q_3,\omega_3)\phi(q_4,\omega_4) + ... \\ & v_2(q,\omega) = 1 - g\chi^{-1}(q,\omega), \end{aligned} \tag{1.17}$$

where $\chi^{-1}(q,\omega) = -\frac{1}{\beta}\sum_{\mathbf{k},\omega_n} G(k,i\omega_n)G(k+q,i\omega_n+\omega)$, and $'$ in the sum indicates the restrictions $\sum_{i=1}^4 q_i = \sum_{i=1}^4 \omega_i = 0$. After expanding for small q and ω, one obtains

$$\chi^{-1}(q,i\omega) \approx \chi^{-1}(0,0) - aq^2 + b\frac{i\omega}{v_F q}, \tag{1.18}$$

where a, b are constants, and v_F the Fermi velocity. The quartic coefficient v_4 was evaluated in the mean-field approximation (all ω_i were set to zero). This resulted in the effective bosonic theory where

$$\mathcal{F} \approx \sum_{q,\omega}\left(r_0 + q^2 + \frac{|\omega|}{q}\right)|\phi|^2 + u_0|\phi|^4, \tag{1.19}$$

where $r_0 = 1 - g\chi^{-1}(0,0)$ is a tunable parameter and $u_0 \sim \rho^{(2)}(\epsilon_F) > 0$ is the second derivative of the density of states at the Fermi surface, which is positive for the free electron dispersion, $\epsilon = k^2$.

We now briefly discuss the physical origin and the role of the Landau damping term $\frac{|\omega|}{q}$ in the free energy. It reflects the fact that in a quantum phase transition statics and dynamics are coupled. The damping occurs due to the presence of the particle-hole continuum. In the paramagnetic phase, excitations are paramagnons

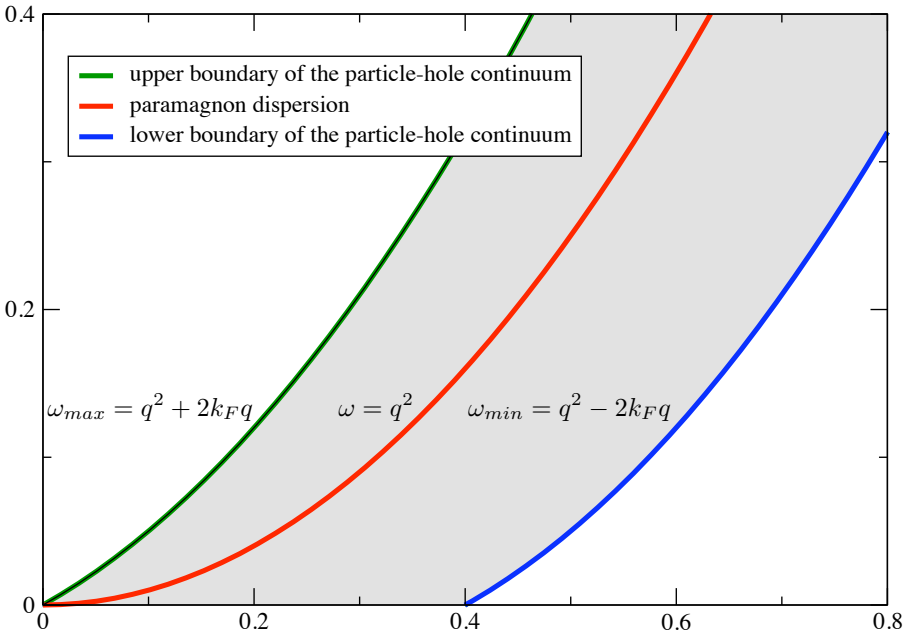

Figure 1.3: **Landau damping due to the particle-hole continuum:** The paramagnon dispersion lies inside the particle-hole continuum. A single paramagnon can decay into a particle-hole pair, which results in a finite lifetime.

with dispersion $\omega(q) = q^2$. The boundaries of the particle-hole continuum are given by $\omega_{min} = q^2 - 2qk_F$, $\omega_{max} = q^2 + 2qk_F$. A paramagnon with momentum q always lies *inside* the continuum of particle-hole pairs of momentum q, see Fig. 1.3. Therefore paramagnons can excite particle-hole pairs and scatter off them. This results in a finite life-time $\tau \approx \frac{1}{qv_F}$, where v_F denotes the Fermi velocity, as seen in the expression for the free energy (1.19).

We summarize the assumptions of Hertz-Millis theory, as we will question them later on. In summary:

1. Decoupling in the spin channel only was performed.
2. The action was expanded about the paramagnetic state $\langle \boldsymbol{\phi} \rangle = 0$.
3. The Lindhardt function was expanded for small momentum q, which lead to the quadratic coefficient in the action of the form $v_2 \approx r_0 + q^2 + \frac{|\omega|}{q}$.
4. The quartic coefficient v_4, was evaluated in the mean field theory.

1.4 The Breakdown of Itinerant Quantum Criticality

In the past decade or so, growing experimental evidence has emerged signalling the breakdown of itinerant quantum criticality. The avoidance of quantum critical points, observed in experiments, manifested itself in the formation of new exotic phases in the vicinity of quantum critical points. We discuss why Hertz-Millis theory fails to account for these observations and present other theoretical methods that address them. These include non-analytic corrections to Hertz-Millis theory, the Coleman-Weinberg mechanism and the quantum order-by-disorder approach. The latter will be pursued throughout this thesis.

1.4.1 Experimental evidence

We present experimental evidence that corroborate the failure of Hertz-Millis theory on two accounts: (i) to predict experimentally observed first order transitions, and (ii) to predict the formation of new phases in the vicinity of a putative quantum critical point.

1.4.1.1 First order transition

There exist many experimental compounds where a second order phase transition was expected, but a first order transition has been seen [9; 10; 11; 12; 13]. Hertz-Millis theory [7; 14] predicts a second order paramagnet-to-ferromagnet transition. This is because the quartic coefficient, Eq. (1.13), in (3.1) is positive. In many experimental compounds, such as MnSi [15], $ZrZn_2$ [16], $Sr_3Ru_2O_7$ [17], the transition becomes first order below a certain temperature.

1.4.1.2 Formation of new phases around itinerant electron quantum critical points

The avoidance of quantum critical points has been observed in many experiments [21; 22]. By trying to avoid a singularity, a system escapes to form new phases in the vicinity of a putative quantum critical point. Examples include an anomalous anisotropic phase around the metamagnetic quantum critical end point of $Sr_3Ru_2O_7$ [17; 23], a possible inhomogeneous magnetic state in $ZrZn_2$ [16], the unusual partially ordered phase of MnSi [20] or the onset of superconductivity close to the itinerant ferromagnetic quantum critical point of UGe_2 [19], see Fig. 1.4. A superconducting dome that appears in the vicinity of a quantum critical point is also a common example in many other heavy fermion systems [24; 25; 26].

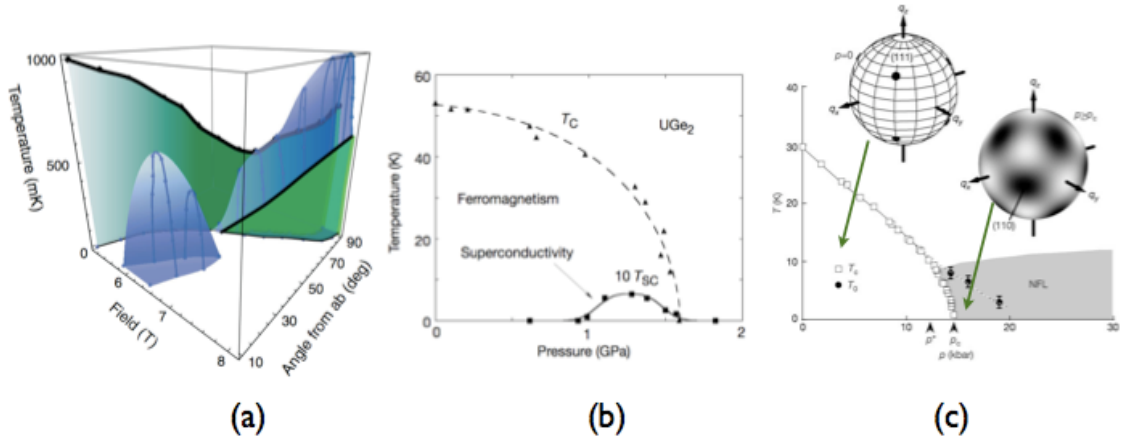

Figure 1.4: **Formation of new phases in the vicinity of quantum critical points:** (a) $Sr_3Ru_2O_7$: phase diagram in temperature-magnetic field strength-magnetic field angle space, taken from [18]. An anomalous anisotropic phase has been detected close to the metamagnetic quantum critical end point. (b) UGe_2: temperature-pressure phase diagram, taken from [19]. A superconducting dome appears inside the ferromagnetic region. (c) MnSi: phase diagram in temperature-pressure plane, taken from [20]. An unusual partially ordered phase emerges in the vicinity of the putative ferromagnetic quantum critical point, as detected in neutron scattering experiments. This is discussed in detail in Chapter 5.

Universality is a central feature in quantum phase transitions. The avoidance of quantum critical points has been seen in many different systems, irrespective of their microscopic details. This has led to the speculation that the onset of new phases close to quantum critical points might represent a generic principle [27].

The physical reason for the formation of new phases is the extreme softness of a system in the vicinity of a quantum critical point. Quantum fluctuations drive the energy scales of many distortions of the electronic state to zero. Equally, they allow weak interactions to reveal themselves.

Recently, it has been argued [28] that the avoidance of naked quantum-critical points can be understood within the AdS/CFT correspondence [29; 30; 31] between conformal field theories, describing critical condensed-matter systems and gravity in Anti-de-Sitter space. In the gravity context, the quantum-critical state at finite temperatures corresponds to a Reissner-Nordstrom black hole in AdS space. It has been realized that such a black hole can become unstable at low temperatures and tends to collapse to a state with lower entropy [32; 33].

1.4.2 Theoretical approaches to the breakdown of the itinerant electron quantum criticality

Here we present theoretical approaches that address the question of instabilities of quantum critical points, and offer an alternative to Hertz-Millis theory.

1.4.2.1 Non-analytic extensions of Hertz-Millis theory

We begin by providing an overview of the non-analytic corrections to Hertz-Millis theory [34; 35; 36; 37; 38; 39; 40; 41; 42; 43; 44]. Vojta *et al.* [45] realized that in an itinerant system, besides order parameter fluctuations, one has to take into account other low-energy modes in order to construct a reliable low-energy model. These additional soft modes correspond to excitations of particle-hole pairs with momentum $2k_F$, where k_F denotes the Fermi momentum. They couple to the order parameter fluctuations, leading to an effective long-range interactions between them. This can change the nature of the transition (i.e. drive it first order) and result in instabilities towards the formation of other phases.

It was argued that because of these additional low-energy modes, it becomes impossible to construct a simple Gizburg-Landau expansion in powers of the order parameter alone [46]. The presence of the additional low-energy modes manifests itself in (i) non-analytic dependence of the free energy on the order parameter [46], or equivalently (ii) non-analytic dependence of the static spin susceptibility [34; 35; 40; 47]. Below, we present a brief outline of the calculations of the free energy $\mathcal{F}(M)$ and static spin susceptibility $\chi(q)$. From the forms of the non-analytic corrections to $\mathcal{F}$ and $\chi(q)$, it is possible to deduce the instabilities that develop in the vicinity of an itinerant ferromagnetic quantum critical point: first order transition, inhomogeneous ferromagnetic state, and spin nematic. Finally, we address the reasons why Hertz-Millis theory failed.

(i) Non-analytic dependence of the free energy. We have seen that the fermionic density operator couples linearly to order parameter fluctuations (1.15). Kirkpatrick and Belitz stressed that one needs to keep the low-energy particle-hole modes P on equal footing to the order parameter fluctuations M. In their work [48], this is done through considering the action $\mathcal{A}[M,P] = \mathcal{A}_M + \mathcal{A}_P + \mathcal{A}_{M,P}$, where $\mathcal{A}_{M,P}$ denotes the coupling of the low-energy particle-hole modes to the order parameter fluctuations. The inclusion of these $2k_F$ low-energy modes leads to the following non-analytic correction to the free energy:

$$\mathcal{F}(M) \sim M^4 + cM^4 \ln\left(M^2 + T^2\right). \tag{1.20}$$

The free energy is divergent at $T = 0$ and $M = 0$, while finite M or finite T cut-off the divergence. When the quartic coefficient becomes negative, the paramagnet-to-ferromagnet transition turns first order.

(ii) Non-analytic dependence of the static spin susceptibility. In the work of Belitz *et al.* [47] a perturbative calculation of the static spin susceptibility to second order in the interaction strength was performed. A non-analytic dependence of the static spin susceptibility $\chi(q)$ on q in $d = 3$ was shown to occur:

$$\frac{\chi^{-1}(q)}{\chi^{-1}(0)} = 1 + c_3 \left(\frac{q}{2k_F}\right)^2 \ln\left(\frac{2k_f}{q}\right), \quad c_3 > 0. \tag{1.21}$$

It was explicitly shown that the non-analytic dependence arises due to a $2k_F$ singularity in the particle-hole polarization bubble [34]. The non-analytic dependence of the static spin susceptibility (1.21) leads to the $\mathcal{F}(M) \sim M^4 \ln(M^2)$ non-analytic dependence of the free energy, see Ref. [49].

Instabilities. It was argued that negative static susceptibility (1.21) up to finite q_1 implies either instability towards an incommensurate state with $q \approx q_1$ or commensurate ordering, but a first order transition. The occurrence of first order transitions is perhaps more easily seen from the free energy dependence (1.20). The work of Chubukov [50] also predicts an instability towards a p-wave spin-nematic state, arguing that this instability can occur before other relevant instabilities.

1.4.2.2 Why did Hertz-Millis theory fail?

After having discussed the framework of non-analytic corrections to Hertz-Millis theory, we are in a position to explain why Hertz-Millis theory failed. First, the theory did not explicitly account for *all* low-energy modes in an itinerant system – it neglected the coupling of order parameter fluctuations to low-energy particle-hole pairs with momentum $2k_F$. Secondly, it breaks spin conservation and SU(2) invariance.

Hertz-Millis theory predicts the leading momentum dependence of the inverse static spin susceptibility $\chi^{-1}_{HM}(q) \approx q^2$. The above result (1.21) signals the failure of Hertz-Millis theory in $d = 3$. This is because the leading "correction" to the q^2 dependence of $\chi^{-1}_{HM}(q)$ is given by $q^2 \ln \frac{2k_f}{q}$. The "correction" is thus bigger than q^2. In d dimensions (apart from the marginal case $d = 3$) the correction to the inverse susceptibility scales as $\chi^{-1}(q) \sim q^{\frac{d+1}{2}}$. This indicates the validity of Hertz-Millis theory for $d \geq 4$, since the corrections become smaller than the q^2 term.

The fact that Hertz-Millis theory breaks spin conservation [50] is a more fundamental problem. Any theory that describes low-energy fermions must be $SU(2)$ invariant. It must preserve the total charge and the total spin. Hertz-Millis theory is fundamentally incomplete since it violates spin conservation. The following argument outlines why this is the case. In Hertz-Millis theory, electron spins are 'split' into spins of itinerant fermions $\mathbf{s} = c^\dagger_\alpha \boldsymbol{\sigma}_{\alpha,\beta} c_\beta$, and spins $\boldsymbol{\phi}$ of collective bosons. In the $SU(2)$ symmetric case the fermion-boson coupling $\mathbf{s} \cdot \boldsymbol{\phi}$ (see Eq. (1.15)) flips the electron spin s^z. $\boldsymbol{\phi}$ is therefore not conserved separately from s, and vice versa. Hertz-Millis theory integrates out the fermions, and writes down an effective low-energy theory in terms of bosonic spins only.

1.4.2.3 Coleman-Weinberg mechanism

Coleman and Weinberg [51] considered a theory of a massless, quartically self-interacting meson field, in order to study spontaneous symmetry breaking. The authors performed an expansion around the classical action and employed a one loop approximation for the effective potential. This resulted in an effective potential of the form $V_{\text{eff}} = \phi^4 \log \phi^2$, which leads to a first order transition.

Condensed matter analogue of the Coleman-Weinberg mechanism. Next, we discuss the condensed matter analogue of the Coleman-Weinberg mechanism, employed by She *et al.* [28]. She and collaborators studied quantum criticality in the presence of competing interactions, in order to address the emergence of new phases in the vicinity of quantum critical points.

They introduced two competing fields: classical (ψ) and quantum (ϕ), that interact repulsively via a bi-quadratic interaction. The main idea behind their work is that integrating out the quantum field provides an effective potential for the classical field. In a way, this is a quantum analogue of the Larkin-Pickin mechanism [52]. Briefly, the starting point for this calculation is the partition function given by

$$\begin{aligned} Z(\psi) &= \int \mathcal{D}\phi \, \exp\left(-\mathcal{F}_\psi/T - S_\phi - S_{\phi,\psi}\right) \\ S_{\phi,\psi} &= g \int d\tau d\mathbf{r} \, \phi^2 \psi^2 \end{aligned} \tag{1.22}$$

They considered the one loop correction to the effective potential of ψ. The saddle point equation for the classical field ψ reads

$$(-\alpha + \beta\psi^2 - \frac{\rho}{2}\nabla^2 + g\langle\phi^2(r)\rangle)\psi = 0, \tag{1.23}$$

where α, β and ρ are constant. The expectation value of $\langle\phi^2(r)\rangle$ is defined by

$$\langle\phi^2(r)\rangle = \frac{1}{\beta}\int D\phi \int d\tau\ \phi^2 \exp\left(-S_\phi - S_{\psi,\phi}\right) = \int_{k,\omega} \frac{1}{\chi^{-1}(k,\omega_n) + g\psi^2}. \quad (1.24)$$

This is equivalent to having an effective potential of the form

$$\frac{\partial V_{\text{eff}}}{\partial \psi} = 2g\langle\phi^2(r)\rangle\psi. \quad (1.25)$$

The Coleman-Weinberg potential $V_{\text{eff}} = \psi^4 \ln \psi^2$ is recovered for $d = 3$, $z = 1$. When the quartic coefficient in the free energy becomes negative (which is inevitable due to the form of the V_{eff}), this results in the occurrence of a first order transition, as observed in experiments.

1.4.2.4 Quantum order-by-disorder

In itinerant electron system, certain deformations of the Fermi surface enhance quantum fluctuations. Enhanced quantum fluctuations lower the free energy of certain phases and stabilize them – this mechanism is known as quantum order-by-disorder. The lowering of the free energy already becomes evident from the self-consistent second order perturbation theory. The presence of a given type of order modifies the mean-field dispersion. The modified mean-field dispersion changes quantum fluctuations. Enhanced quantum fluctuations lower the free energy.

The approach not only establishes the connection to deformations of the Fermi surface, which are accessible by various experimental probes, but also leads to relatively simple analytical calculations. As such, it is more accessible than technically involved diagrammatic techniques [35; 43; 45; 50]. It predicts instabilities towards new phases, such as the d-wave spin nematic.

The two approaches – quantum order-by-disorder and the theory of non-analytic corrections – are formally equivalent; expanding self-consistently about a saddle point with the already established order re-sums selected series of diagrams that give rise to non-analytic corrections to the free energy. In particular, we recover the non-analytic dependence of the free energy of [45] and explicitly show that the non-analytic corrections occur due to particle-hole pairs of momentum $2k_F$.

As will be shown in the thesis, ferromagnetic, spiral or spin-nematic deformations of the Fermi surface enhance the phase space available for the formation of low-energy particle-hole pairs of momentum $2k_F$. These are the relevant instabilities that our approach predicts in the vicinity of an itinerant ferromagnetic quantum critical point.

1.5 Summary

In summary, the instability of quantum critical points is an experimental fact. It manifests itself in the occurrence of new phases in the vicinity of putative quantum critical points. The standard theory of itinerant quantum criticality, Hertz-Millis theory, has failed to provide an explanation for this.

We discussed different theoretical approaches that address the failure of itinerant electron quantum criticality: non-analytic corrections to Hertz-Millis theory, the Coleman-Weinberg mechanism and the quantum order-by-disorder mechanism. It has been argued that Hertz-Millis theory failed because it neglected the presence of low-energy particle-hole pairs that couple to order parameter fluctuations. When these additional soft modes are included in the low-energy theory on an equal footing, it has been shown that they generate non-analytic dependence of the free energy, or, equivalently, non-analyticities in the static spin susceptibility. The non-analytic corrections to Hertz-Millis theory predict a first order transition and spiral and p-wave spin nematic instabilities. The Coleman-Weinberg mechanism, originally discussed in high-energy physics, but with a straightforward condensed-matter analogue, leads to an effective potential of the form $V_{\text{eff}} = \phi^4 \ln \phi^2$. It successfully explains the emergence of first order transitions. The quantum order-by-disorder approach provides an intuitive physical picture – certain deformations of the Fermi surface associated with a particular type of order enhance quantum fluctuations and self-consistently lower the free energy of that order. In the itinerant ferromagnetic system, quantum fluctuations correspond to pairs of particle-hole pairs of opposite spin. The approach results in relatively simple calculations, that can be understood by a broad audience. It predicts spiral and spin-nematic instabilities, as will be shown in this thesis.

All the aforementioned methods ultimately describe the same physics. The $\phi^4 \ln \phi^2$ non-analyticity is present in all theories, and as it has been argued by several authors [34; 45; 53] it results from low-energy particle-hole modes carrying momentum $2k_F$.

1.6 Thesis Outline

The outline of this thesis is as follows. In Chapter 2 we present the main idea of quantum order-by-disorder approach at an itinerant ferromagnetic quantum critical point, and perform an explicit calculation of fluctuation corrections to the free energy. Certain phases have more quantum fluctuations associated with them; this lowers their free energy and renders them stable. The lowering of the free energy becomes evident from self-consistent second order perturbation

theory.

In Chapter 3, we develop the Ginzburg-Landau expansion of various order parameters that characterize the phases that might form in the vicinity of the putative quantum critical point. We allow for the generation of new phases due to quantum fluctuations, and consider phases relevant to the experimental examples mentioned in the Introduction – spiral ferromagnet and spin nematic. First, the Ginzburg-Landau expansion of a uniform ferromagnet is developed. We show that the Ginzburg-Landau coefficients of spiral and spin nematic are related to the Ginzburg-Landau coefficients of the uniform ferromagnet by averages of certain angular functions. In addition, we also construct the Ginzburg-Landau expansion of the uniform ferromagnet, spiral ferromagnet and spin nematic in the presence of a weakly anisotropic dispersion $\epsilon_{\mathbf{k}} = k^2 + \delta\epsilon_{\mathbf{k}}$, where $\delta\epsilon_{\mathbf{k}}$ is small.

The phase diagram of the itinerant ferromagnetic quantum critical point is then constructed in Chapter 4. The mean-field phase diagram consists of a paramagnet and a ferromagnet, separated by a line of second order phase transitions. The inclusion of quantum fluctuations results in the formation of new phases – a spiral ferromagnet and a spin nematic are stabilized near to the putative quantum critical point. In addition, we investigate the modifications of the phase diagram if one allows for the presence of a weakly anisotropic dispersion, rather than the isotropic-free electron one.

In second part of the thesis, we apply the quantum order-by-disorder method to study the phase diagram of MnSi. In Chapter 5, we present the summary of experimental results on MnSi. We discuss the key features of the helical phase and the partially ordered phase, detected in neutron scattering data. In Chapter 6, we construct the simplest extension of the Stoner model by adding weak spin-orbit coupling. This enables us to explain the experimentally observed phase diagram of MnSi. In particular, we show that quantum fluctuations stabilize a phase which shares many of the experimentally observed features with the partially ordered phase of MnSi. In particular, our model explains the experimentally observed wave vector re-orientation when going from the helical phase into the partially ordered phase. The theoretical predictions for the neutron scattering data are presented in Chapter 7, where we also discuss the relation of our approach to other related theories.

Chapter 2

Quantum Order-by-Disorder

In the order-by-disorder mechanism, fluctuations stabilize a particular ground state of a system. There are many simple examples of order arising from disorder in nature, that we encounter in everyday life – the formation by the wind of ripple patterns on sand dunes in deserts or snowflakes of perfect geometric shapes that are created spontaneously from randomly moving water molecules in a snow storm. In such classical systems, thermal fluctuations entropically pick a particular ground state.

In this Chapter we introduce the main concept of this thesis, that of a quantum order-by-disorder, where quantum fluctuations lower the free energy of a particular ground state and stabilize it. This is a familiar concept in field theory (the Coleman-Weinberg mechanism) and there are numerous examples of the mechanism in condensed matter systems [54; 55]. Perhaps the best known examples arise in frustrated magnets, where quantum fluctuations can lift degeneracies [56; 57; 58; 59; 60; 61; 62; 63]. Spin waves select a particular ground state(s) from the otherwise classically degenerate manifold of ground states. We will discuss the $J_1 - J_2$ next-nearest neighbour model on a square lattice in more detail. There, in a certain parameter regime, quantum fluctuations can have even more profound effects and stabilize a **new** ground-state, which is not favoured in the classical theory.

We then concentrate on the quantum order-by-disorder mechanism at itinerant ferromagnetic quantum critical points. We begin by discussing a simple physical picture, where quantum fluctuations correspond to excitations of virtual pairs of particle-hole pairs of opposite spin. Certain deformations of the Fermi surface, such as ferromagnetic, spiral or spin-nematic enhance the phase space for quantum fluctuations. Enhanced quantum fluctuations then lower the free energies of those states. This is, in a sense, the fermionic version of quantum order-by-disorder. In the usual concept, the order-by-disorder mechanism is driven by fluctuations of a bosonic order parameter. Here, the underlying Fermi

statistics and Pauli blocking become important.

We show that the lowering of the free energy becomes evident from: (i) self-consistent second order perturbation theory, as well as (ii) from the equivalent field-theoretical derivation.

(i) We develop a perturbation theory around the mean-field state, for a given type of order. The order modifies the mean-field dispersion, which in turn modifies the quantum fluctuations. The second order free energy shift due to fluctuations is always negative; in this way enhanced quantum fluctuations can lead to the stabilization of new phases.

(ii) The field-theoretical derivation begins by decoupling the interaction in *both spin and charge channels*. We then integrate out the fermions, which leads to an effective bosonic theory. The crucial step comes next, where we expand the action around an **ordered** state – characterized by a non-zero expectation value of some bosonic order parameter – as opposed to expanding around the disordered state, as in Hertz-Millis theory. Integrating out the fluctuations, treated to second order, recovers the second order perturbation theory result for the free energy.

The fluctuation corrections to the free energy are tricky to evaluate. This is due to the fact that (i) they are given by a high-dimensional momentum integral over a kernel, (ii) the kernel is a functional of different mean-field dispersions, which in some cases are not trivial. As a mathematical convenience, we express the fluctuation corrections to the free energy as a lower-dimensional integral over the modified particle-hole densities of states.

2.1 Order-by-Disorder Mechanism

In this section we discuss the quantum order-by-disorder mechanism.

2.1.1 Classical order-by-disorder

We begin by discussing the classical order-by-disorder mechanism, where thermal fluctuations entropically pick a particular ground state. Mathematically, the entropic lowering of the free energy comes from the TS term in the free energy $\mathcal{F} = E - TS$. For example, in reference [64], a diamond-lattice antiferromagnet was studied. With sufficiently strong frustration, the ground-state of the system is highly degenerate – it is given by a manifold of spirals with wave vectors residing on a two-dimensional surface in the momentum space (see Fig. 2.1). The energy associated with each ground-state is the same; however, at finite temperature different ground-states have different entropies, and hence different free energies. In this way thermal fluctuations select a particular subset of ground-states – the

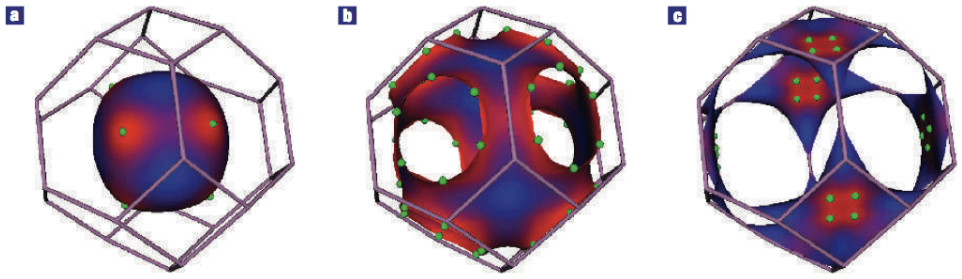

Figure 2.1: $J_1 - J_2$ **next nearest neighbours model on a diamond lattice.** Taken from [64]. Degenerate spiral ground-state wavevectors lie on the 'spiral surfaces' depicted above: (a) $J_2/J_1 = 0.2$, (b) $J_2/J_1 = 0.4$ and (c) $J_2/J_1 = 0.85$. At finite temperatures, thermal fluctuations lift the degeneracy in the free energy. This mechanism is known as order-by-disorder. Areas of high free energy are denoted blue, while areas of low free energy are denoted red. Green dots represent the absolute minima in the free energy – these wavevectors are selected as new ground-states by the order-by-disorder mechanism.

one(s) with the highest entropy, (see Fig. 2.1 – the wave vectors associated with the new ground-states are denoted by green dots).

2.1.2 Quantum order-by-disorder

Similarly to the entropic lowering of the free energy in classical systems, quantum fluctuations can lower the energy of a certain state and stabilize a new order. The order affects the mean-field dispersion, which modifies the quantum fluctuations. Enhanced quantum fluctuations lower the energy of certain states. This is equivalent to the Coleman-Weinberg mechanism in high energy physics [51].

A simple example of quantum order-by-disorder is that of a quantum antiferromagnet. If the neighbouring spins are oriented parallel to each other, no virtual hopping is allowed due to the Pauli exclusion principle. On the other hand, for the anti-parallel orientation of the spins virtual hopping is allowed. The hopping lowers the energy of the system and stabilizes the antiferromagnetic phase. This result can be obtained from the second order perturbation theory: the additional phase space for fluctuations in the antiferromagnet lowers its free energy. Here, the free energy is lowered by reducing the *energy* of the system ($T = 0$), rather than by an increase in the entropy.

Another, maybe more familiar example is that of the $J_1 - J_2$ next-nearest

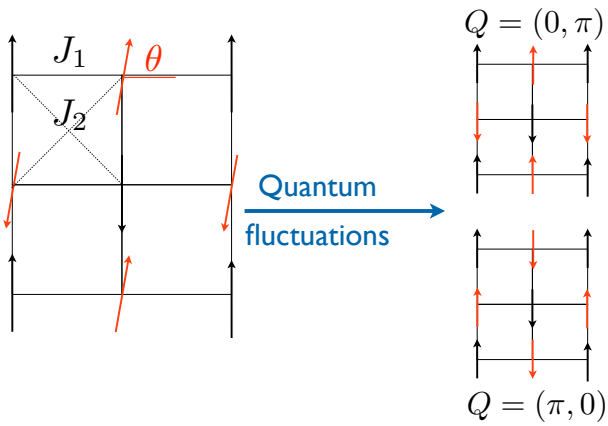

Figure 2.2: $J_1 - J_2$ **next nearest neighbours model on a square lattice – linear spin-wave theory** (courtesy of F. Krüger): Quantum fluctuations, included through linear spin-wave theory, select columnar antiferromagnet ($\mathbf{Q} = (0, \pi)$ or $\mathbf{Q} = (\pi, 0)$) as the ground state, from an otherwise highly degenerate manifold of classical ground states.

neighbour model on a square lattice [61]. The Hamiltonian reads

$$\mathcal{H} = J_1 \sum_{\langle i,j \rangle} \hat{S}_i \cdot \hat{S}_j + J_2 \sum_{\langle\langle i,j \rangle\rangle} \hat{S}_i \cdot \hat{S}_j. \tag{2.1}$$

We will concentrate on the region in parameter space where $J_2 > \frac{J_1}{2}$, with positive J_1, J_2. The classical ground-state energy (see Fig. 2.2) is given by

$$\begin{aligned} E &= J_1 \cos\left(\frac{\pi}{2} - \theta\right) + J_1 \cos\left(\frac{\pi}{2} + \theta\right) - 2J_2 \\ &= -2J_2. \end{aligned} \tag{2.2}$$

The ground state energy is independent of the angle θ. Hence, there is a highly degenerate manifold of classical ground states. Quantum fluctuations, included through linear spin-wave theory in the first approximation, select $\mathbf{Q} = (0, \pi)$ or $\mathbf{Q} = (\pi, 0)$ (columnar antiferromagnets) as ground states for $J_2 > \frac{J_1}{2}$ (see Fig. 2.2). Beyond the linear spin-wave theory, quantum fluctuations stabilize the new ground state – the region of Neel antiferromagnet (blue line in Fig. 2.3) now penetrates into the region where the columnar antiferromagnet was previously stabilized in linear spin-wave theory (green line in Fig. 2.3). This demonstrates how quantum fluctuations can **change** the ground state and stabilize a new phase, which was not favoured in mean-field theory.

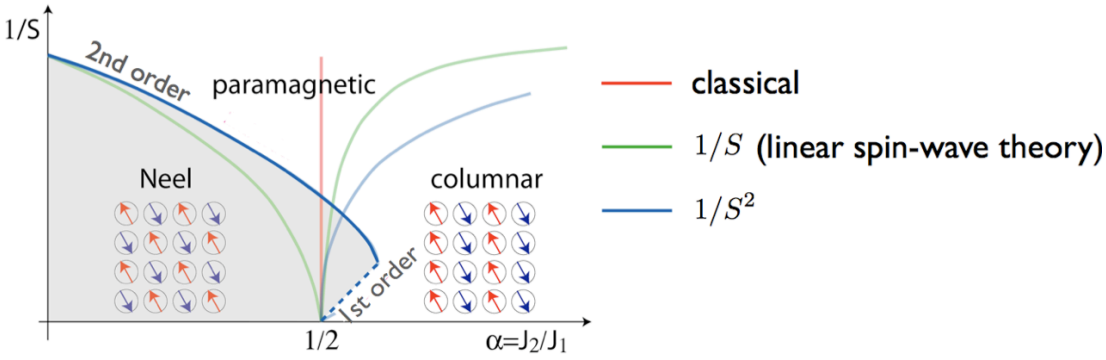

Figure 2.3: $J_1 - J_2$ **next nearest neighbours model on a square lattice – phase diagram beyond the linear spin-wave theory** (courtesy of F. Kruger): Phase diagram in $1/S$ (inverse spin) vs $\frac{J_2}{J_1}$ plane. In the region of the phase diagram where $J_2 > \frac{J_1}{2}$, quantum fluctuations, included through linear spin-wave theory (green line), select columnar antiferromagnet ($\mathbf{Q} = (0, \pi)$ or $\mathbf{Q} = (\pi, 0)$) as the ground state, from otherwise highly degenerate manifold of classical ground states. Beyond the linear spin-wave theory (order $1/S^2$), quantum fluctuations stabilize new ground state – a Neel ferromagnet (blue line) in the region where columnar antiferromagnet was previously found.

2.2 Quantum Order-by Disorder for an Itinerant Ferromagnet

We describe the quantum order-by-disorder mechanism at itinerant ferromagnetic quantum critical points. We begin by presenting a simple heuristic picture and then embark on a more rigorous mathematical journey.

2.2.1 Heuristic picture

In the case of an itinerant ferromagnet, quantum fluctuations correspond to virtual pairs of particle-hole pairs of opposite spin and equal and opposite momenta. The dominant low-energy quantum fluctuations are the particle-hole pairs with momentum $q \approx 2k_F$. Certain Fermi-surface deformations can enhance the phase-space for the formation of these low-energy particle-hole pairs, see Fig. 2.4.

2.2.2 Self-consistent perturbation theory

We start from the Stoner model

$$\mathcal{H} = \sum_{\mathbf{k},\sigma=\pm} (\epsilon_{\mathbf{k}} - \mu)\, \hat{n}_{\mathbf{k},\sigma} + g \int \mathrm{d}^3\mathbf{r}\; \hat{n}_+(\mathbf{r})\hat{n}_-(\mathbf{r}), \tag{2.3}$$

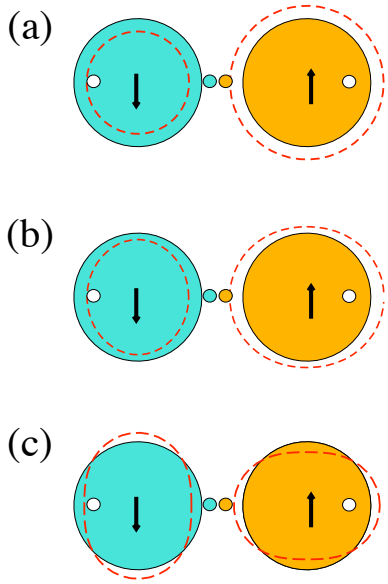

Figure 2.4: **Distortions of the Fermi surface (dashed lines) enhance the phase-space for quantum fluctuations:** (a) uniform ferromagnet (b) spiral and (c) d-wave spin nematic. Quantum fluctuations correspond to excitations of pairs of particle-hole pairs of opposite spin and equal and opposite momenta.

and perform a mean-field decoupling in the spin channel

$$g \int \mathrm{d}^3\mathbf{r}\; \hat{n}_+(\mathbf{r})\hat{n}_-(\mathbf{r}) \approx g \sum_{\mathbf{r},\nu,\nu'} \mathbf{M}(\mathbf{r}) \cdot \boldsymbol{\sigma}_{\nu,\nu'} c^\dagger_{\mathbf{r}\nu} c_{\mathbf{r}\nu'} \tag{2.4}$$

where the magnetization is given $\mathbf{M}(\mathbf{r}) = \langle \boldsymbol{\sigma}_{\nu,\nu'} c^\dagger_{\mathbf{r}\nu} c_{\mathbf{r}\nu'} \rangle$. After diagonalization (the choice of basis depends on the specific form of $\mathbf{M}(\mathbf{r})$ – we will explicitly consider spiral ferromagnet later on), this leads to the mean-field Hamiltonian

$$\mathcal{H}_{MF} = \sum_{\mathbf{k},\sigma=\pm} (\epsilon^\sigma_{\mathbf{k}} - \mu)\, \hat{n}_{\mathbf{k},\sigma} + g \int \mathrm{d}^3\mathbf{r} M^2(\mathbf{r}), \tag{2.5}$$

where $\epsilon^\sigma_{\mathbf{k}}$ is the mean-field dispersion in the presence of a given type of order (we will not consider charge ordering). We perform a self-consistent perturbation theory around the mean-field solution.

2.2.2.1 Free energy

We calculate the corrections to the free energy. The first order energy shift is zero, while the second order energy shift reads

$$\mathcal{F} = \sum_{\{i\}} \frac{\langle\langle T|\mathcal{H}^{int}|i\rangle\langle i|\mathcal{H}^{int}|T\rangle\rangle}{\epsilon_T - \epsilon_i}, \tag{2.6}$$

where $|T\rangle$ is a state from the thermal ensemble, $|i\rangle$ represents a virtual intermediate state and $\langle\langle ...\rangle\rangle$ indicates quantum and thermal averaging. With the form of $\mathcal{H}^{int}$ given in Eq. (2.3), non-zero averages occur for intermediate states of the form

$$|i\rangle = \sum_{\mathbf{p}\neq\mathbf{k},\mathbf{q}\neq\mathbf{l}} c^\dagger_{\mathbf{p},\uparrow} c^\dagger_{\mathbf{q},\downarrow} c_{\mathbf{l},\downarrow} c_{\mathbf{k},\uparrow} |0\rangle, \tag{2.7}$$

so that $\epsilon_T - \epsilon_i = \epsilon^+_{\mathbf{k}} + \epsilon^-_{\mathbf{l}} - \epsilon^+_{\mathbf{p}} - \epsilon^-_{\mathbf{q}}$. This leads to

$$\mathcal{F} = \sum_{\mathbf{p}\neq\mathbf{k},\mathbf{q}\neq\mathbf{l}} \frac{|{}_0\langle \mathbf{p}\uparrow,\mathbf{q}\downarrow|\mathcal{H}^{int}|\mathbf{k}\uparrow,\mathbf{l}\downarrow\rangle_0|^2}{\epsilon^+_{\mathbf{k}} + \epsilon^-_{\mathbf{l}} - \epsilon^+_{\mathbf{p}} - \epsilon^-_{\mathbf{q}}}, \tag{2.8}$$

where $|\mathbf{k}\uparrow,\mathbf{l}\downarrow\rangle_0$ labels the two-particle free-electron state. We obtain

$$\mathcal{F}^{(0)}_{\rm fl} = -2g^2 {\sum_{}}' \frac{n(\epsilon^+_{\mathbf{k_1}}) n(\epsilon^-_{\mathbf{k_2}})(1 - n(\epsilon^+_{\mathbf{k_3}}))(1 - n(\epsilon^-_{\mathbf{k_4}}))}{\epsilon^+_{\mathbf{k_1}} + \epsilon^-_{\mathbf{k_2}} - \epsilon^+_{\mathbf{k_3}} - \epsilon^-_{\mathbf{k_4}}}, \tag{2.9}$$

where the prime over the sum indicates momentum conservation, $\mathbf{k}_1 + \mathbf{k}_2 = \mathbf{k}_3 + \mathbf{k}_4$, and for brevity, we have written the Fermi functions as

$$n^\sigma_{\mathbf{k}} := n(\epsilon^\sigma_{\mathbf{k}}) = (e^{\beta(\epsilon^\sigma_{\mathbf{k}} - \mu)} + 1)^{-1}. \tag{2.10}$$

Note that the fluctuation corrections to the free energy are calculated self-consistently; the energies entering the Fermi functions are the mean-field dispersions in the presence of a given type of order. From Eq.(2.9) we see that the fluctuations correspond to excitations of virtual pairs of particle-hole pairs of opposite spin and equal and opposite momenta (spin up particle-hole pairs carry momentum $\mathbf{k}_1 - \mathbf{k}_3$ and spin down particle-hole pairs carry momentum $\mathbf{k}_2 - \mathbf{k}_4$). Since we need to put in energy to create the particle-hole pairs, the denominator of (2.9) is always positive, which results in *negative* contributions to the free energy. Certain deformations of the Fermi-surface enhance the phase space available for low-energy, virtual particle-hole excitations and in that way self-consistently stabilize new phases. Ferromagnetic, spiral or spin-nematic Fermi-surface distortions – which are shown schematically in Fig. (2.4) – all open up extra phase-space for the low-energy particle-hole pairs to form.

Renormalization of the interaction strength. A careful inspection of the term

$$\mathcal{F}_{\rm fl}^{\infty} = -2g^2 {\sum}' \frac{n(\epsilon^+_{\mathbf{k_1}})n(\epsilon^-_{\mathbf{k_2}})}{\epsilon^+_{\mathbf{k_1}} + \epsilon^-_{\mathbf{k_2}} - \epsilon^+_{\mathbf{k_3}} - \epsilon^-_{\mathbf{k_4}}}, \tag{2.11}$$

in Eq.(2.9) reveals an unphysical divergent contribution to the free energy. To avoid this, we need to take into account the renormalization of the interaction matrix element g [65]. In the presence of interactions, the eigenstates of the Hamiltonian are not plane waves any more; hence we need to re-evaluate the matrix element between the set of new, perturbed eigenstates

$$|\mathbf{k}\uparrow,\mathbf{l}\downarrow\rangle \;=\; |\mathbf{k}\uparrow,\mathbf{l}\downarrow\rangle_0 + \sum_{\mathbf{p}\neq\mathbf{k},\mathbf{q}\neq\mathbf{l}} \frac{{}_0\langle\mathbf{p}\uparrow,\mathbf{q}\downarrow|\mathcal{H}^{int}|\mathbf{k}\uparrow,\mathbf{l}\downarrow\rangle_0}{\epsilon^+_{\mathbf{k}} + \epsilon^-_{\mathbf{l}} - \epsilon^+_{\mathbf{p}} - \epsilon^-_{\mathbf{q}}} |\mathbf{p}\uparrow,\mathbf{q}\downarrow\rangle_0 \tag{2.12}$$

where $|\mathbf{k}\uparrow,\mathbf{l}\downarrow\rangle$ labels the first order corrected two-particle state. With this identification, we must make a corresponding alteration to the interaction strength,

$$g_{\mathbf{k}_1,\mathbf{k}_2} \to g - 2g^2 {\sum_{\mathbf{k}_3,\mathbf{k}_4}}' \frac{1}{\epsilon^+_{\mathbf{k}_1} + \epsilon^-_{\mathbf{k}_2} - \epsilon^+_{\mathbf{k}_3} - \epsilon^-_{\mathbf{k}_4}}. \tag{2.13}$$

The renormalization that we have chosen to adopt is conventional in the atomic physics community, and accounts for modification due to scattering of two particles when no others are around. It leads to a regular expression for the free energy,

$$\begin{aligned} \mathcal{F} &= \mathcal{F}_{MF} + \mathcal{F}_{\rm fl} \\ \mathcal{F}_{\rm fl} &= 2g^2 {\sum_{\mathbf{k}_1\ldots\mathbf{k}_4}}' \frac{n^+_{\mathbf{k}_1} n^-_{\mathbf{k}_2}(n^+_{\mathbf{k}_3} + n^-_{\mathbf{k}_4})}{\epsilon^+_{\mathbf{k}_1} + \epsilon^-_{\mathbf{k}_2} - \epsilon^+_{\mathbf{k}_3} - \epsilon^-_{\mathbf{k}_4}}, \end{aligned} \tag{2.14}$$

where $\mathcal{F}_{MF}$ represents the mean-field contribution.

2.2.3 Equivalent field-theoretical derivation

We sketch how the same result can be derived using field theoretical methods [66; 67]. This approach reveals the connection between the self-consistent second order perturbation theory [68; 69; 70] and field theoretical calculations that explicitly show non-analytic behavior of the free energy.

2.2.3.1 Free energy

We start from the fermionic partition function,

$$\begin{aligned} \mathcal{Z} &= \int \mathcal{D}(\bar{\psi},\psi) e^{-S[\bar{\psi},\psi]}, \\ S[\bar{\psi},\psi] &= \int_0^\beta \mathrm{d}\tau \int \mathrm{d}^3\mathbf{r} \left[\bar{\psi}\partial_\tau \psi + \mathcal{H}(\bar{\psi},\psi)\right], \end{aligned} \tag{2.15}$$

where $\psi = (\psi_+, \psi_-)^T$ and $\bar{\psi} = (\bar{\psi}_+, \bar{\psi}_-)$ denote Grassman fields which vary throughout space and imaginary time, and the Hamiltonian is given by Eq. (2.3). After performing a Hubbard-Stratonovich decoupling of the interaction in spin ($\boldsymbol{\phi}$) and charge (ρ) channels we obtain

$$\begin{aligned} \mathcal{Z} &= \int \mathcal{D}(\bar{\psi},\psi)\mathcal{D}\boldsymbol{\phi}\mathcal{D}\rho e^{-S[\bar{\psi},\psi,\boldsymbol{\phi},\rho]}, \\ S[\bar{\psi},\psi,\boldsymbol{\phi},\rho] &= \int \bar{\psi}(\hat{G}_0^{-1} + g(\rho - \boldsymbol{\phi}\cdot\boldsymbol{\sigma}))\psi + g\int(\boldsymbol{\phi}^2 - \rho^2), \end{aligned} \tag{2.16}$$

where $\hat{G}_0^{-1}$ is the free-electron Green function and $\boldsymbol{\sigma}$ denotes the vector of Pauli matrices. While Hertz and Millis decoupled the interaction in the spin channel only [7; 8], Conduit *et al.* [66] (and later Chubukov and Maslov [50]) stressed the necessity of decoupling in both spin and charge channels, since the contributions of the spin and charged bosons are of the same magnitude. Integrating out the fermions, we obtain an effective theory in terms of the fluctuations of the bosonic order parameter

$$\begin{aligned} \mathcal{Z} &= \int \mathcal{D}\boldsymbol{\phi}\mathcal{D}\rho e^{-S[\boldsymbol{\phi},\rho]}, \\ S[\boldsymbol{\phi},\rho] &= -\mathrm{Tr}\ln\left[\hat{G}_0^{-1} + g(\rho - \boldsymbol{\sigma}\cdot\boldsymbol{\phi})\right] + g\int(\boldsymbol{\phi}^2 - \rho^2). \end{aligned} \tag{2.17}$$

A saddle point approximation of this action recovers the mean-field solution. So far all the steps closely resemble the derivation of Hertz and Millis. In their theory, however, the aim was to derive an effective action for dynamical fluctuations of the bosonic order parameter in the **paramagnetic** state. In contrast, we wish to derive a Ginzburg-Landau expansion in the static order parameter. In order to do this we separate $\boldsymbol{\phi}$ and ρ into zero-frequency ($\rho_0, \mathbf{M}$) and finite-frequency parts ($\tilde{\rho}, \tilde{\boldsymbol{\phi}}$): $\rho = \rho_0 + \tilde{\rho}$ and $\boldsymbol{\phi} = \mathbf{M} + \tilde{\boldsymbol{\phi}}$. The action then becomes

$$\begin{aligned} S[\phi,\rho] &= -\mathrm{Tr}\ln\left[\underbrace{\hat{G}_0^{-1} + g\rho_0 - g\boldsymbol{\sigma}.\mathbf{M}}_{\hat{G}_{\mathbf{M}}^{-1}} + g(\tilde{\rho} - \tilde{\boldsymbol{\phi}}\cdot\boldsymbol{\sigma})\right] \\ &+ g\int(\mathbf{M}^2 + \tilde{\boldsymbol{\phi}}^2 - \tilde{\rho}^2). \end{aligned} \tag{2.18}$$

So far all the analysis has been exact. Next, we expand this action to quadratic order in finite-frequency fluctuations

$$\begin{aligned} S[\mathbf{M},\tilde{\rho},\tilde{\phi}] &= g\int d\mathbf{r}\ \mathbf{M}^2 - Tr\ln\hat{G}^{-1}_{\mathbf{M}} + g(\tilde{\boldsymbol{\phi}}^2-\tilde{\rho}^2) \\ &- gTr[\hat{G}_{\mathbf{M}}(\tilde{\rho}-\boldsymbol{\sigma}.\tilde{\boldsymbol{\phi}}) + \frac{g}{2}\hat{G}_{\mathbf{M}}(\tilde{\rho}-\boldsymbol{\sigma}.\tilde{\boldsymbol{\phi}})\hat{G}_{\mathbf{M}}(\tilde{\rho}-\boldsymbol{\sigma}.\tilde{\boldsymbol{\phi}})]. \quad (2.19) \end{aligned}$$

We separate two different contributions to the action

$$S[\tilde{\rho},\tilde{\boldsymbol{\phi}}] = S_{\parallel}[\tilde{\rho},\tilde{\phi}_z] + S_{\perp}[\tilde{\phi}_x,\tilde{\phi}_y]. \quad (2.20)$$

Integrating out fluctuations, we obtain the following expression for the free energy:

$$\begin{aligned} \mathcal{F}[\mathbf{M}] &= gM^2 - \mathrm{Tr}\ln\hat{G}^{-1} + \underbrace{\frac{1}{2}\mathrm{Tr}\ln(1+2g\Pi^{+-}+g^2\Pi^{+-}\Pi^{-+})}_{\mathcal{F}_{fl,\perp}} \\ &+ \underbrace{\frac{1}{2}\mathrm{Tr}\ln(1-g^2\Pi^{++}\Pi^{--})}_{\mathcal{F}_{fl,\parallel}}. \quad (2.21) \end{aligned}$$

The term $\mathcal{F}_{\mathrm{fl},\perp}$ arises from transverse magnetic fluctuations, while the term $\mathcal{F}_{\mathrm{fl},\parallel}$ accounts for charge-density and longitudinal magnetic fluctuations. The polarization bubbles are given by

$$\Pi^{\sigma\sigma'}(\mathbf{q},\omega) = \frac{1}{\beta}\sum_{\mathbf{k},\omega'}\hat{G}_{\sigma}(\mathbf{k},\omega')\hat{G}_{\sigma'}(\mathbf{k}-\mathbf{q},\omega'-\omega), \quad (2.22)$$

where $\hat{G}^{-1}_{\sigma} = \hat{G}^{-1}_{0} + g\rho_0 - \sigma gM$. The polarization bubbles $\Pi^{\sigma\sigma'}$ explicitly depend on the interaction strength g.

Next, we perform a rather strange expansion in g. We expand the Tr ln-terms to second order in g by only expanding in powers of g that stand in front of the polarization bubbles, whilst keeping the full g dependence of the polarization bubbles as it is. This looks like a second order expansion in g, but self-consistency actually implies resummation of certain classes of contributions to infinite order – see Fig. 2.5. This expansion captures the relevant physics and recovers the non-analytic dependence of the free energy on the order parameter $\mathcal{F} \sim M^4\ln(M^2+T^2)$, as we will see later on. After performing the summations over the Matsubara frequencies, we arrive at the expression (2.9).

Further, we need to renormalize g to cancel the ultraviolet divergence. Doing so according to Eq. (2.13) recovers expression Eq. (2.14) for the free energy. Note that this choice of renormalization is not equivalent to a standard field-theoretical choice – the one loop correction, but still cancels the unphysical divergences in the free energy.

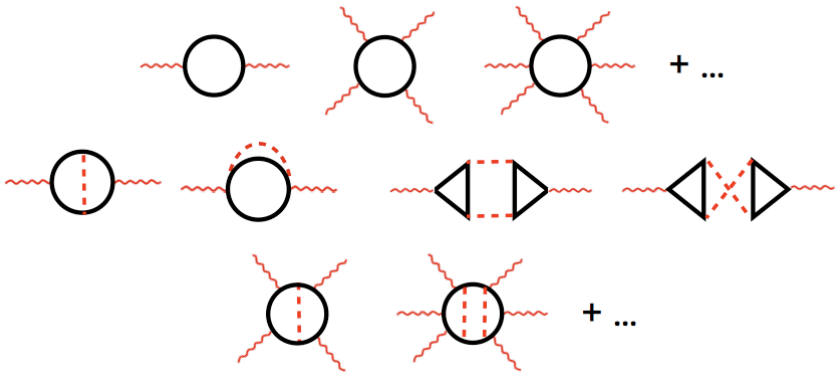

Figure 2.5: **Diagrammatic contributions to the partition function in the quantum order-by-disorder approach:** Black lines denote fermionic propagators, while red wiggly lines denote bosonic propagators that carry zero frequency. Finite frequency bosonic modes are denoted by dashed red lines. We include finite frequency fluctuations of the bosonic field to second order. *All* diagrams with an arbitrary number of zero-frequency lines are taken into account. In this way, the non-analytic dependence of the free energy on the order parameter is recovered.

2.2.4 Explicit calculation of fluctuation corrections

The second order perturbative corrections to the free energy Eq. (2.14) at zero temperature in the disordered phase were evaluated by Abrikosov and Khalatnikov [69]. The challenge is to evaluate the free energy in the presence of a certain type of order at finite temperature. We will prepare the ground for it now and deal with the explicit calculations of free energies of different types of order in Chapter 3.

From Eq. (2.14), we see that the fluctuation corrections are quite tricky to evaluate. The reason for this is two-fold. First, they are given by an integral over three three-dimensional momenta over a kernel. Secondly, non-trivial mean-field dispersions can enter the fluctuation corrections. This can result in significant calculational difficulty when expanding such a free energy in powers of the order parameter(s).

Some previous studies [66; 70] attempted a brute force numerical evaluation of the free energy (2.14). They evaluated the free energies of a uniform ferromagnet and a spiral state for different values of order parameters M, Q (where Q is the spiral wave vector) at a given (g, T). After that they extracted the values of M, Q that minimize the free energy at a given (g, T) and plotted the phase diagram. This procedure is not very accurate at low temperatures as the Fermi functions entering (2.14) fall off sharply as one approaches the Fermi energy, which might

lead to the incorrect identification of the actual minima of the free energy.

2.2.4.1 Free energy in terms of particle-hole densities of states

Here, we outline a mathematical trick that will allow us to evaluate the fluctuation contributions to the free energy.

As we have seen, the fluctuation corrections to the free energy (2.9) correspond to excitations of virtual pairs of particle-hole pairs of opposite spin, and equal and opposite momenta. It is therefore possible to rewrite the regularized fluctuation corrections $\mathcal{F}_{\text{fl}}$ (2.14) as a lower dimensional integral over modified particle-hole densities of states. We replace the momentum sum in (2.14) by an integral and use the identity

$$\frac{1}{\epsilon^+_{\mathbf{k_1}} + \epsilon^-_{\mathbf{k_2}} - \epsilon^+_{\mathbf{k_3}} - \epsilon^-_{\mathbf{k_4}}} = \int_{-\infty}^{+\infty} \mathrm{d}\epsilon_1 \int_{-\infty}^{+\infty} \mathrm{d}\epsilon_2 \; \delta(\epsilon_2 - \epsilon^-_{\mathbf{k}_2} + \epsilon^-_{\mathbf{k}_4}) \delta(\epsilon_1 - \epsilon^+_{\mathbf{k}_1} + \epsilon^+_{\mathbf{k}_3}) \frac{1}{\epsilon_1 + \epsilon_2} \tag{2.23}$$

to obtain

$$\begin{aligned} \mathcal{F}_{\text{fl}} \;=\; & 2g^2 \int_{\mathbf{k}_3} \int_{\epsilon_1} \int_{\epsilon_2} \frac{\int_{\mathbf{k}_1} n(\epsilon^+_{\mathbf{k}_1}) n(\epsilon^+_{\mathbf{k}_3}) \delta(\epsilon_1 - \epsilon^+_{\mathbf{k}_1} + \epsilon^+_{\mathbf{k}_3}) \int_{\mathbf{k}_2} n(\epsilon^-_{\mathbf{k}_2}) \delta(\epsilon_2 - \epsilon^-_{\mathbf{k}_2} + \epsilon^-_{\mathbf{k}_4})}{\epsilon_1 + \epsilon_2} \\ & 2g^2 \int_{\mathbf{k}_3} \int_{\epsilon_1} \int_{\epsilon_2} \frac{\int_{\mathbf{k}_2} n(\epsilon^-_{\mathbf{k}_2}) n(\epsilon^-_{\mathbf{k}_4}) \delta(\epsilon_2 - \epsilon^-_{\mathbf{k}_2} + \epsilon^-_{\mathbf{k}_4}) \int_{\mathbf{k}_1} n(\epsilon^+_{\mathbf{k}_1}) \delta(\epsilon_1 - \epsilon^+_{\mathbf{k}_1} + \epsilon^+_{\mathbf{k}_3})}{\epsilon_1 + \epsilon_2}, \end{aligned} \tag{2.24}$$

where we have defined $\int_{\mathbf{k}} := \int \frac{\mathrm{d}^3\mathbf{k}}{(2\pi)^3}$ and $\int_{\epsilon} := \int_{-\infty}^{\infty} \mathrm{d}\epsilon$. We change the variables from $\mathbf{k}_3$ to $\mathbf{q} = \mathbf{k}_1 - \mathbf{k}_3$, and then shift $\mathbf{k}_1 \to \mathbf{k}_1 + \frac{\mathbf{q}}{2}$, $\mathbf{k}_2 \to \mathbf{k}_2 + \frac{\mathbf{q}}{2}$. After doing so, the fluctuation corrections to the free energy can be written as

$$\mathcal{F}_{\text{fl}} = 2g^2 \sum_{\sigma=\pm 1} \int_{\mathbf{q},\epsilon_1,\epsilon_2} \frac{\Delta\rho^{\sigma}(\mathbf{q},\epsilon_1)\rho^{-\sigma}(-\mathbf{q},\epsilon_2)}{\epsilon_1 + \epsilon_2}, \tag{2.25}$$

where the modified particle-hole densities of states as a function of momentum $\mathbf{q}$ and energy ϵ are given by

$$\begin{aligned} \rho^{\sigma}(q,\epsilon) \;&=\; \int_{\mathbf{k}} n(\epsilon^{\sigma}_{\mathbf{k}-\frac{\mathbf{q}}{2}}) \delta(\epsilon - \epsilon^{\sigma}_{\mathbf{k}+\frac{\mathbf{q}}{2}} + \epsilon^{\sigma}_{\mathbf{k}-\frac{\mathbf{q}}{2}}), \\ \Delta\rho^{\sigma}(q,\epsilon) \;&=\; \int_{\mathbf{k}} n(\epsilon^{\sigma}_{\mathbf{k}-\frac{\mathbf{q}}{2}}) n(\epsilon^{\sigma}_{\mathbf{k}+\frac{\mathbf{q}}{2}}) \delta(\epsilon - \epsilon^{\sigma}_{\mathbf{k}+\frac{\mathbf{q}}{2}} + \epsilon^{\sigma}_{\mathbf{k}-\frac{\mathbf{q}}{2}}), \end{aligned} \tag{2.26}$$

and are related to the particle-hole density of states as $\rho^{\sigma}_{ph} = \Delta\rho_{\sigma} - \rho_{\sigma}$. Note that the modified particle-hole densities of states are a functional of the mean-field dispersion. This form of the fluctuation correction will prove useful in our subsequent

evaluation of the Ginzburg-Landau expansion of the uniform ferromagnet, since the modified particle-hole density of states of the uniform ferromagnet can be calculated analytically. This leads to a tremendous simplification of the fluctuation integral, as it reduces to three dimensions. In Chapter 3, we show that, knowing the free energy of the uniform ferromagnet, we can deduce the free energies of a spiral and spin-nematic to leading order.

To summarize, we have described quantum order-by-disorder at itinerant ferromagnetic quantum critical points. The physical picture is that certain Fermi-surface deformations enhance the phase-space for quantum fluctuations. Enhanced quantum fluctuations then lower free energies of certain states. The lowering of the free energy due to fluctuations is evident from either self-consistent perturbation theory or the field-theoretical approach.

We developed a self-consistent second order perturbation theory around the mean-field state, for a given type of order. The order modified the mean-field dispersion, which in turn modified quantum fluctuations. We have shown how quantum fluctuations provide a negative contribution to the free energy, which enables them to stabilize certain states that are not necessarily favoured in the mean-field theory. The field theoretical derivation consisted of decoupling the interaction in spin and charge channels and of considering spin and charge fluctuations around an **ordered** state. It led to equivalent results to self-consistent perturbation theory. As a mathematical convenience, we then expressed fluctuation corrections as an integral over particle-hole densities of states. The explicit evaluation of fluctuation corrections to the free energy for different phases that might form in the vicinity of a quantum critical point is performed in Chapter 3.

Chapter 3

Ginzburg-Landau Theory

We wish to determine the phase diagram of the near critical itinerant ferromagnet allowing for the generation of new phases near the quantum critical point. In order to obtain the phase diagram, we develop a Ginzburg-Landau expansion of the free energy in powers of the order parameters for the various types of phases that might form.

We briefly discuss the basic ideas behind the Ginzburg-Landau expansion. As we have seen in Chapter 2, the free energy is a functional of the mean-field dispersion. The order parameter enters the free energy through the mean-field dispersion. In the vicinity of a phase transition, the value of the order parameters is sufficiently small. We can therefore expand the free energy in powers of the order parameter, and truncate this expansion at a certain order. This will enable us to deduce the phase boundaries and the nature of the transitions between different phases.

It turns out that our task is simplified considerably by relationships between the expansion coefficients for the different types of order and those for the uniform ferromagnet. We evaluate the Ginzburg-landau coefficients of the uniform ferromagnet analytically. The fluctuation corrections to the Ginzburg-Landau coefficients provide a negative contribution and drive the quartic coefficient β negative.

Next, we allow for spatial modulations of the ferromagnetic order; in particular we consider a spiral modulation of the magnetization. We use the fact that the free energy can be expressed (to all orders) as a functional of the mean-field electron dispersion in the presence of the spiral order. Using the fact that the spiral wave vector $\mathbf{Q}$ enters the dispersion like an angle-dependent magnetization, we show how the coefficients of the expansion in Q are related (by angular averages of certain functions) to those of the uniform ferromagnet.

For other order parameters that cannot be introduced by a mean-field decoupling of the electron-electron interaction, we introduce a field conjugate to

the order parameter and construct an expansion of the generating function in terms of the conjugate field. We are able to relate the coefficients of the generating function to the Ginzburg-Landau coefficients of the uniform ferromagnet by performing some simple angular integrals. We use a Legendre transformation of the generating function to recover the Ginzburg-Landau expansion of the free energy. Quantum fluctuations generate an interaction in the new channel. We demonstrate this on the case of a d-wave spin nematic.

Finally, we allow for a more generic energy dispersion by considering small anisotropic deviations from the isotropic free-electron dispersion. We calculate the corrections to the coefficients of the Ginzburg-Landau expansion due to the anisotropic distortion. The coefficients of this expansion are proportional to parts of the Ginzburg-Landau coefficients of the uniform ferromagnet in the presence of an isotropic dispersion. The proportionality factors are determined by angular averages of functions that encode the specific form of the deviation from the isotropic free-electron dispersion.

3.1 Introduction

The Ginzburg-Landau expansion [1] relies on the fact that close to a second order phase transition, or a weakly first order transition, the value of an order parameter is small. Therefore, we can Taylor expand the free energy in powers of the order parameter and truncate this expansion at a certain order. The form of the expansion reflects the symmetry of the order parameter. For example, for a ferromagnet without an external magnetic field, where $M \to -M$ symmetry is present, the expansion should contain only even powers of M. We can write

$$\mathcal{F}(M) = \alpha M^2 + \beta M^4 + \gamma M^6 + ... \tag{3.1}$$

We analyse this expression for the free energy.

(i) A second order phase transition occurs when the minimum at $M = 0$ turns into a local maximum, and minima adjacent to $M = 0$ start developing (see Fig. 3.1 (a)). The necessary condition for this is that $\beta > 0$. The second order transition happens along the $\alpha = 0$ line.

(ii) Another possible scenario for the transition is the one where the magnetization discontinously jumps from $M = 0$ to a finite value M^* (see Fig. 3.1 (b)). This will happen when these two minima become degenerate, i.e when $\mathcal{F}(0) = \mathcal{F}(M^*)$. The necessary condition for the existence of a minimum at $M^* \neq 0$, is that $\beta < 0$ and $\alpha > 0$. The degeneracy condition that yields the transition line is $\beta^2 = 4\alpha\gamma$.

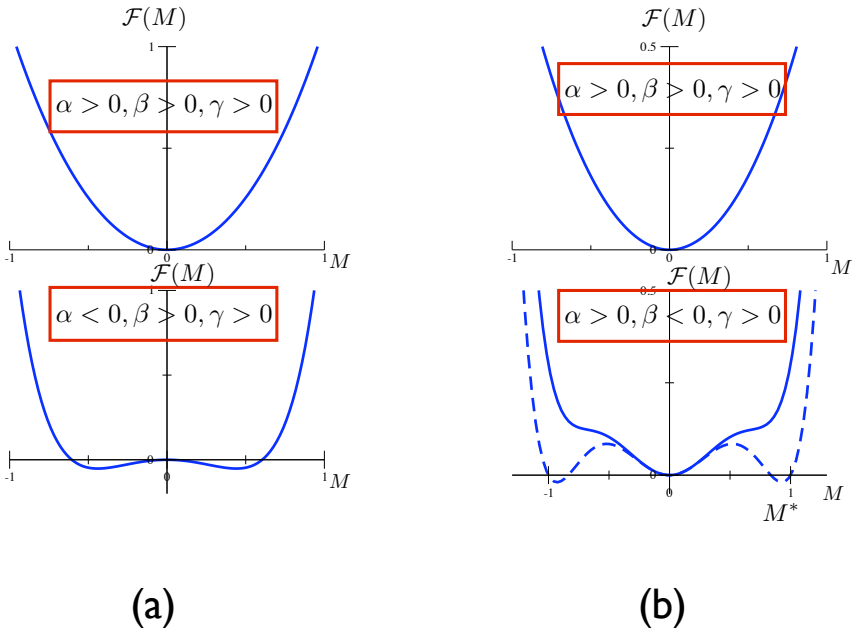

Figure 3.1: **Free energy profiles for first and second order phase transitions:** (a) In a second order transition, the magnetization rises continuously from zero – the minimum at $M = 0$ turns into a local maximum, and minima adjacent to $M = 0$ emerge. (b) In a first order transition, a secondary minimum develops at a non-zero value M^*. The transition takes place when $M = 0$ and M^* become degenerate.

3.2 Uniform Ferromagnet

The dispersion of the uniform ferromagnet is given by $\epsilon^\sigma(\mathbf{k}) = \frac{\mathbf{k}^2}{2} - \sigma g M$. We Taylor expand the free energy in powers of M, according to (3.1). The Ginzburg-Landau coefficients α, β, γ are functions of the interaction strength g and temperature T.

3.2.1 Mean-field Ginzburg-Landau coefficients

The mean-field energy was derived in Chapter 2, and is given by

$$\mathcal{F}_{MF}(M) = -\frac{1}{\beta}\sum_{\mathbf{k},\sigma} \ln\left(1 + e^{-\beta(\epsilon^\sigma_{\mathbf{k}} - \mu)}\right) + g\int \mathrm{d}^3\mathbf{r}\; M^2(\mathbf{r}), \tag{3.2}$$

The expansion of the mean-field free energy Eq. (3.2) in powers of M leads to the following coefficients:

$$\begin{aligned} \alpha_{MF} &= g + g^2 \sum_{\mathbf{k}} n^{(1)}(\epsilon_{\mathbf{k}}), \\ \beta_{MF} &= \frac{2}{4!} g^4 \sum_{\mathbf{k}} n^{(3)}(\epsilon_{\mathbf{k}}), \\ \gamma_{MF} &= \frac{2}{6!} g^6 \sum_{\mathbf{k}} n^{(5)}(\epsilon_{\mathbf{k}}), \end{aligned} \tag{3.3}$$

where $n^{(j)}(\epsilon) = \partial_\epsilon^j n(\epsilon)$ denotes the jth derivative of the Fermi function with respect to its energy argument.

3.2.2 Fluctuation contributions to the Ginzburg-Landau coefficients

We wish to evaluate the fluctuation corrections to the Ginzburg-Landau coefficients of the uniform ferromagnet

$$\alpha_{\text{fl}} = \frac{1}{2} \left. \frac{\partial^2 \mathcal{F}_{\text{fl}}}{\partial M^2} \right|_{M=0} \text{ and } \quad \beta_{\text{fl}} = \frac{1}{4!} \left. \frac{\partial^4 \mathcal{F}_{\text{fl}}}{\partial M^4} \right|_{M=0}. \tag{3.4}$$

This is achieved by rewriting the fluctuation corrections to the free energy in terms of modified particle-hole densities of states. The modified particle-hole densities of states can be calculated analytically, in the form of a Taylor series expansion in M. The sixth order coefficient γ will be evaluated in mean-field theory only.

In Chapter 2, it was shown that the fluctuation corrections to the free energy can be expressed in terms of integrals over the modified particle hole densities of states

$$\mathcal{F}_{\text{fl}} = 2g^2 \sum_{\sigma=\pm 1} \int_{\mathbf{q},\epsilon_1,\epsilon_2} \frac{\Delta\rho^\sigma(\mathbf{q},\epsilon_1)\rho^{-\sigma}(-\mathbf{q},\epsilon_2)}{\epsilon_1+\epsilon_2}, \tag{3.5}$$

where we have defined $\int_{\mathbf{q}} := \int \frac{\mathrm{d}^3\mathbf{q}}{(2\pi)^3}$ and $\int_\epsilon := \int_{-\infty}^{\infty} \mathrm{d}\epsilon$. The modified particle-hole densities of states as a function of momentum $\mathbf{q}$ and energy ϵ are given by

$$\begin{aligned} \rho^\sigma(q,\epsilon) &= \int_{\mathbf{k}} n(\epsilon^\sigma_{\mathbf{k}-\frac{\mathbf{q}}{2}}) \delta(\epsilon - \epsilon^\sigma_{\mathbf{k}+\frac{\mathbf{q}}{2}} + \epsilon^\sigma_{\mathbf{k}-\frac{\mathbf{q}}{2}}), \\ \Delta\rho^\sigma(q,\epsilon) &= \int_{\mathbf{k}} n(\epsilon^\sigma_{\mathbf{k}-\frac{\mathbf{q}}{2}}) n(\epsilon^\sigma_{\mathbf{k}+\frac{\mathbf{q}}{2}}) \delta(\epsilon - \epsilon^\sigma_{\mathbf{k}+\frac{\mathbf{q}}{2}} + \epsilon^\sigma_{\mathbf{k}-\frac{\mathbf{q}}{2}}), \end{aligned} \tag{3.6}$$

They relate to the particle-hole density of states through $\rho^{ph}_\sigma = \Delta\rho_\sigma - \rho_\sigma$. Note that the modified particle-hole densities of states represent a functional of the

mean-field dispersion. They are functions of the magnetization M, which enters through the dispersion $\epsilon^\sigma_{\mathbf{k}} = \epsilon_{\mathbf{k}} - \sigma g M$ of the uniform ferromagnet. We want to Taylor expand (3.5) with respect to M. In doing so we will require the derivatives of ρ^σ and $\Delta\rho^\sigma$ with respect to M. However, since in ρ^σ and $\Delta\rho^\sigma$ the dispersion only enters for either spin up or spin down (and not both) we can relate the derivatives with respect to M to derivatives with respect to the chemical potential μ,

$$\begin{aligned} \partial^i_M \Delta\rho^\sigma(q,\epsilon)\big|_{M=0} &= (\sigma g)^i \partial^i_\mu \Delta\rho^\sigma(q,\epsilon)\big|_{M=0} \\ &= (\sigma g)^i \partial^i_\mu \Delta\rho(q,\epsilon). \end{aligned} \tag{3.7}$$

The modified particle hole densities of states and their derivatives with respect to μ have been calculated analytically at finite temperature in Appendix 1. We define $J_{i,j}$ by

$$J_{i,j} = \int_{\mathbf{q},\epsilon_1,\epsilon_2} \frac{\partial^i_\mu \Delta\rho(q,\epsilon_1)\partial^j_\mu \rho(q,\epsilon_2)}{\epsilon_1+\epsilon_2}. \tag{3.8}$$

By Taylor expanding the fluctuation corrections to the free energy, we obtain the fluctuation contributions to the Ginzburg-Landau coefficients,

$$\begin{aligned} \alpha_{\text{fl}} &= 2g^4 \sum_{i=0}^{2} (-1)^i \begin{pmatrix} 2 \\ i \end{pmatrix} J_{i,2-i}, \\ \beta_{\text{fl}} &= \frac{g^6}{6} \sum_{i=0}^{4} (-1)^i \begin{pmatrix} 4 \\ i \end{pmatrix} J_{i,4-i}. \end{aligned} \tag{3.9}$$

Some of the integrals $J_{i,j}$ are difficult to evaluate numerically, since, at very low temperatures, higher derivatives of Fermi functions (which enter through the derivatives of modified particle-hole densities of states, see Appendix 1) are strongly peaked around the Fermi energy and rapidly change sign. The fluctuation contributions to the free energy at zero magnetization $\mathcal{F}^{(0)}_{\text{fl}} = \mathcal{F}_{\text{fl}}\big|_{M=0}$ are given by $\mathcal{F}^{(0)}_{\text{fl}} = 4g^2 J_{0,0}$. We evaluated the integral $J_{0,0}$ numerically for finite temperatures and analytically at $T = 0$. The analytical calculation at $T = 0$ correctly reproduces the result of Abrikosov and Khalatnikov [69].

3.2.2.1 Quadratic coefficient α_{fl}

First, we explicitly evaluate the quadratic coefficient α_{fl}. The coefficients $J_{1,1}$, $J_{2,0}$ and $J_{0,2}$ that appear in (3.9) have been evaluated numerically at finite temperatures, and analytically at $T = 0$. The explicit evaluation at zero temperature is outlined in Appendix 2. At zero temperature we obtain

$$\alpha_{\text{fl}} \simeq -\lambda(1 + 2\ln 2)g^4, \tag{3.10}$$

where $\lambda = \frac{16\sqrt{2}}{3(2\pi)^6}$. Numerical results for $\alpha_{\rm fl}$ correctly converge towards the analytically calculated $T = 0$ limit, which can be seen in the Fig. 3.2.

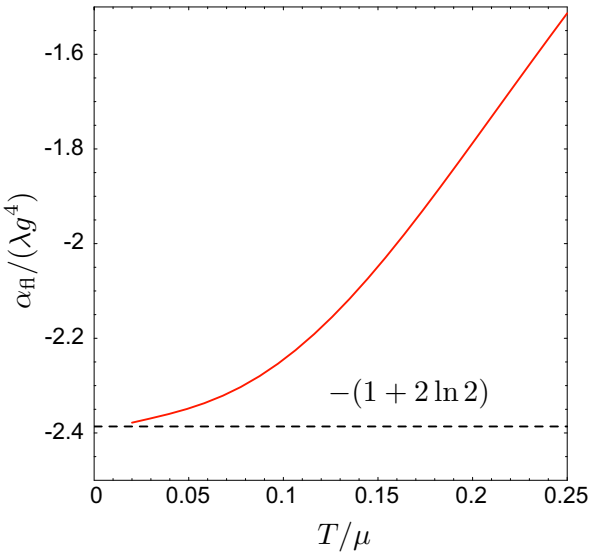

Figure 3.2: **Fluctuation contributions to α:** Comparison of numerics (solid line) with leading low-temperature analytical dependence (dashed line).

3.2.2.2 Quartic coefficient $\beta_{\rm fl}$

In order to evaluate $\beta_{\rm fl}$ we need to evaluate five terms in Eq. (3.9). As they contain higher order derivatives of Fermi functions (entering through the derivatives of the particle-hole densities of states) they are even more difficult to evaluate numerically, especially the terms $J_{0,4}$ and $J_{4,0}$. This is because higher derivatives of Fermi functions are strongly peaked around the Fermi energy at low temperatures, and they rapidly change sign. We collect some of the terms together by noting that

$$\partial_\mu^4 \mathcal{F}_{\rm fl}^{(0)} = 4g^2 \sum_{i=0}^{4} \begin{pmatrix} 4 \\ i \end{pmatrix} J_{i,4-i}, \tag{3.11}$$

to get

$$\beta_{\rm fl} = \frac{g^4}{4!}\partial_\mu^4 \mathcal{F}_{\rm fl}^{(0)} - \frac{4g^6}{3}(J_{1,3} + J_{3,1}). \tag{3.12}$$

In this way we avoid the explicit calculation of integrals $J_{0,4}$ and $J_{4,0}$, which contain third derivatives of Fermi functions. We can further simplify by noting that

$$\partial_\mu^2 J_{1,1} = J_{3,1} + 2J_{2,2} + J_{1,3}. \tag{3.13}$$

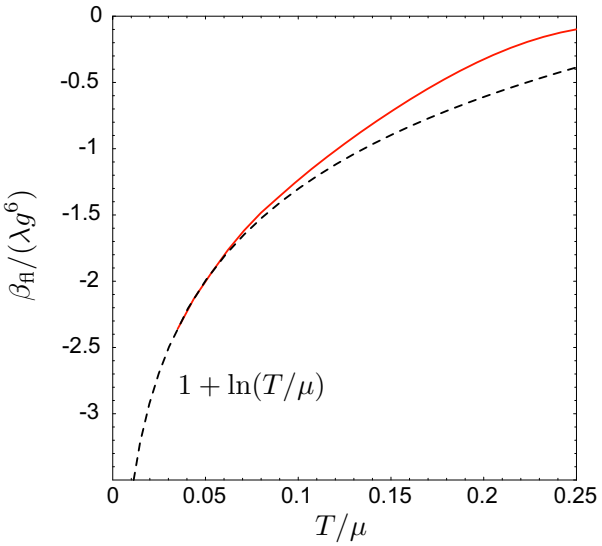

Figure 3.3: **Fluctuation contributions to β:** Comparison of numerics (solid line) with leading low-temperature analytical dependence (dashed line).

If we re-express $J_{3,1} + J_{1,3}$ in Eq. (3.12) using Eq. (3.13), we obtain

$$\beta_{\rm fl} = \frac{g^4}{4!}\partial_\mu^4 \mathcal{F}_{\rm fl}^{(0)} - \frac{4}{3}g^6 \partial_\mu^2 J_{1,1} + \frac{8}{3}g^6 J_{2,2}. \tag{3.14}$$

We have already calculated the functions $\mathcal{F}_{\rm fl}^{(0)}$ and $J_{1,1}$, when we evaluated $\alpha_{\rm fl}$. Both are smooth functions and the numerical evaluation of the derivatives with respect to μ is trivial. The leading temperature dependence of $\beta_{\rm fl}$ comes from the $J_{2,2}$ integral, which diverges as $T \to 0$ (see Appendix 2 for the analytical derivation of the leading temperature dependence of $J_{2,2}$). In this limit

$$\beta_{\rm fl} \simeq \lambda \left(1 + \ln \frac{T}{\mu}\right) g^6. \tag{3.15}$$

The $\ln(T/\mu)$ dependence of β is a remnant of the $M^4 \ln[M^2 + (T/\mu)^2]$ term in the free energy of Vojta *et al* [46] . It arises from particle-hole pairs with momenta $q \approx 2k_F$. The good agreement between our numerical and analytical results in the low-temperature regime is shown in Fig. 3.3.

3.3 Spiral

Next, we calculate the coefficients of the Ginzburg-Landau expansion allowing for a spatial modulation of the magnetic order. We restrict our consideration to a single planar spiral, with $\mathbf{Q} \parallel \hat{z}$ and the magnetization vector

$$\mathbf{M} = M(\cos(2\mathbf{Q}.\mathbf{r}), \sin(2\mathbf{Q}.\mathbf{r}), 0). \tag{3.16}$$

A general form for the Ginzburg-Landau expansion reads

$$\begin{aligned} \mathcal{F}[M,Q] &= \left(\alpha + \beta_1 Q^2 + \gamma_1 Q^4\right) M^2 \\ &\quad + \left(\beta + \gamma_2 Q^2\right) M^4 + \gamma M^6, \end{aligned} \tag{3.17}$$

We will exploit the fact that the free energy is a functional of the mean-field dispersion in the presence of the spiral magnetic order, in order to determine the Ginzburg-Landau coefficients.

3.3.1 Mean-field electron dispersion in the presence of spiral magnetic order

First, we determine the mean-field dispersion in the presence of spiral magnetic order. The mean-field decoupling in the magnetization channel leads to the following mean-field Hamiltonian

$$\mathcal{H}_{MF} = \int_{\mathbf{k}} \sum_{\nu} (\epsilon_k - \mu) c^{\dagger}_{\mathbf{k},\nu} c_{\mathbf{k},\nu} - g \sum_{\mathbf{r}} \sum_{\nu,\nu'} (\mathbf{M}(\mathbf{r}).\boldsymbol{\sigma}_{\nu,\nu'}) c^{\dagger}_{\mathbf{r},\nu} c_{\mathbf{r},\nu'}, \tag{3.18}$$

where $\mathbf{M}(\mathbf{r})$ is given by (3.16). We then perform a rotation to the spiral basis. In this local reference frame the magnetization is uniform and given by M. Fermionic operators transform as

$$\begin{pmatrix} c_{\mathbf{r},\uparrow} \\ c_{\mathbf{r},\downarrow} \end{pmatrix} \rightarrow e^{i\sigma_z \mathbf{Q}.\mathbf{r}} \begin{pmatrix} c_{\mathbf{r},\uparrow} \\ c_{\mathbf{r},\downarrow} \end{pmatrix}. \tag{3.19}$$

The mean-field Hamiltonian is given by

$$\mathcal{H} = \sum_{\mathbf{k}} \tilde{\psi}^{\dagger}_{\mathbf{k}} \begin{pmatrix} \epsilon_{\mathbf{k}+\mathbf{Q}} & gM \\ gM & \epsilon_{\mathbf{k}-\mathbf{Q}} \end{pmatrix} \tilde{\psi}_{\mathbf{k}} + gM^2, \tag{3.20}$$

where

$$\tilde{\psi}^{\dagger}_{\mathbf{k}} = \left(c^{\dagger}_{\mathbf{k}+\mathbf{Q},\uparrow},\, c^{\dagger}_{\mathbf{k}-\mathbf{Q},\downarrow}\right). \tag{3.21}$$

The dispersion can be obtained by diagonalizing the matrix in (3.20). We obtain

$$\epsilon^{\pm} = \frac{\epsilon_{\mathbf{k}-\mathbf{Q}} + \epsilon_{\mathbf{k}+\mathbf{Q}}}{2} - \sigma\sqrt{\left(\frac{\epsilon_{\mathbf{k}-\mathbf{Q}} - \epsilon_{\mathbf{k}+\mathbf{Q}}}{2}\right)^2 + (gM)^2}. \tag{3.22}$$

For the free-electron dispersion this reduces to

$$\epsilon^{\sigma}_{\mathbf{k}} = \frac{k^2}{2} - \sigma\sqrt{(\mathbf{k}\cdot\mathbf{Q})^2 + (gM)^2}. \tag{3.23}$$

We see that the wave vector Q enters the dispersion like an angle-dependent magnetization.

3.3.2 Mean-field Ginzburg-Landau coefficients

We will now make use of this mean-field electron dispersion in the presence of spiral in order to determine the Ginzburg-Landau expansion coefficients $\beta_1, \gamma_1, \gamma_2$. We begin by evaluating the mean-field contributions. We use two facts: (i) that the free energy is a functional of the mean-field dispersion, and (ii) that Q enters the dispersion like an angle-dependent magnetization.

A useful simplification at this stage is to rescale the spiral wave vector according to $Q \to \frac{k_F}{g}Q$, so that it has the same dimensions as M. In this way, β and β_1, and γ, γ_1 and γ_2 have the same dimensions. Let us first consider β_1. The mean-field contribution is given by

$$\beta_{1,MF} = 2\frac{2}{4!}g^4\int_{\mathbf{k}}\left(\frac{\mathbf{k}\cdot\mathbf{Q}}{k_F Q}\right)^2 n^{(3)}(\epsilon_k). \tag{3.24}$$

Since $T \ll \mu$, derivatives of Fermi functions are strongly peaked around the Fermi energy and we can set $|\mathbf{k}| = k_F$ in the scalar product which leads to a simple angular weight,

$$\frac{\mathbf{k}\cdot\mathbf{Q}}{k_F Q} \approx \cos\theta, \tag{3.25}$$

where θ is the angle between the vectors $\mathbf{k}$ and $\mathbf{Q}$. After carrying out the angular integral we obtain $\beta_{1,MF} \approx \frac{2}{3}\beta_{MF}$. Similarly, we obtain the proportionalities $\gamma_{1,MF} \approx \frac{3}{5}\gamma_{MF}$ and $\gamma_{2,MF} \approx \gamma_{MF}$.

3.3.3 Fluctuation contributions to the Ginzburg-Landau coefficients

Now, we proceed to analyze the fluctuation corrections to the expansion coefficients in Eq. (3.17). As in the evaluation of the mean-field coefficients, it turns

out that the fluctuation contributions to the expansion coefficients in Q are related to those of the uniform ferromagnet by angular factors. The angular factors are identical to those found in the mean-field case.

The fluctuation corrections to the free energy are given by an integral over momenta $\mathbf{k}_1, \ldots, \mathbf{k}_4$ of a kernel that depends explicitly on each of the momenta through the mean-field dispersion (3.23). The fluctuation contributions to the Ginzburg-Landau coefficients are obtained by differentiating Eq. (2.14) with respect to M and Q. First we differentiate the kernel with respect to the dispersion – this places derivatives on Fermi functions, and then the dispersion with respect to M and Q – the differentiation with respect to Q brings down angular factors. For example, the fluctuation contribution to the M^2Q^2 coefficient is given by

$$\beta_{1,\mathrm{fl}} = \left.\frac{\partial^2 \mathcal{F}_{\mathrm{fl}}}{\partial M^2 \partial Q^2}\right|_{Q=0,M=0}. \tag{3.26}$$

We use two important facts in order to calculate this: (i) that the free energy is a functional of the dispersion and (ii) that the spiral wave vector enters the mean-field dispersion Eq. (3.23) like an angle dependent magnetization.

The dispersion enters for each of the momenta $\mathbf{k}_i$, where $i = 1, ...4$, in the momentum sum in Eq. (2.14). Differentiating with respect to Q^2, therefore, will bring down factors of $(\mathbf{k}_i \cdot \mathbf{Q}/(k_F Q))^2$, each of which will contribute with an angular factor as in the mean-field case. This leads to the proportionality $\beta_{1,\mathrm{fl}} \approx \frac{2}{3}\beta_{\mathrm{fl}}$. Combining this with the identical result for the mean-field contribution we obtain $\beta_1 \approx \frac{2}{3}\beta$. When the proportionality between all of the coefficients is taken into account [1] the free energy (3.17) becomes

$$\begin{aligned} \mathcal{F}[M,Q] &= \left(\alpha + \frac{2}{3}\beta Q^2 + \frac{3}{5}\gamma Q^4\right) M^2 \\ &\quad + (\beta + \gamma Q^2) M^4 + \gamma M^6. \end{aligned} \tag{3.27}$$

3.4 d-wave Spin Nematic

3.4.1 In search of new phases of matter: electron nematic states

Nematic phases – phases that break the full rotational symmetry, but preserve the translational symmetry – are known to occur in the context of liquid crystals [71].

[1] If we were to calculate the fluctuation corrections to the Q^4M^2 coefficient (but we will not as it is sixth order term), to leading order, this coefficient would be equal to $\frac{3}{5}\gamma_{fl}$. This is because the dominant contribution would arise from all $\{\mathbf{k}_i\}$ in the kernel of (2.14) parallel to each other.

Liquid crystals are made up of elongated molecules known as directors. These molecules are positioned randomly in space, preserving translational invariance, but they have a preferred direction, breaking the rotational symmetry.

In condensed matter physics, one is always searching for new, exotic phases of matter and trying to create them in a lab. A very interesting question that arises is: Can similar phases, that break the rotational symmetry, but not the translational one, be realized in electronic systems? This question has generated a great deal of theoretical and experimental interest [72; 73; 74; 75; 76; 77; 78; 79; 80; 81; 82; 83]. Signatures of the electron nematic phases have recently been observed in $2d$ electron gases in magnetic fields [74] and in the vicinity of striped phases of cuprates and pnictides [84]. They show anisotropies in transport measurements, can be detected in STM measurements, and trigger of simultaneous structural transitions and orbital ordering in pnictides [83].

The nematic instability can occur in a) the charge (symmetric) channel or b) the spin channel. In what follows, we will concentrate on the case b) – spin-nematic states. These states break rotational symmetry in momentum space and in spin space. Fermi surfaces of these states display spin antisymmetric Pomeranchuk instabilities, which can be characterized by the angular dependence l. Fermi surfaces of spin-up and spin-down electrons are rotated from each-other by π/l, for example see sketch of the $l = 2$ (d-wave) spin-nematic Fermi surface distortion in Fig (2.4). The spin nematics with even l break the time reversal symmetry. These states would also show anisotropies in transport measurements, and hence could potentially be of some relevance to $Sr_3Ru_2O_7$. The theoretical models that these states arise from include non-analytic extensions of Hertz-Millis theory [50; 85] and α-phases [81]. We aim to investigate if such a spin-nematic state can be stabilized in the vicinity of an itinerant ferromagnetic quantum critical point. In what follows, we will develop the Ginzburg-Landau expansion of the spin nematic.

Ginzburg-Landau expansion of spin nematic – a simple recipe. Phases with order parameters that cannot be introduced by a Hubbard-Stratonovich, mean-field decoupling of the point Hubbard interaction, are slightly more difficult to analyze. Examples include p-wave superconductors and spin-nematic phases. To circumvent this problem, we begin by introducing a field h_N conjugate to the order parameter N. We calculate the generating function $\varphi[h_N]$ following the procedure outlined for the uniform ferromagnet in Section 2.2.2. The free energy $\mathcal{F}[N]$ is then obtained by a Legendre transform of the generating function.

To be more specific, we introduce a d-wave spin-nematic [72; 79] order pa-

rameter

$$\begin{aligned} N &= \sum_{\mathbf{k},\sigma} \sigma d_{\mathbf{k}} n_{\mathbf{k},\sigma}, \\ d_{\mathbf{k}} &= \frac{1}{k_F^2}(k_x^2 - k_y^2) \approx \sin^2(\theta)\cos(2\phi), \end{aligned} \tag{3.28}$$

where $d_{\mathbf{k}}$ is the d-wave distortion. The spin-nematic order parameter looks like a magnetization weighted by an angular factor. It corresponds to Fermi-surface distortions which have opposite signs for spin-up and spin-down electrons. The net magnetization however, vanishes since the volumes of the distorted spin-up and spin-down Fermi surfaces are the same (see Fig. 2.4(c)). As we will see later, it is straightforward to generalize our final results to spin-nematic states with different symmetries.

3.4.2 Generating function

The concept of conjugate variables is familiar in physics. Some of examples include the magnetization M and magnetic field h, chemical potential μ and number density n or generalized coordinates and momenta in Hamiltonian dynamics.

The generating function for the spin nematic order is obtained by introducing a fictitious field h_N conjugate to the spin nematic order parameter, N. This is achieved by adding a term

$$\mathcal{H}_{h_N} = \sum_{\mathbf{k},\sigma} h_N \sigma d_{\mathbf{k}} \hat{n}_{\mathbf{k},\sigma} \tag{3.29}$$

to the Hamiltonian, Eq.(2.3). The electron dispersion in the presence of the conjugate field is modified to

$$\epsilon_{\mathbf{k}}^{\sigma} = \epsilon_{\mathbf{k}} - \sigma h_N \sin^2(\theta)\cos(2\phi). \tag{3.30}$$

The partition function in the presence of the field h_N is evaluated in precisely the manner outlined in Sec. 2.2.2 for the uniform ferromagnet. The logarithm of this partition function is the generating function $\varphi[h_N]$. Explicitly, using self-consistent second-order perturbation theory, the generating function is given by

$$\varphi[h_N] = -\frac{1}{\beta}\sum_{\mathbf{k},\sigma} \ln\left(1 + e^{-\beta(\epsilon_{\mathbf{k}}^{\sigma} - \mu)}\right) + 2g^2 {\sum_{\mathbf{k}_1 \ldots \mathbf{k}_4}}' \frac{n_{\mathbf{k}_1}^{+} n_{\mathbf{k}_2}^{-} (n_{\mathbf{k}_3}^{+} + n_{\mathbf{k}_4}^{-})}{\epsilon_{\mathbf{k}_1}^{+} + \epsilon_{\mathbf{k}_2}^{-} - \epsilon_{\mathbf{k}_3}^{+} - \epsilon_{\mathbf{k}_4}^{-}}, \tag{3.31}$$

as a functional of the dispersion, Eq. (3.30).

Expanding the generating function $\varphi[h_N]$, Eq. (3.31), in powers of h_N we obtain

$$\varphi[h_N] = \alpha^\varphi h_N^2 + \beta^\varphi h_N^4 + \gamma^\varphi h_N^6, \tag{3.32}$$

where the superscript φ is used to distinguish coefficients of the generating function from those of the Ginzburg-Landau expansion. Here and in the following h_N is rescaled by g. The coefficients of this expansion may be related by angular averages to those of the Ginzburg-Landau expansion for the uniform ferromagnet. Note that in comparing the expansion of $\varphi[h_N]$ with the expansion of the free energy for the ferromagnet, there is no term directly related to gM^2, since the Hubbard point interaction is local in position space and therefore has no weight in the spin-nematic channel.

3.4.2.1 Mean-field coefficients of the generating function

The mean-field coefficients of the generating function are given by

$$\begin{aligned}
\alpha_{MF}^\varphi &= g^2 \langle d_{\mathbf{k}}^2 \rangle \sum_{\mathbf{k}} n^{(1)}(\epsilon_{\mathbf{k}}) = \langle d_{\mathbf{k}}^2 \rangle (\alpha_{MF} - g) \\
\beta_{MF}^\varphi &= \frac{2}{4!} g^4 \langle d_{\mathbf{k}}^4 \rangle \sum_{\mathbf{k}} n^{(3)}(\epsilon_{\mathbf{k}}) = \langle d_{\mathbf{k}}^4 \rangle \beta_{MF} \\
\gamma_{MF}^\varphi &= \frac{2}{6!} g^6 \langle d_{\mathbf{k}}^6 \rangle \sum_{\mathbf{k}} n^{(5)}(\epsilon_{\mathbf{k}}) = \langle d_{\mathbf{k}}^6 \rangle \gamma,
\end{aligned} \tag{3.33}$$

where $\langle \ldots \rangle = \frac{1}{4\pi} \int_0^\pi \mathrm{d}\theta \sin\theta \int_0^{2\pi} \mathrm{d}\phi \ldots$ denotes the angular average. Note that the term linear in g in the quadratic mean-field coefficient is absent. The coefficients are proportional to the corresponding Ginzburg-Landau coefficients of the uniform ferromagnet; the constants of proportionality are angular averages of powers of the nematic distortion. The resulting integrals are easy to calculate, yielding $\langle d_{\mathbf{k}}^2 \rangle = \frac{4}{15}$, $\langle d_{\mathbf{k}}^4 \rangle = \frac{16}{105}$, and $\langle d_{\mathbf{k}}^6 \rangle = \frac{320}{3003}$.

3.4.2.2 Fluctuation contributions to the coefficients

As we found in the case of the spiral, the fluctuation corrections to the coefficients in the spin-nematic expansion are related to those of the uniform ferromagnet by the same angular averages as the mean-field coefficients. For example, let us consider the fluctuation contribution to the h_N^4 coefficient. We first differentiate the kernel in Eq. (3.31) with respect to the dispersion, and then the dispersion with respect to h_N. This brings down terms like $\langle d_{\mathbf{k}_1} d_{\mathbf{k}_2} d_{\mathbf{k}_3} d_{\mathbf{k}_4} \rangle$, where $|\mathbf{k}_i| \approx k_F$ since derivatives of Fermi functions are peaked around the Fermi energy. Angular averages of this type are potentially more complicated as the directions of different $\mathbf{k}$'s are not independent. However, the fact that the dominant contribution comes

from the particle-hole pairs with momenta $|\mathbf{k}_1 - \mathbf{k}_3| = |\mathbf{k}_2 - \mathbf{k}_4| \approx 2k_F$ leads to a tremendous simplification. Within this approximation, $\mathbf{k}_1, \mathbf{k}_2, \mathbf{k}_3$ and $\mathbf{k}_4$ are either parallel or antiparallel to one another, rendering $\langle d_{\mathbf{k}_1} d_{\mathbf{k}_2} d_{\mathbf{k}_3} d_{\mathbf{k}_4} \rangle \approx \langle d_{\mathbf{k}}^4 \rangle$. Similar arguments hold for other types of terms that appear in the expansion. Thus, to leading order, the same proportionality holds as for the mean-field coefficients and consequently, the generating function is given by

$$\begin{aligned} \varphi[h_N] &= \langle d_{\mathbf{k}}^2 \rangle (\alpha - g) h_N^2 + \langle d_{\mathbf{k}}^4 \rangle \beta h_N^4 \\ &\quad + \langle d_{\mathbf{k}}^6 \rangle \gamma h_N^6. \end{aligned} \tag{3.34}$$

3.4.3 Ginzburg-Landau expansion of the d-wave spin nematic

In order to obtain the Ginzburg-Landau expansion of the free energy $\mathcal{F}[N]$ of the d-wave spin nematic, we perform the Legendre transform of the generating function,

$$\begin{aligned} \mathcal{F}[N] &= \varphi[h_N[N]] + h_N N \\ \frac{\partial \varphi}{\partial h_N} &= -N. \end{aligned} \tag{3.35}$$

Carrying out this transformation to leading order, we obtain the free-energy expansion in powers of the nematic order parameter N,

$$\mathcal{F}[N] = -\langle d_{\mathbf{k}}^2 \rangle (\alpha - g) N^2 + \langle d_{\mathbf{k}}^4 \rangle \beta N^4 + \langle d_{\mathbf{k}}^6 \rangle \gamma N^6. \tag{3.36}$$

Since $\beta \sim \ln T$, the $\sim \ln T N^4$ term is a remnant of the non-analytic dependence $\mathcal{F}(N) \sim N^4 \ln (N^2 + T^2)$ of Ref. [85]. Note that the derivation of the free-energy functional for the spin nematic is general and not constrained to a particular symmetry of the distortion. To obtain the free energy of a p-wave spin nematic,[50; 81; 86] we simply replace the d-wave distortion $d_{\mathbf{k}}$ by the p-wave angular weight $p_{\mathbf{k}} \approx \cos\theta$. This leads to slightly different angular averages, $\langle p_{\mathbf{k}}^2 \rangle = \frac{1}{3}$, $\langle p_{\mathbf{k}}^4 \rangle = \frac{1}{5}$, and $\langle p_{\mathbf{k}}^6 \rangle = \frac{1}{7}$ and hence to slightly different coefficients in the Ginzburg-Landau expansion.

3.5 Deviations from the Isotropic Free-Electron Dispersion

Our approach also enables us to analyze the modifications to the phase diagram in the presence of a dispersion that deviates slightly from the free-electron dispersion

$$\epsilon_{\mathbf{k}} = \frac{k^2}{2} + \delta\epsilon_{\mathbf{k}}. \tag{3.37}$$

This will enable us to produce a more realistic phase diagram.

3.5.1 Free energy of the uniform ferromagnet

In order to obtain the Ginzburg-Landau expansion of the uniform ferromagnet in the presence of a small anisotropy $\delta\epsilon_{\mathbf{k}}$ in the dispersion (3.37), we first differentiate the free energy with respect to the full dispersion $\epsilon^{\sigma}_{\mathbf{k}} = \epsilon_{\mathbf{k}} + \delta\epsilon_{\mathbf{k}} - \sigma g M$. Then we differentiate the dispersion $\epsilon^{\sigma}_{\mathbf{k}}$ with respect to the magnetization M. Finally we expand the resulting Ginzburg-Landau coefficients in powers of $\delta\epsilon_{\mathbf{k}}$. The additional contribution to the free energy (3.1), arising from small $\delta\epsilon_{\mathbf{k}}$ terms is given by

$$\delta\mathcal{F}[M] = \left(6\beta_{MF} + \frac{g^2}{2}\frac{\partial^2\alpha_{\text{fl}}}{\partial^2\mu^2}\right)\frac{\langle\delta\epsilon^2_{\mathbf{k}}\rangle}{g^2}M^2 + 15\gamma\frac{\langle\delta\epsilon^2_{\mathbf{k}}\rangle}{g^2}M^4 \tag{3.38}$$

The presence of an anisotropy in the dispersion introduces mixing between the coefficients – for example the M^2 coefficient contains parts of both α and β.

3.5.2 Spiral free energy

In the presence of anisotropic dispersion (3.37), the mean-field dispersion in the presence of a spiral order, Eq. (3.22), is given by

$$\epsilon^{\sigma}_{\mathbf{k}} \approx \frac{k^2}{2} + \delta\epsilon_{\mathbf{k}} - \sigma\sqrt{\left[\mathbf{Q}\cdot(\mathbf{k}+\nabla\delta\epsilon_{\mathbf{k}})\right]^2 + (gM)^2}. \tag{3.39}$$

In order to calculate the corrections to the Ginzburg-Landau coefficients (3.27), we first differentiate the free energy with respect to the dispersion $\epsilon^{\sigma}_{\mathbf{k}}$ and then the dispersion (3.39) with respect to M and Q. Finally, we expand the resulting Ginzburg-Landau coefficients in powers of $\delta\epsilon_{\mathbf{k}}$, assumed small. The free energy is now given by the sum of $\mathcal{F}_{M,Q}$ (3.27) and the additional contribution

$$\begin{aligned}\delta\mathcal{F}[M,\mathbf{Q}] &= \left(6\beta_{MF} + \frac{g^2}{2}\frac{\partial^2\alpha_{\text{fl}}}{\partial^2\mu^2}\right)\frac{\langle\delta\epsilon^2_{\mathbf{k}}\rangle}{g^2}M^2 \\ &+ 15\gamma\frac{\langle\delta\epsilon^2_{\mathbf{k}}\rangle}{g^2}M^4 + 30\gamma\frac{\langle(\frac{\mathbf{k}\cdot\mathbf{Q}}{k_F})^2\delta\epsilon^2_{\mathbf{k}}\rangle}{g^2}M^2 \\ &+ 2\beta_{MF}\Big\langle\left(\frac{\mathbf{Q}\cdot\nabla\delta\epsilon_{\mathbf{k}}}{k_F}\right)^2\Big\rangle M^2,\end{aligned} \tag{3.40}$$

where $\langle ...\rangle$ denotes an angular average and we have assumed that the deviation $\delta\epsilon_{\mathbf{k}}$ is such that the odd-power angular averages give zero. Mixing between coefficients

at different total order in M and Q now occurs, since the angular distortion enters in both spin-symmetric and spin-antisymmetric ways. For example the M^2Q^2 coefficient is no longer proportional to the M^4 coefficient.

3.5.3 d-wave spin-nematic free energy

Following the same steps, we obtain the additional contribution to the free energy $\mathcal{F}[N]$, Eq. (3.36), of the spin-nematic state

$$\begin{aligned}\delta\mathcal{F}[N] = &- \left(6\beta_{\mathrm{MF}} + \frac{g^2}{2}\frac{\partial^2\alpha_{\mathrm{fl}}}{\partial^2\mu^2}\right)\frac{\langle\delta\epsilon_{\mathbf{k}}^2 d_{\mathbf{k}}^2\rangle}{g^2}N^2 \\ &+ 15\gamma\frac{\langle\delta\epsilon_{\mathbf{k}}^2 d_{\mathbf{k}}^4\rangle}{g^2}N^4. \end{aligned} \tag{3.41}$$

In summary, in this chapter we have developed the Ginzburg-Landau expansion of the various phases that might form in the vicinity of an itinerant ferromagnetic quantum critical point: a uniform ferromagnet, spiral and spin nematic. This will enable us to construct the phase diagram in the next chapter.

To construct the expansion of the free energy, we used the fact that the free energy is a functional of the dispersion, and that the order parameter enters through the dispersion. We evaluated the Ginzburg-Landau coefficients of the uniform ferromagnet analytically at low temperatures, as well as numerically at a finite temperature. First, we evaluated the mean-field contributions to the Ginzburg-Landau coefficients. The fluctuation corrections to the coefficients provide negative contribution (as expected in the quantum order-by-disorder approach). Moreover, fluctuations *drive* the quartic coefficient β negative.

When evaluating the spiral Ginzburg-Landau coefficients, we used the fact that the wave vector Q enters the dispersion like an angle-dependent magnetization. We showed that the expansion coefficients of the spiral are related to those of the uniform ferromagnet by averages of certain angular functions.

In order to develop the Ginzburg-Landau expansion of the phases for which a mean-field Hubbard-Stratonovich decoupling in terms of order parameter cannot be performed, we introduced a field conjugate to the order parameter. We then expanded the generating function in powers of the conjugate field. For the case of d-wave spin nematic, coefficients of the generating function were found to be proportional to the Ginzburg-Landau coefficients of the uniform ferromagnet. The free energy of spin nematic was then recovered by a Legendre transform of the generating function.

We further considered the modifications to the Ginzburg-Landau coefficients of the uniform ferromagnet, spiral and spin nematic in the presence of a small anisotropy added to the isotropic free-electron dispersion. The Ginzburg-Landau

coefficients in the presence of the anisotropic dispersion are proportional to certain combinations of the Ginzburg-Landau coefficients of the uniform ferromagnet without the anisotropy. Mixing between coefficients of different total orders in M and Q now occurs – for example the M^2Q^2 coefficient is no longer proportional to the M^4 coefficient. In the next chapter, we will investigate the consequences of this on the phase diagram.

Chapter 4

Phase Diagram of the Itinerant Ferromagnet

In Chapter 1, we briefly discussed mean-field theory of the Stoner model. Mean-field theory predicts a paramagnet and a uniform ferromagnet, separated by a line of second order phase transitions. On the contrary, there are numerous experimental examples where i) the paramagnet-to-ferromagnet transition turns first order below a certain temperature and where ii) new phases emerge, such as superconductivity or anomalous anisotropic phases. This was discussed in Section 1.4.1. Obviously, the mean-field theory does not capture these findings. We are forced to go beyond and include the effect of quantum fluctuations. We do so by using the quantum order-by-disorder approach, developed in Chapter 2. The questions that we aim to address are: Can quantum fluctuations modify the nature of the paramagnet-to-ferromagnet transition? Can they stabilize new phases? And finally, what does the reconstructed phase diagram in the vicinity of an itinerant ferromagnetic quantum critical point look like (including quantum fluctuations)?

The Ginzburg-Landau theory of the uniform ferromagnet, spiral and spin nematic, including the effect of quantum fluctuations, was developed in Chapter 3. First we considered an isotropic free electron dispersion, and then re-derived the Ginzburg-Landau coefficients for the case of a small anisotropic correction to the isotropic free electron dispersion. In this Chapter, we will use the Ginzburg-Landau expansion to construct the phase diagram. A simple recipe follows three steps:

- We minimize the free energies with respect to the order parameter(s).
- We compare the free energies of different phases.
- The phase with the lowest free energy wins.

We first calculate the phase diagram for the isotropic free-electron dispersion. We begin our analysis by investigating the modifications to the phase boundaries between the uniform ferromagnet and paramagnet, due to the effect of quantum fluctuations. We show that i) ferromagnetism is favoured for lower values of the interaction strength than in the mean-field theory and ii) that the paramagnet-to-ferromagnet transition turns first order below a tri-critical point. Quantum fluctuations can be thought of as virtual excitations of pairs of particle-hole pairs, of opposite spin and equal and opposite momenta. There are more low-energy fluctuations associated with the ferromagnetic phase than with the paramagnetic phase, and they further lower the free energy of the ferromagnetic phase. This results in ferromagnetism being favoured for lower interaction strength g. Further, quantum fluctuations change the nature of the paramagnet-to-ferromagnet transition and drive it first order as they become strong enough at low temperatures. This occurs due to the low-energy particle-hole pairs with momentum $2k_F$, which give the dominant contribution to the free energy. Mathematically, quantum fluctuations drive the quartic coefficient β negative at low temperatures, which is a necessary condition for a first order transition.

Not only do fluctuations change the nature of the transition, but they can have even more drastic effects and stabilize new phases, not present in the mean-field phase diagram. First, we consider the possibility that quantum fluctuations stabilize an inhomogeneous ferromagnetic state. We show that the formation of a single spiral state pre-empts the first order paramagnet-to-uniform ferromagnet transition. In this region of the phase diagram, the spiral Fermi-surface distortion enhances quantum fluctuations even more than the ferromagnetic one. Mathematically, we have shown that the M^2Q^2 coefficient of the Ginzburg-Landau expansion is proportional to the M^4 coefficient β. For $\beta < 0$ (below the tri-critical point) it becomes favourable to form a state with non-zero Q, as this lowers the free energy. Motivated by the fact that the d-wave spin-nematic state produces a very similar Fermi surface distortion to that of a spiral, we begin our search for the spin nematic – a state characterized by antisymmetric deformations of the Fermi surfaces of spin-up/down electrons, that carries no net magnetization. We predict a thin region of d-wave spin-nematic forming at very low temperatures. Here, spin and charge fluctuations mediate the coupling in the spin-nematic channel.

It is well-known that the choice of a dispersion can have profound effects upon a phase diagram. We thus consider a more realistic, weakly anisotropic dispersion, which slightly deviates from the previously considered isotropic free-electron dispersion. There are two main modifications to the phase diagram in the presence of such a dispersion. First, we find that the onset of the spiral is no longer coincident with the putative tri-critical point of the uniform ferromagnet. Secondly, the regions of the phase diagram occupied by the spiral and spin nematic

enlarge at the expense of the uniform ferromagnet.

4.1 Isotropic Free-Electron Dispersion

4.1.1 Uniform ferromagnet

Before investigating how fluctuations may favour the formation of new phases, we first investigate their effect on the uniform ferromagnet.

In Chapter 1 we calculated the mean-field phase diagram of the Stoner model. The mean-field theory predicts a second order phase transition from a paramagnet into a ferromagnet, since the quartic coefficient is positive, $\beta_{MF} > 0$. The transition happens when the quadratic coefficient, α_{MF}, changes sign. Our aim is to include quantum fluctuations and see if they can modify the nature of the transition.

4.1.1.1 Line of second order transitions

We have seen that quantum fluctuations provide a negative contribution to the Ginzburg-Landau coefficients. Ferromagnetism is thus favored for lower values of the interaction strength, g, than in the mean-field theory. This becomes evident if we consider the line of second order transitions, $\alpha = 0$. A simple physical picture of why this happens can be developed. When the system is magnetized, the spin-up and spin-down Fermi surfaces are split and have different volumes. This Fermi surface distortion increases the phase space available for low-energy particle-hole pairs to form, and these quantum fluctuations further lower the free energy of the ferromagnetic phase. Thus, a lower interaction strength g is needed to magnetize the system.

4.1.1.2 Line of first order transitions

In the presence of fluctuations, the quartic coefficient, β, *inevitably* becomes negative for low enough temperatures due to the $\sim \ln(T/\mu)$ divergence. For $\beta < 0$, fluctuations become strong enough to drive the paramagnet-to-ferromagnet transition first order. The line of first order transitions is given by $\beta^2 = 4\alpha\gamma$ (the condition for degeneracy of the minima of the Ginzburg-Landau function). The location of the tricritical point, at the intercept of the first-order and second-order lines, is found to be $T^* = 0.24\mu$, which is in good agreement with previous numerical calculations [66] .

The occurrence of the first order transition in the presence of quantum fluctuations is in the spirit of the Coleman-Weinberg mechanism. At low temperature the free energy adopts the form $\mathcal{F} \sim M^4 \ln(M^2 + T^2)$, which reduces to the

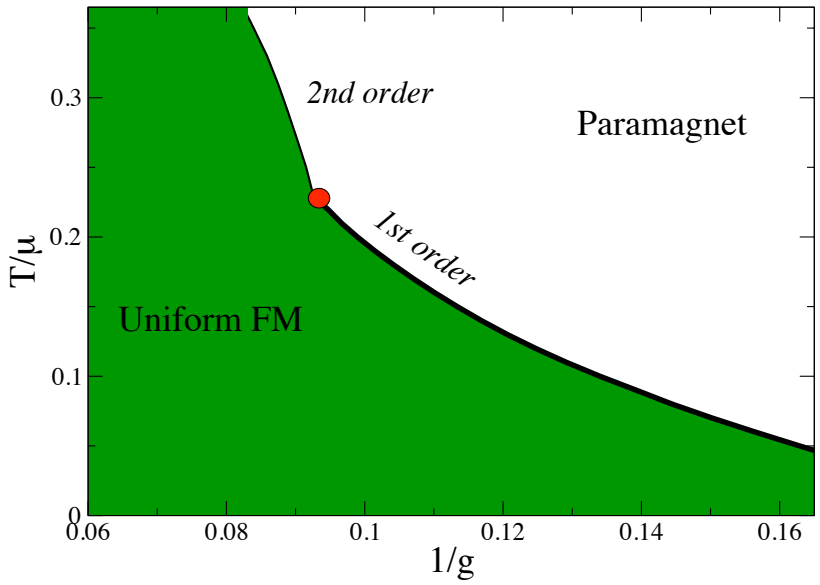

Figure 4.1: **Phase diagram of the uniform ferromagnet, including quantum fluctuations:** Below the tricritical point (shown as circle), quantum fluctuations drive the transition first order.

Coleman-Weinberg potential at $T = 0$. As previously shown, this form of the free energy leads to a first order transition. Finite temperature, T, cuts off the divergence of the M^4 coefficient and renders the Ginzburg-Landau expansion in powers of M meaningful. This is another example of fluctuation-driven first order transition [87; 88]. First order transitions have been observed in many experiments [15; 16; 89; 90; 91].

4.1.2 Fluctuation-driven spiral phase

From the expression for the spiral free energy Eq. (3.17) we see that the Q^2M^2 term favors non-zero Q for $\beta_1 < 0$. The particular relationship between coefficients that is found in the free-electron case implies that this occurs when $\beta < 0$, *i.e.* the spiral first forms at the tricritical point where the transition into a uniform magnet would have become first order. The phase diagram showing the instability towards the formation of a magnetic spiral is shown in Fig. 4.2. We now derive it from the Ginzburg-Landau functional.

Minimizing the free energy Eq. (3.27) with respect to Q, we obtain the optimal wave vector

$$\bar{Q}^2 = -\frac{5}{6\gamma}\left(\frac{2}{3}\beta + M^2\gamma\right). \tag{4.1}$$

After substituting this value of Q back in (3.27), we obtain the free energy at the optimal wavevector as a function of M,

$$\begin{aligned} \mathcal{F}_{\bar{Q}}[M] &= \alpha_{\bar{Q}} M^2 + \beta_{\bar{Q}} M^4 + \gamma_{\bar{Q}} M^6, \\ \alpha_{\bar{Q}} &= \left(\alpha - \frac{5}{27}\frac{\beta^2}{\gamma}\right), \\ \beta_{\bar{Q}} &= \frac{4}{9}\beta, \\ \gamma_{\bar{Q}} &= \frac{7}{12}\gamma. \end{aligned} \tag{4.2}$$

4.1.2.1 Spiral-to-paramagnet transition

In principle, there are two ways in which the system can make a transition from a paramagnet into a spiral state:

i. *A second order transition in* M, along which $M = 0$. This line is given by $\alpha_{\bar{Q}} = 0$, and the necessary condition for its existence is that $\beta_{\bar{Q}} > 0$.

ii. *A first order transition in* M, along which M changes discontinuously from zero to a finite value. This transition happens along the line $\beta_{\bar{Q}}^2 = 4\alpha_{\bar{Q}}\gamma_{\bar{Q}}$, as long as $\beta_{\bar{Q}} < 0$ and $\alpha_{\bar{Q}} > 0$.

Since we have already established that we can have a spiral state only for $\beta_1 < 0$ and hence $\beta, \beta_{\bar{Q}} < 0$ (following from the proportionalities of coefficients), we rule out the first possibility and conclude that the transition from the paramagnet into the spiral ferromagnet must be first order in M (and also first order in Q, according to Eq. (4.1)). Substituting $\alpha_{\bar{Q}}$, $\beta_{\bar{Q}}$ and $\gamma_{\bar{Q}}$ from Eq. (4.2), the equation for this line becomes $\alpha\gamma = \frac{17}{63}\beta^2$. This transition pre-empts the transition from the paramagnet into the uniform ferromagnetic state [see Fig. 4.2].

Usually, it is either nesting or a spin-orbit coupling that leads to a helical modulation of the ferromagnetic order. Here the spiral state is stabilized entirely by quantum fluctuations through the quantum order-by-disorder mechanism. The spiral state is not energetically favoured in the mean-field theory. However, there are more low-energy particle-hole pairs associated with the spiral Fermi-surface distortion than with the ferromagnetic one. This lowers the spiral free energy and stabilizes the spiral state. The phase boundary between the spiral and the uniform ferromagnet is determined by a subtle balance of the mean-field terms and quantum fluctuations. We expect the spiral phase to be stabilized inside the region where the free energy of the uniform ferromagnet is close to that of the paramagnetic state; certainly not deep in the ferromagnetic phase where the mean-field drive of the uniform ferromagnet is big. Further, low temperatures are

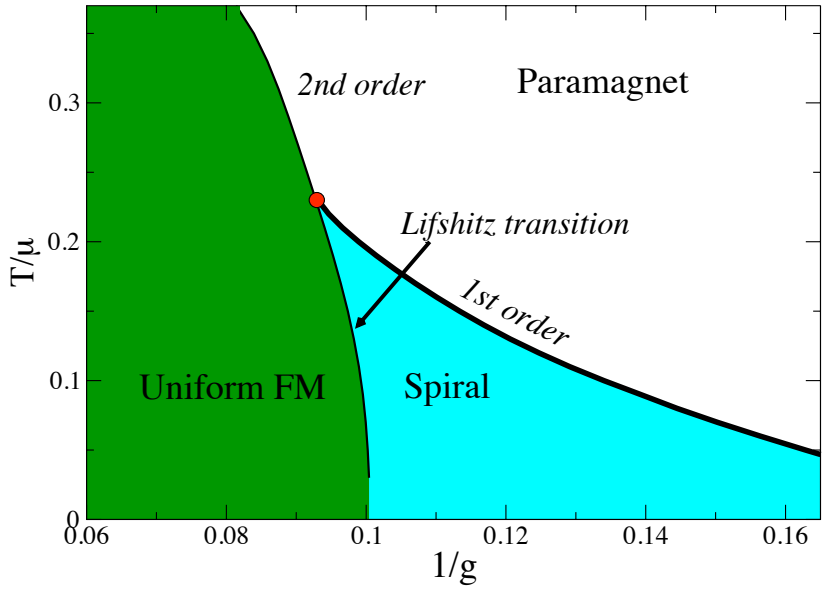

Figure 4.2: **Phase diagram of the itinerant ferromagnet allowing for the possibility of spatially modulated ferromagnetism:** Quantum fluctuations drive the formation of a spiral phase which sets in below the tricritical point and pre-empts the first-order transition between the uniform ferromagnet and the paramagnet.

needed to enhance the effect of quantum fluctuations. Therefore, it is not surprising that the spiral pre-empts the first order paramagnet-to-uniform ferromagnet transition below the tri-critical point.

4.1.2.2 Spiral-to-uniform ferromagnet transition

Next, we wish to determine the boundary between the spiral phase and the uniform ferromagnet. In principle, the transition may occur either discontinuously or smoothly along the $Q = 0$ line. In order to determine which of the scenarios holds, we calculate $Q = Q(g, T)$. From Eq. (4.1), we see that we first need to evaluate the magnetization M. The value of magnetization that minimizes the free energy $\mathcal{F}_{\bar{Q}}$, Eq. (4.2), is given by

$$M^2 = \frac{-2\beta}{7\gamma}\left(\frac{8}{9} + \sqrt{\left(\frac{8}{9}\right)^2 - 7\left(\frac{\alpha\gamma}{\beta^2} - \frac{5}{27}\right)}\right). \tag{4.3}$$

Substituting this into Eq. (4.1) for $\bar{Q}$, we find that the transition occurs via a Lifshitz line (line along which $Q = 0$) which coincides with the $\alpha = 0$ line. The magnetization M varies continuously along this line.

4.1.2.3 Evolution of the order parameters

The expressions for $M(g,T)$ and $Q(g,T)$ are given by (4.3) and (4.1), respectively. The evolution of the order parameters M and Q in the vicinity of the first order transition from the paramagnet into the spiral state is plotted in Fig. 4.3. We see that the jumps in M and Q get smaller as we approach the tricritical point (where $Q = M = 0$).

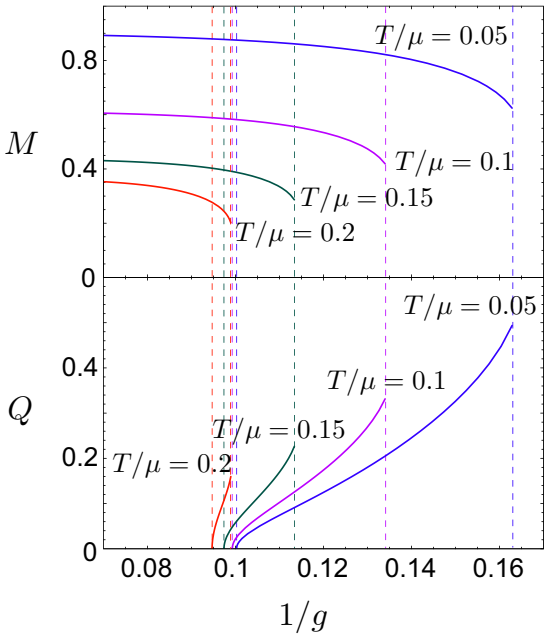

Figure 4.3: **The evolution of the order parameters M and Q in the spiral phase:** As we approach the tricritical point, the jumps in M and Q along the line of first order transitions become smaller. At the tricritical point $M = Q = 0$. At the Lifshitz transition between the uniform ferromagnet and the spiral ferromagnet, Q goes continuously to zero while M remains finite and behaves smoothly.

4.1.2.4 Comparison to previous work

Previous analyses [66] determined the phase diagram of spiral and uniform ferromagnets (they did not consider a spin nematic phase) by brute force numerical (Monte-Carlo) evaluation of the fluctuation corrections to the free energy, given by Eq. (2.14), for a given g, T and M,Q. We, instead, evaluate the phase diagram within a Ginzburg-Landau expansion and obtain an analytical approximation at low temperatures. The agreement between the two methods is good

in the vicinity of the tricritical point where the expansion is controlled. At low temperatures, numerics becomes less accurate. The re-entrance of first order transition line between the paramagnet and uniform ferromagnet in [66] could be an artefact of numerical errors. Our analytical results do not predict this. Our approach offers some complementary information – we determined the location of the boundary between the uniform and spiral ferromagnet as well as the nature of this transition.

4.1.3 d-wave spin nematic

The Stoner Hamiltonian is rotationally invariant; hence the momentum-dependent distortion of the Fermi surface is not favoured in mean-field theory. In the case of a spiral ferromagnet we have seen that the momentum-dependent (and spin antisymmetric) distortion has more low-energy quantum fluctuations associated with it. This leads us to believe that a spin nematic phase might be stabilized by a similar mechanism where quantum fluctuations generate an effective coupling in the spin-nematic channel.

We start from the expression for the free energy of the spin nematic (3.36). The goal is to see if, for certain values of the interaction strength and temperature the spin nematic phase represents the phase with the lowest free energy.

4.1.3.1 d-wave spin nematic-to-paramagnet boundary

By inspection of the free energy Eq. (3.36), we see that the N^2 coefficient is always positive. This implies that only the possibility of a first order transition into the $N = 0$ state exists, in agreement with Ref. [85]. For temperatures below $T = 0.02\mu$, the paramagnet-to-spin nematic transition pre-empts the paramagnet-to-spiral transition. The first order transition line between the paramagnet and the spin nematic is given by the equation

$$\beta^2 = 4\frac{\langle d_{\mathbf{k}}^2\rangle\langle d_{\mathbf{k}}^6\rangle}{\langle d_{\mathbf{k}}^4\rangle^2}(g-\alpha)\gamma. \tag{4.4}$$

From the evaluation of this equation for spin-nematic states with d- and p-wave symmetry we find that the instability to the formation of the d-wave spin nematic occurs at slightly higher temperatures and is, therefore, favored. This might change, however, with dimensionality, the form of the electron dispersion, or the range of the interactions.

4.1.3.2 d-wave spin nematic-to-spiral boundary

Comparing the free energies $F(N)$ and $F(M, Q)$ of the spin-nematic and spiral phases, we find that the spin-nematic state penetrates into the region where

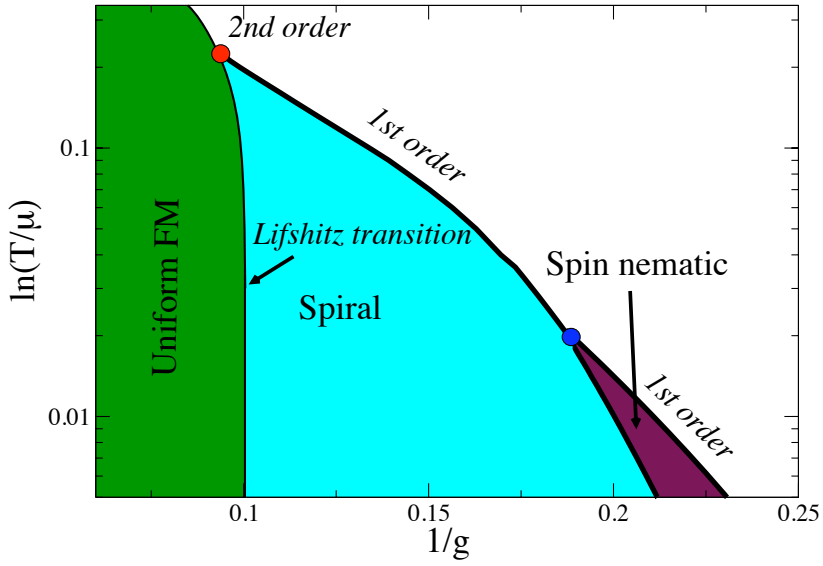

Figure 4.4: **Phase diagram of the itinerant ferromagnet, allowing for the possibility for the formation of spiral and spin-nematic phases:** At temperatures which are about an order of magnitude smaller than the temperature of the tricritical point, a d-wave spin nematic forms between the spiral ferromagnet and the paramagnet.

the spiral state was previously favored. The details of the transition between the spiral and spin-nematic phases are potentially very interesting but hard to analyze. Introducing phase slips into the spiral restores translational symmetry and renders the phase nematic. Whether this is indeed the spin-nematic phase identified here, or something more exotic [92] is not clear.

The phase diagram, including the spin-nematic state is shown in Fig. 4.4. Note that this phase diagram is plotted on a logarithmic scale, since the spin-nematic state onsets at a temperature which is an order of magnitude lower than the temperature of the tricritical point where the spiral forms.

In summary, quantum fluctuations have generated a coupling in the spin-nematic channel and stabilized a spin-nematic phase. This is similar to the mechanism by which a superconducting state is stabilized in spin-fluctuation theory [93; 94], and we anticipate that our approach can be applied to study superconductivity as well. We emphasize that the quantum order-by-disorder approach incorporates charge fluctuations on the same footing as spin fluctuations. As pointed out by Chubukov and Maslov [50], charge fluctuations are essential to mediate the formation of a spin-nematic state.

4.2 Small Deviations from the Isotropic Free-Electron Dispersion

Changing from a free-electron dispersion to a band dispersion can have a profound effect upon the magnetic phase diagram. In the extreme, it has been shown that the tight-binding dispersion can lead to the formation of a spiral phase even on the mean-field level [18; 95]. Here, we consider the effect of a weakly anisotropic dispersion $\epsilon_{\mathbf{k}} = \frac{k^2}{2} + \delta\epsilon_{\mathbf{k}}$, with $\delta\epsilon_{\mathbf{k}} = \delta\cos(4\phi)\sin\theta$. This deformation makes the dispersion more tight-binding like. By changing the subtle balance between kinetic energy and fluctuation corrections the regions occupied by the different phases, and the nature (*e.g.* first or second order) of the transitions are altered.

4.2.1 Uniform ferromagnet

First, we investigate the changes to the phase diagram of the uniform ferromagnet. Summing Eqs. (3.1) and (3.38), we arrive at the following expression for the free energy:

$$\begin{aligned} \tilde{\mathcal{F}} &= \tilde{\alpha}M^2 + \tilde{\beta}M^4 + \tilde{\gamma}M^6, \\ \tilde{\alpha} &= \alpha + \left(6\beta_{MF} + \frac{g^2}{2}\frac{\partial^2\alpha_{\text{fl}}}{\partial^2\mu^2}\right)\frac{\langle\delta\epsilon_{\mathbf{k}}^2\rangle}{g^2}, \\ \tilde{\beta} &= \beta + 15\gamma\frac{\langle\delta\epsilon_{\mathbf{k}}^2\rangle}{g^2}, \\ \tilde{\gamma} &= \gamma. \end{aligned} \tag{4.5}$$

There are two ways to make the transition from the paramagnet into the ferromagnet

1. A second order transition, where the magnetization rises continously from zero,
2. A first order transition where the magnetization jumps from zero to a finite value.

4.2.1.1 Line of second order transitions

As in the case of the isotropic k^2 dispersion, we find that the transition between the uniform ferromagnet and the paramagnet is continuous at high temperatures – see Fig. 4.5. The line of second order transitions between the uniform ferromagnet and the paramagnet is given by $\tilde{\alpha} = 0$. The necessary condition for its existence is that $\tilde{\beta} > 0$. The effect of the anisotropic correction to the dispersion is to slightly shift the locations of the phase boundaries, e.g. the temperature of the tricritical point (where $\tilde{\beta} = \tilde{\alpha} = 0$) is reduced to $T^* = 0.225\mu$ (see Fig. 4.5).

4.2.1.2 Line of first order transitions

At lower temperatures, the transition becomes first order due to a sign change of $\tilde{\beta}$. The line of first order transitions is given by $\tilde{\beta}^2 = 4\tilde{\alpha}\tilde{\gamma}$.

4.2.2 Spiral phase

Our analysis of the spiral phase follows the same steps as in the case of the free-electron dispersion in Section 4.1.2. The resulting expressions are lengthy and not particularly revealing in themselves. Therefore, we simply outline the main steps. The free energy of the spiral state is the sum of Eqs. (3.27) and (3.40), and is given by

$$\mathcal{F}[M, \mathbf{Q}] = \left(\tilde{\alpha} + \tilde{\beta}_1(\hat{\mathbf{Q}})Q^2 + \tilde{\gamma}_1 Q^4\right) M^2 + \left(\tilde{\beta} + \tilde{\gamma}_2 Q^2\right) M^4 + \tilde{\gamma} M^6, \quad (4.6)$$

with $\tilde{\alpha}$, $\tilde{\beta}$, and $\tilde{\gamma}$ defined in Eq. (4.5), $\tilde{\gamma}_1 = \gamma_1 = \frac{3}{5}\gamma$, $\tilde{\gamma}_2 = \gamma_2 = \gamma$, and

$$\tilde{\beta}_1(\hat{\mathbf{Q}}) = \frac{2}{3}\beta + 2\beta_{MF}\Big\langle \left(\frac{\mathbf{Q}\cdot\nabla\delta\epsilon_{\mathbf{k}}}{k_F Q}\right)^2 \Big\rangle + 30\frac{\gamma}{g^2}\Big\langle \left(\frac{\mathbf{k}\cdot\mathbf{Q}}{k_F Q}\right)^2 \delta\epsilon_{\mathbf{k}}^2 \Big\rangle. \quad (4.7)$$

This free energy now depends upon the direction $\hat{\mathbf{Q}} = \mathbf{Q}/Q$ and is no longer invariant under rotations of the spiral. This is the consequence of the anisotropic dispersion which breaks the continuous rotation symmetry. It turns out that for the particular anisotropy $\delta\epsilon_{\mathbf{k}} = \delta\cos(4\phi)\sin\theta$, the free energy is minimized for spirals with $\hat{\mathbf{Q}}$ along the z-axis.

Notice that the proportionality between coefficients found in the case of the free-electron dispersion is broken by the anisotropic dispersion. For example, the coefficient of the term Q^2M^2 is no longer proportional to that of the M^4 term. This broken proportionality between the coefficients changes the nature of the transition between the spiral ferromagnet and the paramagnet (see Fig. 4.5).

The optimum wavevector is obtained by minimizing the free energy Eq. (4.6) with respect to Q for a given magnetization M. In this way, we obtain $\bar{Q} \equiv \bar{Q}[M]$. Substituting this value of Q back into Eq. (4.6) we obtain the free energy at the optimum wavevector as a function of M, equation where $\tilde{\alpha}_{\bar{Q}}$, $\tilde{\beta}_{\bar{Q}}$ and $\tilde{\gamma}_{\bar{Q}}$ are the appropriate generalizations of the free-electron forms given in Eq. (4.2). In this way we obtain

$$\tilde{\mathcal{F}}_{\bar{Q}}[M] = \tilde{\alpha}_{\bar{Q}} M^2 + \tilde{\beta}_{\bar{Q}} M^4 + \tilde{\gamma}_{\bar{Q}} M^6. \quad (4.8)$$

4.2.2.1 Spiral-to-paramagnet boundary

In the presence of an anisotropic dispersion, we expect the onset of the spiral below or above the tri-critical point, due to the mixing between the coefficients

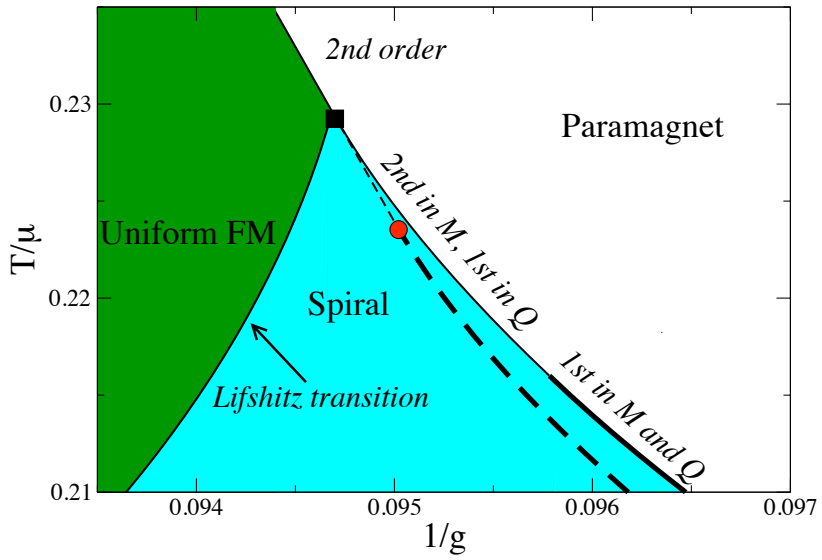

Figure 4.5: **Modification to the phase diagram of the spiral state with a weakly anisotropic dispersion:** The onset of the spiral no longer coincides with the uniform tricrital point (circle). Instead, the spiral forms at a slightly higher temperature (square) and pre-empts a portion of the continuous transition between the uniform ferromagnet and the paramagnet (thin dashed line) as well as the first-order transition (thick dashed line). Note that because of the anisotropy also the nature of the spiral-to-paramagnet transition changes. At higher temperatures M now behaves continuously while at low temperatures the transition is first order in M as in the isotropic case.

of different total order in M and Q in the free energy (3.40). As discussed in the case of the isotropic free-electron dispersion, in principle, there are two ways in which the system can make a transition form the paramagnet into the spiral state:

1. A second order transition in M (which occurs along the line $\tilde{\alpha}_{\bar{Q}} = 0$ for $\tilde{\beta}_{\bar{Q}} > 0$), and

2. A first order transition in M (which occurs along the line $\tilde{\beta}_{\bar{Q}}^2 = 4\tilde{\alpha}_{\bar{Q}}\tilde{\gamma}_{\bar{Q}}$ for $\tilde{\beta}_{\bar{Q}} < 0$ and $\tilde{\alpha}_{\bar{Q}} > 0$).

For the free-electron dispersion only the latter possibility occurred. Now that we have broken the proportionality between Ginzburg-Landau coefficients by allowing for an anisotropic dispersion, both of the possibilities exist.

1. Line of second order transitions in M. The transition begins as second order in M (and first order in Q) (thin solid line in Fig. 4.5, extending below the square symbol). The equation of this line is given by $\tilde{\alpha}_{\bar{Q}} = 0$. This line was not present in the phase diagram with free-electron dispersion, because the quartic coefficient β was negative in the region where the spiral existed. This line pre-empts a portion of the line of second order phase transitions between the paramagnet and the uniform ferromagnet (thin dashed line) and the line of first order transitions from the paramagnetic to the uniform ferromagnetic state (thick dashed line). The formation of the spiral phase is, therefore, no longer coincident with the putative tricritical point of the uniform ferromagnet (shown as circle in Fig. 4.5) but sets in at higher temperatures as indicated by a square symbol in Fig. 4.5.

2. Line of first order transitions. The second order transition between the paramagnetic and spiral phases gives way to a first order transition at lower temperatures - shown as thick solid line in Fig. 4.5, and given by the equation $\tilde{\beta}_{\bar{Q}}^2 = 4\tilde{\alpha}_{\bar{Q}}\tilde{\gamma}_{\bar{Q}}$.

4.2.2.2 Uniform ferromagnet-to-spiral transition

The boundary between the spiral and uniform ferromagnetic phases remains a Lifshitz transition, where the optimal wave vector falls continuously to zero and along which M is continuous. In the case of the free-electron dispersion, this has turned out to be coincident with the $\alpha = 0$ line. The situation is not so simple when we allow for an anisotropic dispersion. While the magnetization remains continuous, within our numerical resolution, we cannot exclude that the derivative of M becomes discontinuous.

The anisotropic dispersion has had two key effects upon the phase diagram. Firstly, the region occupied by the spiral phase has increased, and secondly, the onset of the spiral decoupled from the new tricritical point of the uniform ferromagnet.

4.2.3 d-wave spin nematic

The free energy of the d-wave spin-nematic state in the presence of a distortion is given by the sum of Eqs. (3.36) and (3.41). We can rewrite this in the form

$$\tilde{\mathcal{F}}[N] = \tilde{\alpha}_N N^2 + \tilde{\beta}_N N^4 + \tilde{\gamma}_N N^6, \tag{4.9}$$

where

$$\tilde{\alpha}_N \;=\; -\langle d_{\mathbf{k}}^2\rangle(\alpha - g) - \left(6\frac{\beta_{MF}}{g^2} + \frac{1}{2}\frac{\partial^2 \alpha_{\text{fl}}}{\partial \mu^2}\right)\langle \delta\epsilon_{\mathbf{k}}^2 d_{\mathbf{k}}^2\rangle,$$

$$\begin{aligned}\tilde{\beta}_N &= \langle d_{\mathbf{k}}^4\rangle\beta + 15\frac{\gamma}{g^2}\langle\delta\epsilon_{\mathbf{k}}^2 d_{\mathbf{k}}^4\rangle, \\ \tilde{\gamma}_N &= \langle d_{\mathbf{k}}^6\rangle\gamma. \end{aligned} \tag{4.10}$$

4.2.3.1 d-wave spin nematic-to-paramagnet boundary

In the region where the spin nematic is stabilized, the quartic coefficient is negative (while the quadratic coefficient is positive). This implies that the transition from the paramagnet into the d-wave spin nematic is of first order. It occurs when $\tilde{\beta}_N^2 = 4\tilde{\alpha}_N\tilde{\gamma}_N$. The spin-nematic state forms at slightly higher temperatures than in the presence of the isotropic free-electron dispersion – it onsets below $T = 0.025\mu$.

4.2.3.2 d-wave spin nematic-to-spiral boundary

The boundary between the spiral and spin-nematic is obtained by comparison of their free energies $\tilde{\mathcal{F}}(N)$ and $\tilde{\mathcal{F}}(M, Q)$. In the presence of the anisotropy the spin nematic wins over the spiral phase at higher temperatures than in the isotropic case. The spin-nematic region is enlarged (compared to the case of the isotropic free-electron dispersion) since it becomes easier to redistribute the kinetic energy cost of forming a spin nematic when the dispersion is anisotropic.

In summary, we have used the Ginzburg-Landau expansion of the free energy to determine the phase diagram of an itinerant ferromagnet in the vicinity of the quantum critical point. Quantum fluctuations were included through the quantum order-by-disorder approach.

First, we investigated the effect of quantum fluctuations upon the phase diagram of the uniform ferromagnet. It was found that a lower interaction strength is needed to magnetize the system in the presence of quantum fluctuations. Below a certain temperature (the tricritical temperature) the paramagnet-to-ferromagnet transition becomes first order.

Next, we allowed for the generation of new phases in the vicinity of the putative quantum critical point. We showed that quantum fluctuations stabilize a spiral and spin-nematic phase. For temperatures lower than the tricritical temperature, the putative first order transition between the paramagnet and the uniform ferromagnet is pre-empted by a transition into the spatially modulated spiral state. A d-wave spin-nematic state is stabilized for temperatures below $T \approx 0.02\mu$, in between the paramagnet and the spiral phase. We have demonstrated that, in the presence of an anisotropic dispersion, the relative sizes of the regions occupied by different phases and the nature of the transitions change.

The onset of spiral order no longer coincides with the putative tricritical point of the uniform ferromagnet. The nature of the transition from the paramagnet into the spiral state changes – initially the transition is second order in M, and then it turns first order as the temperature is lowered. The regions occupied by the spiral and spin nematic increase at the cost of the uniform ferromagnetic region getting smaller.

Chapter 5

Experimental Phase Diagram of MnSi

We consider a simple extension of the Stoner model of an itinerant quantum critical point – we add a small spin-orbit coupling term. As we will see, this model proves suitable to explain many features of the experimentally observed phase diagram of MnSi.

For a long time MnSi was considered to be a textbook example of a Fermi liquid, developing helical ferromagnetic order at low temperatures. However, in recent years this material has revealed some fascinating and poorly understood behaviour. In this Chapter we present a brief summary of existing experimental data.

At ambient pressure, MnSi orders ferromagnetically below a certain transition temperature. Due to a small Dzyaloshinski-Moriya interaction, the ground state is a spiral. The spiral wave vector aligns along the lattice-favoured (111) directions, due to even smaller anisotropic spin-orbit terms allowed by the lattice symmetry. This behaviour is well understood.

By applying hydrostatic pressure, the helical ferromagnet-to-ferromagnet transition can be tuned towards a quantum critical point. Under the application of sufficiently strong hydrostatic pressure, the transition turns first order. Upon suppression of the magnetic order under hydrostatic pressure, experiments found a radical departure from conventional metallic physics, characterized by a $T^{\frac{3}{2}}$ dependence of the resistivity. The occurrence of this behaviour over a wide pressure range, not just close to the transition, suggests a new phase of matter.

A clue to its nature was provided by neutron scattering, which revealed an unusual partially ordered phase, characterized by a small increase in the magnitude of the helical wave vector and relatively broad neutron scattering peaks along the (110) directions. The neutron scattering pattern was found to be very weakly temperature dependent within a large window of temperatures, suggest-

ing that the broadening of the peaks is not a thermal effect. The order seen in the experiments is dynamic – its time-scales have been estimated from μSR data. The ordering has not been seen in resistivity or susceptibility measurements, most likely due to the fact that they operate on different time scales. Most recently, signatures of the partially ordered phase have been observed in thermo-power measurements. The partially ordered phase has been suggested as the key to understanding the mysterious non-Fermi behaviour.

A number of open questions arises from the experimental results, the most important of which are:

- What is the origin of the partially ordered phase?
- Can we explain the unusual neutron-scattering pattern in the partially ordered phase? In particular, why does the spiral wave vector re-orient from the (111) direction to the (110) direction?
- What is the mechanism behind the non-Fermi liquid resistivity in the vicinity of the putative quantum critical point, and why does this region extend to such a wide range of pressures? Can the partially order phase be the origin of the anomalous transport properties in MnSi?

5.1 Helical phase

MnSi has been one of the most extensively studied weak itinerant ferromagnets. At ambient pressures it orders ferromagnetically below the temperature of $T_c = 29.5K$. The ground state is a helix with a wave vector of magnitude $Q = 0.037\mathring{A}^{-1}$, due to a small spin-orbit coupling. The helical wave vector is pinned to the (111) direction in the crystal axis frame, as observed by a sharp peak along this (and equivalent) direction in the neutron scattering data [96]. The Curie temperature can be tuned to zero by the application of hydrostatic pressure. The helical phase exhibits expected Fermi-liquid behaviour, and can be well described by Stoner mean-field theory in the presence of a spin-orbit coupling.

5.1.1 Role of the spin-orbit coupling in MnSi

The lack of inversion symmetry in MnSi leads to a Dzyaloshinskii-Moriya interaction of the form $\int d\mathbf{r}\,(\mathbf{M}.\nabla \times \mathbf{M})$. The Dzyaloshinskii-Moriya interaction introduces a helical modulation of the ferromagnetic order, such that the $\mathbf{M} \perp \mathbf{Q}$, where $\mathbf{Q}$ denotes the spiral wave vector, since this configuration minimizes the

free energy. Even smaller anisotropic spin-orbit terms, allowed by the lattice symmetry, lock the direction of the spiral to the (111) direction in the crystal axes frame. The locking can be easily understood from a phenomenological Ginzburg-Landau expansion [97]. There are three clearly distinguishable energy scales in MnSi [97; 98]:

1. The strongest being Coulomb repulsion between electrons (responsible for ferromagnetic order).

2. An order of magnitude weaker Dzyaloshinskii-Moriya interaction, since spin-orbit coupling is a relativistic effect. The Dzyaloshinskii-Moriya interaction is responsible for a helical modulation of the ferromagnetic order; the wavelength is $\lambda = 175\mathring{A}$.

3. Anisotropic spin-orbit coupling. This is the weakest scale; almost two orders of magnitude weaker than the Dzyaloshinskii-Moriya interaction. It determines the directional dependence of the spiral wave vector.

5.2 Partially ordered phase

5.2.1 MnSi under hydrostatic pressure - a world of mysteries

Upon approaching the critical pressure and beyond, several experiments found a radical departure from conventional metallic physics. First, it has been noticed that the helical ferromagnet-to-paramagnet transition turns first order for pressures greater than $p^* = 1.2GPa$ [89]. This is inconsistent with Hertz-Millis theory which predicts a second order phase transition. The critical pressure of $p_c = 1.46GPa$ suppresses the ferromagnetic order, see Fig. 5.1. The first order transition is characterized by a sharp drop in electrical resistivity at the critical temperature T_c, see Fig. 5.2. Secondly, for pressures greater than p_c, non-Fermi liquid behaviour was measured in a region adjacent to the helical phase [99; 100]. It is characterized by a $T^{3/2}$ dependence of the resistivity (shaded region in Fig. 5.1). Normally, a non-Fermi liquid behaviour is expected in a quantum critical region that extends from a quantum critical point like a cone (see Fig. 1.1). However, here it extends over a *wide* region of the phase diagram, almost three decades in temperature and at least up to pressures $\sim 3p_C$. Similar behaviour has been noticed in other itinerant ferromagnets, for example $ZrZn_2$ [101] and Ni_3Al (see Ref. [5] and references therein), which indicates that it might be a generic principle for itinerant ferromagnets. This behaviour suggests a novel phase of matter.

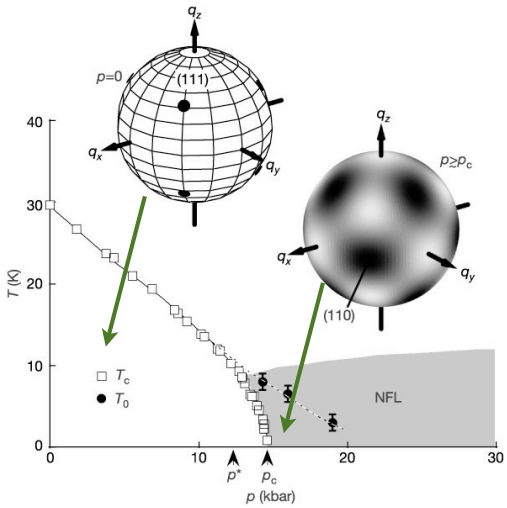

Figure 5.1: **Temperature versus pressure phase diagram of MnSi:** Adapted from Fig. 1 of Ref. [20]. Resistivity and susceptibility reveal a second order transition between the helical ferromagnet and paramagnet up to $p^* \approx 12$ kbar ($T^* \approx 12$ K). Above this pressure, the same measurements show a weakly first order transition that reaches zero temperature at $p_c = 14.6$ kbar. Beyond this pressure, resistivity shows a non-Fermi liquid temperature dependence of $T^{3/2}$. Neutron scattering in the helimagnetic phase shows resolution-limited peaks corresponding to spiral wave vectors $Q \sim 0.037 \mathring{A}^{-1}$ parallel to the [111] directions. These measurements also reveal a partially ordered phase - not apparent in resistivity or susceptibility - where the spirals unpin from the [111] directions. The scattering signal (shown in the inset taken from Ref. [20]) spreads diffusely over a sphere of radius $Q \sim 0.043 \mathring{A}^{-1}$, weakly favouring the [110] directions and antifavouring the [111] and [100] directions.

The measurements of the resistivity and susceptibility suggested that the long-range order in MnSi is suppressed for $p > p_c$. However, more recent neutron scattering experiments [20] and NMR [91] challenge this view. They indicate the emergence of a partially ordered phase in the vicinity of the putative quantum critical point, within the non-Fermi liquid region, where a true long-range order is lost, but a peculiar helical ordering survives on intermediate time and length scales. The neutron scattering intensity still remains spread over a surface of a sphere, now with a slightly increased radius, see Fig. 5.1. However, there is almost no signal left along the (111) direction and equivalent – the intensity shifts to the (110) direction. The peaks along the (110) are characterized by a relatively broad distribution in angular directions. The signal is lost above a crossover temperature T_0. For details, see Fig. 5.1. The distribution of the magnetic moments

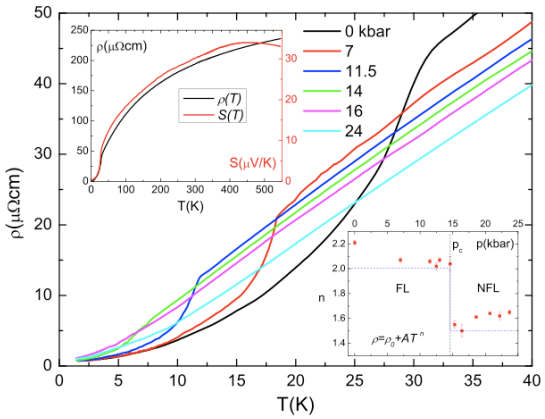

Figure 5.2: **Resistivity as a function of temperature for MnSi:** Taken from Ref. [102]). The resistivity shows pronounced jumps along the line of first order transitions into the helical ferromagnetic phase. Bottom inset shows non-Fermi liquid behaviour of the resistivity in the partially ordered phase (and beyond), characterized by the temperature exponent of $\frac{3}{2}$. Top inset shows the temperature dependence of resistivity and thermo-power at ambient pressure.

is effectively temperature independent, suggesting that the broadening is not a thermal effect, but a dynamical one. The μSR measurements [103] support this view and estimate that spin correlations have dynamic character at time-scales between 10^{-11} and 10^{-10}s. This offers an explanation why signatures of the partial order have not been previously seen in resistivity or susceptibility measurements – the order fluctuates too rapidly on the scale for these measurements. On the other hand, the partially ordered phase has been detected in neutron scattering experiments and NMR measurements, which probe shorter time scales (NMR measurements actually probe somewhat longer time-scales than neutrons).

5.2.2 Signatures of the partially ordered phase in thermo-power measurements

Very recently, signatures of the partially ordered phase have been observed for the first time in a transport property [102]. Measurements of the thermo-power S showed anomalous increase when crossing from the long-ranged ordered phase (helical phase) to the partially ordered phase (see Fig. 5.3). This is attributed to the increase in entropy of the system in the partially ordered phase. Fig. 5.3 shows the values of S/T mapped out in temperature vs pressure plane. The authors see a crossover between the partially ordered phase and the rest of the non-Fermi liquid phase, consistent with the neutron scattering data.

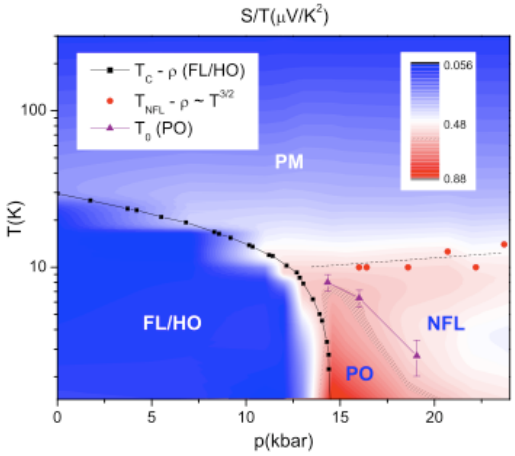

Figure 5.3: **Thermo-power mapped out over the phase diagram in temperature-pressure plane:** Taken from Ref. [102]. The partially ordered phase (PO) is characterized by an increase in the thermo-power S from its value in the helical phase (denoted as FL/HO), associated with an increase in the entropy. Red dots (T_{NFL}) denote the onset of the Non-Fermi liquid phase (NFL). Black dots (T_c) denote the boundary of the helical phase. Purple triangles (T_0) denote the line beyond which the unusual neutron scattering signal in the partially ordered phase disappears.

5.3 Open questions and problems

The experimental results presented above have been a subject of extensive theoretical and experimental debates. Various possible theoretical scenarios (discussed later) have been proposed in order to resolve the origin of the partially ordered phase and the occurrence of non-Fermi-liquid behaviour in the vicinity of the putative quantum critical point. Several intriguing questions still remain to be answered:

- What is the origin of the partially ordered phase?
- How can we explain a small increase in the spiral wave vector when going from the helical phase into the partially ordered phase?
- Why does the wave vector change the direction from (111) to (110)?
- Can we explain the unusual neutron-scattering pattern?
- Can we propose a mechanism which leads to an anomalous behaviour of the resistivity, $\rho \sim T^{\frac{3}{2}}$?

To summarize, the experimental data presented above demonstrates that the partially ordered phase in MnSi is yet another example of an onset of an unusual phase in the vicinity of a putative quantum critical point. The partially ordered phase is characterized by a small increase in the spiral wave vector from its value in the helical phase and its shift in the direction from (111) in the helical phase to (110). No true long range order exists in this phase, but a peculiar partial order 'responsible' for relatively broad neutron scattering peaks and an increase in entropy (seen in thermopower measurements). μSR and neutron scattering data indicate the presence of a dynamical order. These experiments raise several open questions - i) what is the origin of this phase? ii) why does the wave vector shift to a new direction? iii) what is the mechanism behind the non-Fermi liquid resistivity that extends to a large pressure range? In our subsequent analysis we attempt to answer the first two questions in order to resolve this long-standing experimental puzzle.

Chapter 6

Quantum Order-by-Disorder in MnSi

In this Chapter, we construct an analytical model that describes MnSi and enables us to explain its experimentally observed phase diagram [104]. The model is a simple extension of the Stoner model of an itinerant ferromagnetic quantum critical point, discussed in Chapters 3 and 4. We add a small spin-orbit coupling to the model and treat it as a perturbation. We show that quantum fluctuations naturally lead to the formation of an unusual phase near to the putative quantum critical point, which shares many of the observed features of the partially ordered phase in MnSi, most notably the unusual directional dependence of magnetic structure.

We show that the helical phase emerges as the mean-field solution of the model, with the wave vector pinned along the (111) direction. The partially ordered phase is a fluctuation-modified spiral phase stabilized through the quantum order-by-disorder mechanism. The spiral wave vector reorientation to the (110) direction in the partially ordered phase happens as quantum fluctuations stabilize directions of the spiral wave vector far away from the mean-field pinning along the (111) direction.

Mean-field theory. First we discuss the mean-field theory of the model. We begin our analysis by deriving the mean-field dispersion of the Stoner model in the presence of the spin-orbit coupling. The Dzyaloshinski-Moriya interaction D turns the ferromagnet into a helimagnet. Even smaller anisotropic spin-orbit terms allowed by the lattice symmetry pin the wave vector $\mathbf{Q}$ along the (111) direction. This is exactly what has been seen in the neutron scattering pattern in the helical phase. Equivalent results can be obtained from a phenomenological Ginzburg-Landau expansion.

Quantum order-by-disorder in MnSi. We aim to answer the question: How do quantum fluctuations modify the phase diagram? In Chapter 2 we have shown that the free energy is a functional of the mean-field dispersion. We will show that the mean-field dispersion in the presence of a weak Dzyaloshinsky-Moriya interaction D is of the same form as the dispersion of the spiral in a system without spin-orbit coupling, with a shifted wave vector $\tilde{Q} = Q - D$. This will result in the phase diagram with the same phase boundaries as in the case of a system without the spin-orbit coupling; however, the corresponding phases will come with a wave vector shifted by D. The partially ordered phase then corresponds to the fluctuation-modified spiral phase, with non-zero $\tilde{Q} = Q - D$. This explains a small increase in the wave vector in the partially ordered phase from its value D in the helical phase.

In order to deduce the directional dependence of $\mathbf{Q}$, we analyze the directional dependent terms in the free energy, arising from a small anisotropic spin-orbit coupling. We show that quantum fluctuations weakly favour the (110) direction, and that the change of direction from (111) to (110) happens as we cross the boundary from helical phase to partial order.

6.1 Central Idea of Our Approach

6.1.1 Recap of Chapter 4

We begin by summarizing the results of Chapter 4, as they will prove extremely useful in our subsequent analysis.

There, we considered the Stoner model in a system without spin-orbit coupling and deduced the phase diagram in the vicinity of the putative quantum critical point. First we demonstrated how quantum fluctuations can drive the paramagnet-to-ferromagnet transition first order. Next, we showed that this first order transition is actually pre-empted by the transition into a spiral ferromagnetic state.

6.1.2 Connection to Chapter 4

Next, we investigate the changes to the phase diagram in the presence of a weak spin-orbit coupling. Since the spin-orbit terms are considerably smaller than the Stoner terms (an order of magnitude in MnSi), they will not affect the location of the phase boundaries significantly. However, they change the nature of the phases:

- A Dzyaloshinskii-Moriya interaction D will turn a uniform ferromagnet into a helimagnet with a pitch $Q = D$.

- Instead of a fluctuation-driven spiral phase in a system without spin-orbit coupling, we will now encounter a fluctuation-modified spiral phase characterized by a small increase in the wave vector from its value D in the helical phase, *i.e.* non-zero $\tilde{Q} = Q - D$. We will show this explicitly by calculating the mean-field dispersion in the presence of spin-orbit coupling and by showing that it is the same as the spiral dispersion of a system without a spin-orbit coupling, but with the wave vector shifted to $\tilde{Q} = Q - D$. We will convince the reader that this phase closely resembles the partially ordered phase.

Apart from explaining a small increase in the wave vector, the model offers an intuitive explanation why dynamical order has been seen in the experiments – due to the phase being stabilized by quantum fluctuations.

6.1.3 Directional dependence of the wave vector

Determining the directional dependence of $\mathbf{Q}$ requires some additional work, although an intuitive picture can still be developed. The directional dependence originates from small anisotropic spin-orbit terms allowed by the lattice symmetry. These terms generate directional dependent terms in the free energy. It has long been known that the mean-field-like directional dependent terms pin $\mathbf{Q}$ to the lattice-favoured (111) direction in the helical phase. As quantum fluctuations become strong enough, in the partially ordered phase, we expect them to stabilize the directions far away from the mean-field pinning. The wave vector will therefore shift in direction in order to open up and benefit energetically from the extra phase space for low-energy particle-hole excitations.

We explicitly show this by introducing a tiny anisotropic spin-orbit coupling specific to the cubic B20 structure of MnSi, and examining the directional dependent terms in the free energy. We show that the free energy is minimized for $\mathbf{Q} \parallel (111)$ in the helical phase, and for $\mathbf{Q} \parallel (110)$ in the partially ordered phase.

6.2 Mean-field theory

In this section we outline a theoretical model that describes the helical phase of MnSi. The helical phase can be understood from two different perspectives that eventually lead to exactly the same results: a phenomenological Ginzburg-Landau expansion and microscopic mean field theory of the Stoner model in the presence of a weak spin-orbit coupling.

The phenomenological expansion considers all terms allowed by the lattice symmetry in the Ginzburg-Landau expansion (up to a certain order). We will show that this leads to a spiral ground state. Smaller terms, that explicitly break

the rotational symmetry, lead to the directional dependence of $\mathbf{Q}$ and align $\mathbf{Q}$ along the (111) direction.

The microscopic model consists of adding small spin-orbit terms to the Stoner model. Adding a small isotropic spin-orbit coupling results in a helical modulation of the ferromagnetic order. Even smaller anisotropic spin-orbit terms, that depend on the lattice symmetry, generate directional dependent terms in the free energy. The wave vector $\mathbf{Q}$ picks a certain direction in the crystal axes frame, such that the free energy is minimized. Using a specific form of the spin orbit coupling in the cubic B20 environment, we show that the wave vector is pinned along the (111) direction.

6.2.1 Ginzburg - Landau phenomenology

The chiral ferromagnet MnSi can be characterized by the symmetry group $P2_13$. We write down all the leading terms in the Ginzburg-Landau expansion allowed by this symmetry. By minimizing the free energy, we deduce the ground state.

The main contribution to the free energy of a chiral magnet is given by

$$\mathcal{F}^{(0)} = (\nabla \mathbf{M})^2 + r_0 \mathbf{M}^2 + 2D\mathbf{M} \cdot (\nabla \times \mathbf{M}) + \dots, \tag{6.1}$$

The spin-orbit coupling that arises due to the absence of inversion symmetry manifests itself in the Ginzburg-Landau expansion of the order parameter (6.1) in the form of the Dzyaloshinskii-Moriya interaction $2D\mathbf{M} \cdot (\nabla \times \mathbf{M})$. Since spin-orbit coupling is a relativistic effect D is expected to be a small parameter. The free energy is minimized by $\mathbf{M}(\mathbf{r}) = M\left[\mathbf{n}_x \cos(\mathbf{Q}.\mathbf{r}) + \mathbf{n}_y \sin(\mathbf{Q}.\mathbf{r})\right]$, see Fig. 6.1. The ground state is a spiral with the pitch determined by the Dzyaloshinskii-Moriya interaction, $Q = D$.

Directional dependence of Q. Next, we introduce smaller terms in the phenomenological expansion that explicitly break the rotational symmetry, but which are allowed by the lattice symmetry. For the B20 cubic structure, the leading anisotropy is of the form

$$\mathcal{F}^{(1)} = \kappa \sum_{\alpha=a,b,c} (\partial_\alpha M_\alpha)^2. \tag{6.2}$$

These terms are much smaller than the Dzyaloshinskii-Moriya interaction in MnSi (see Section 5.1.1). As such, they don't affect the magnitude of $\mathbf{Q}$ significantly. However, they generate the directional dependence of $\mathbf{Q}$. In order to investigate the directional dependence, we consider two coordinate frames as demonstrated in Fig. 6.1:

- the crystal axes frame $(\mathbf{n}_a, \mathbf{n}_b, \mathbf{n}_c)$

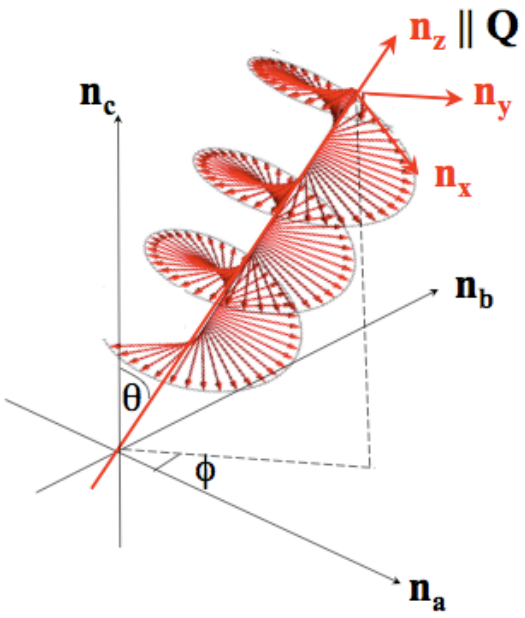

Figure 6.1: **Two coordinate frames: the crystal axes frame and the spiral frame:** The wave vector $\mathbf{Q} \parallel \mathbf{n}_z$ will orient with respect to the crystal axes frame $(\mathbf{n}_a, \mathbf{n}_b, \mathbf{n}_c)$ in such a way that the free energy is minimized.

- the spiral frame $(\mathbf{n}_x, \mathbf{n}_y, \mathbf{n}_z)$, where $\mathbf{Q} \parallel \mathbf{n}_z$.

The spiral wave vector $\mathbf{Q}$ will pick a certain direction in the crystal axes frame in such a way that the free energy is minimized. We can rewrite the directional dependent term as

$$\mathcal{F}^{(1)} \propto -\kappa Q^2 M^2 \sum_{\alpha=a,b,c} \lambda_\alpha^4, \tag{6.3}$$

where $\lambda_\alpha = \mathbf{n}_z.\mathbf{n}_\alpha$ and $\kappa < 0$ for MnSi. The free energy is minimized for $\lambda_a = \lambda_b = \lambda_c$, that is for $\mathbf{Q}$ along the $(1,1,1)$ direction in the crystal axes frame.

6.2.2 Microscopic mean-field theory

Here, we explicitly show how the helical phase emerges as the mean-field solution of the Stoner model in the presence of the spin-orbit coupling in the B20 cubic environment. Our starting point is the Hamiltonian given by

$$\begin{aligned} \mathcal{H} &= \mathcal{H}_{St} + \mathcal{H}_{SO}^{(1)} + \mathcal{H}_{SO}^{(2)} \\ \mathcal{H}_{St} &= \sum_{\mathbf{k},\nu=\uparrow,\downarrow} k^2 c_{\mathbf{k}\nu}^\dagger c_{\mathbf{k}\nu} + g \sum_{\mathbf{r}} \hat{n}_{\mathbf{r}\uparrow} \hat{n}_{\mathbf{r}\downarrow}, \end{aligned} \tag{6.4}$$

where $\mathcal{H}_{St}$ represents the Stoner Hamiltonian, $\mathcal{H}_{SO}^{(1)}$ isotropic spin-orbit coupling and $\mathcal{H}_{SO}^{(2)}$ anisotropic spin-orbit Hamiltonian. As found in the experiments (see Section 5.1.1), the energy scales indicate that $\mathcal{H}_{St} \gg \mathcal{H}_{SO}^{(1)} \gg \mathcal{H}_{SO}^{(2)}$.

6.2.2.1 Spin-orbit coupling in MnSi

We present the form that the spin-orbit coupling takes in MnSi.

Isotropic spin-orbit coupling. The isotropic spin-orbit coupling is given by

$$\mathcal{H}_{SO}^{(1)} = -\frac{1}{2}\sum_{\mathbf{k},\nu,\nu'} D\mathbf{k}\cdot\boldsymbol{\sigma}_{\nu,\nu'} c^{\dagger}_{\mathbf{k}\nu} c_{\mathbf{k}\nu'}. \tag{6.5}$$

It breaks the inversion symmetry of the lattice, and it is responsible for the helical modulation of the ferromagnetic order. As previously mentioned, in mean-field theory it generates the term $2D\mathbf{M}\cdot(\nabla\times\mathbf{M})$ in the free energy .

Anisotropic spin-orbit coupling. The small anisotropic spin-orbit coupling in the B20 structure is given by

$$\begin{aligned}\mathcal{H}_{SO}^{(2)} &= -\frac{1}{2}\sum_{\mathbf{k},\nu,\nu'} \mathbf{h}_c(\mathbf{k})\cdot\boldsymbol{\sigma}_{\nu,\nu'} c^{\dagger}_{\mathbf{k}\nu} c_{\mathbf{k}\nu'} \\ \mathbf{h}_c &= \tilde{D}\begin{pmatrix} k_a(k_b^2-k_c^2) \\ k_b(k_c^2-k_a^2) \\ k_c(k_a^2-k_b^2)\end{pmatrix},\end{aligned} \tag{6.6}$$

where $D \gg \tilde{D}$ for MnSi and a,b and c stand for vector components in the crystal axes frame. Anisotropic spin-orbit coupling breaks the rotational symmetry and generates directional dependent terms in the free energy. As a result, the wave vector $\mathbf{Q}$ will pick a certain direction in the crystal axes frame. To leading order, this spin-orbit coupling produces $\sum_\alpha(\partial_\alpha M_\alpha)^2$ ($\alpha = a,b,c$) terms in the phenomenological free energy expansion.

6.2.2.2 Mean-field dispersion

We derive the mean-field dispersion in the presence of the spin-orbit coupling (6.4). The effects of isotropic (6.5) and anisotropic (6.6) spin-orbit coupling to the dispersion are included to leading order. Anisotropic spin-orbit coupling generates terms in the dispersion that explicitly depend upon the direction of the wave vector $\mathbf{Q}$ with respect to the crystal axes frame (different $\mathbf{Q}$ directions are not degenerate any more). Since they are very small, these terms do not affect the

magnitude of the wave vector or position of the boundaries in the phase diagram significantly.

The spin-orbit terms are given in the crystal axes basis a, b, c. In order to diagonalize the Hamiltonian and determine the dispersion, we need to rotate the spin-orbit terms to the spiral basis. A similar procedure was performed in Section 3.3.1.

Rotation to the spiral basis. We have previously shown that the mean-field decoupling of the Stoner interaction takes the form

$$\mathcal{H}_{St} \approx g \sum_{\mathbf{r},\nu,\nu'} \mathbf{M}(\mathbf{r}) \cdot \boldsymbol{\sigma}_{\nu,\nu'} c^{\dagger}_{\mathbf{r}\nu} c_{\mathbf{r}\nu'} = gM \int_{\mathbf{k}} (c^{\dagger}_{\mathbf{k}+\mathbf{Q}/2\uparrow} c_{\mathbf{k}-\mathbf{Q}/2\downarrow} + \text{h.c.}), \tag{6.7}$$

where $\mathbf{M}(\mathbf{r}) = M\left[\mathbf{n}_x \cos(\mathbf{Q}\mathbf{r}) + \mathbf{n}_y \sin(\mathbf{Q}\mathbf{r})\right]$ is a planar spiral with $\mathbf{Q} = Q\mathbf{n}_z$.

The components of the wave vector in the crystal axes frame (see Fig. 6.1) are given by

$$\begin{aligned} Q\hat{n}_z &= Q(\lambda_a \mathbf{n}_a + \lambda_b \mathbf{n}_b + \lambda_c \mathbf{n}_c) \\ &= Q(\sin\theta\cos\phi\,\mathbf{n}_a + \sin\theta\sin\phi\,\mathbf{n}_b + \cos\theta\,\mathbf{n}_c). \end{aligned} \tag{6.8}$$

We perform the rotation by an angle θ around the axis $(-\sin\phi, \cos\phi, 0)$ (this axis is orthogonal to both $\mathbf{n}_z$ and $\mathbf{n}_c$), which leads to $\mathbf{R}_{\phi,\theta}\mathbf{n}_c = \mathbf{n}_z$. The rotation matrix is given by

$$\mathbf{R}_{\phi,\theta} = \begin{pmatrix} \cos\theta + \sin^2\phi(1-\cos\theta) & -\sin\phi\cos\phi(1-\cos\theta) & \cos\phi\sin\theta \\ -\sin\phi\cos\phi(1-\cos\theta) & \cos\theta + \cos^2\phi(1-\cos\theta) & \sin\phi\sin\theta \\ -\cos\phi\sin\theta & -\sin\phi\sin\theta & \cos\theta \end{pmatrix}. \tag{6.9}$$

In order to diagonalize the Hamiltonian, we need to rotate the spin-orbit interaction to the spiral basis. The isotropic spin-orbit terms transform like

$$\mathbf{R}_{\phi,\theta}(k_a, k_b, k_c) = (k_x, k_y, k_z). \tag{6.10}$$

The anisotropic spin-orbit coupling in the spiral coordinate frame takes the form

$$\mathbf{h}(\mathbf{k}) = \mathbf{R}_{\phi,\theta}\mathbf{h}_c(\mathbf{k}\mathbf{R}^T_{\phi,\theta}) = \tilde{D}\mathbf{f}(\mathbf{k}, \phi, \theta), \tag{6.11}$$

where the components of $\mathbf{f}$ are lengthy polynomials in k_x, k_y, k_z with coefficients that depend on the direction of $\mathbf{Q}$. It turns out that we will only need the z

component of $\mathbf{f}$, which is given by $f_z(\mathbf{k} \pm \frac{\mathbf{Q}}{2}) = \Gamma_1(\mathbf{k}, \mathbf{Q}) \pm \Gamma_2(\mathbf{k}, \mathbf{Q})$, where

$$\begin{aligned}
\Gamma_1(\mathbf{k}, \mathbf{Q}) &= Q\gamma_1(\mathbf{k}, \phi, \theta), \\
\gamma_1(\mathbf{k}, \phi, \theta) &= \frac{1}{2}(k_x^2 - k_y^2)\cos^2(2\phi)\cos(2\theta) + \frac{1}{16}(k_x^2 - k_y^2)[5\cos\theta + 3\cos(3\theta)]\sin^2(2\phi) \\
&\quad -\frac{1}{8}\sin(2\phi)[\sin\theta - 3\sin(3\theta)]k_z(k_y\cos\phi - k_x\sin\phi) \\
&\quad -\frac{1}{2}\cos(2\phi)[4k_xk_y(2 + 3\cos\theta)\sin(2\phi)\sin^4(\theta/2) \\
&\qquad\qquad + k_z(k_x\cos\phi + k_y\sin\phi)\sin(2\theta)], \\
\Gamma_2(\mathbf{k}, \mathbf{Q}) &= Q^2\gamma_2(\mathbf{k}, \phi, \theta), \\
\gamma_2(\mathbf{k}, \phi, \theta) &= \frac{1}{32}(k_x\sin\phi - k_y\cos\phi)\sin(2\phi)[\sin\theta - 3\sin(3\theta)] \\
&\quad -\frac{1}{8}(k_x\cos\phi + k_y\sin\phi)\cos(2\phi)\sin(2\theta). \qquad (6.12)
\end{aligned}$$

The mean-field dispersion. We aim to obtain the **leading** order contributions to the dispersion from i) isotropic spin-orbit coupling, and ii) anisotropic spin-orbit coupling. For this purpose, it is enough to keep only Dk_z and $\tilde{D}f_z$ terms in the spin-orbit coupling. This leads to the Hamiltonian

$$\begin{aligned}
\mathcal{H} &= \sum_{\mathbf{k}} \tilde{\psi}^\dagger_{\mathbf{k}} \mathcal{M}_{\mathbf{k}} \tilde{\psi}_{\mathbf{k}}, \\
\tilde{\psi}^\dagger_{\mathbf{k}} &= (c^\dagger_{\mathbf{k}+\frac{\mathbf{Q}}{2},\uparrow}, c^\dagger_{\mathbf{k}-\frac{\mathbf{Q}}{2},\downarrow}), \\
\mathcal{M}_{\mathbf{k}} &= \begin{pmatrix} \epsilon_{\mathbf{k}+\frac{\mathbf{Q}}{2}} + D(k_z + \frac{Q}{2}) + \tilde{D}f_z(\mathbf{k} + \frac{\mathbf{Q}}{2}) & gM \\ gM & \epsilon_{\mathbf{k}-\frac{\mathbf{Q}}{2}} - D(k_z - \frac{Q}{2}) - \tilde{D}f_z(\mathbf{k} - \frac{\mathbf{Q}}{2}) \end{pmatrix}. \qquad (6.13)
\end{aligned}$$

Note that the anisotropic deformations $\gamma_{1/2}(\mathbf{k}, \mathbf{Q})$, given by (6.12), depend upon the direction of the spiral wave vector (ϕ, θ). We evaluate the eigenvalues of $\mathcal{M}$ to obtain the energy dispersion

$$\begin{aligned}
\epsilon^{\pm}(\mathbf{k}) &= k^2 - \mu - \tilde{D}\gamma_1(\mathbf{k}, \mathbf{Q})Q \\
&\quad \pm\sqrt{\left[k_z(Q - D) - \tilde{D}\gamma_2(\mathbf{k}, \mathbf{Q})Q^2\right]^2 + (gM)^2}. \qquad (6.14)
\end{aligned}$$

The components $Dk_{x,y}$ (and similarly $\tilde{D}h_{x,y}$) would have given rise to the contributions of $\mathcal{O}(D^2)$ and do not change the results qualitatively. They give rise to exponentially flat minibands for long-period spirals.

The ground state. After having calculated the dispersion, we can explicitly show that the mean-field ground state is the spiral whose pitch is determined by the value of the spin orbit coupling, $Q = D$. Let us neglect small $\tilde{D}$ terms, for a moment, since they do not affect the magnitude of the wave vector significantly. **We note that the dispersion looks the same as that of a spiral ferromagnet without spin orbit coupling, just with the shifted wave vector $\tilde{Q} = Q - D$.** In the *mean-field* theory the state with $\tilde{Q} = 0$ is favoured, due to the $\beta_{MF}\tilde{Q}^2M^2 > 0$ term in the free energy (we have explicitly shown this in Section 3.3.2). The mean-field ground-state of MnSi is therefore a spiral with the wave vector $Q = D$, as we have already shown from the phenomenological expansion. Next, we determine the directional dependence of the wave vector.

6.2.2.3 Directional dependence of Q

By inspection of the dispersion (6.14), we see that the directional dependence is encoded in the two terms γ_1 and γ_2. They generate different directional-dependent terms in the free energy, the balance of which will determine the orientation of $\mathbf{Q}$. The leading directional-dependent term arises from the coupling of γ_1 to Q (γ_2 couples to Q^2 and generates higher order terms). For the sole purpose of extracting this term, the dispersion can be reduced to $\epsilon^{\sigma}_{\mathbf{k}} \approx k^2 - \mu + \tilde{D}\gamma_1(\mathbf{k}, \mathbf{Q})Q - \sigma g M$. We differentiate the mean-field contribution to the free energy (1.11) with respect to M twice and with respect to Q twice, to obtain

$$\begin{aligned} \delta F_1^{MF} &= \frac{1}{4}\tilde{D}^2Q^2M^2 \int_{\mathbf{k}} n^{(3)}(k^2-\mu)\gamma_1^2(\mathbf{k},\mathbf{Q}) \\ \delta F_1^{MF} &= \frac{15}{8}\tilde{D}^2\langle\gamma_1^2\rangle\alpha_{MF}Q^2M^2 \\ \langle\gamma_1^2\rangle &= \frac{1}{40}\left(\sum_{\alpha=a,b,c}\lambda_\alpha^4 - \frac{1}{3}\right), \end{aligned} \tag{6.15}$$

where $\lambda_\alpha = \mathbf{n}_z \cdot \mathbf{n}_\alpha$. To get from the first to the second line of (6.15), we performed integration by parts with respect to variable $\epsilon = k^2$ (Note that $\gamma_1 \sim k^2$). The small directional-dependent contribution to the free energy δF_1^{MF} is minimized for $\lambda_a = \lambda_b = \lambda_c$. This corresponds to $\mathbf{Q}$ along the (111) direction, in agreement with the phenomenology.

In summary, we have shown that the mean-field theory ground state corresponds to a spiral with $|\mathbf{Q}| = D$ and $\mathbf{Q} \parallel (1,1,1)$. These are the features of the helical phase in MnSi, seen in the neutron scattering data.

6.3 Quantum Order-by-Disorder in MnSi

In the previous section, we have shown how the helical phase emerges as the mean-field solution of our model. Next, we include quantum fluctuations through the quantum order-by-disorder approach. How will this modify the phase diagram? We show that quantum fluctuations stabilize a new phase which shares striking similarities with the partially ordered phase of MnSi.

6.3.1 Phase diagram

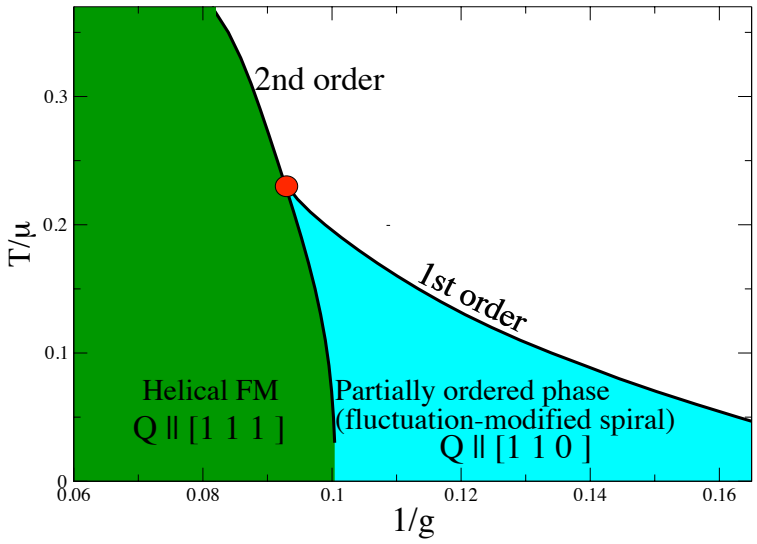

Figure 6.2: **Phase diagram of MnSi, determined using the quantum order-by-disorder approach:** In the helical phase $Q = D$, and $\mathbf{Q} \parallel (111)$. Quantum fluctuations stabilize the fluctuation-modified spiral phase, characterized by a small increase in the magnitude of the wave vector Q from its value in the helical phase, and the wave vector re-orientation to the (110) direction. These are the signatures of the partially ordered phase.

Here, we explicitly show that the phase boundaries of the system with spin-orbit coupling map onto the phase boundaries of a system without the spin-orbit coupling, but with the nature of the phases changed – the wave vector in every phase is shifted by D. We argue that the partially ordered phase can be identified with the fluctuation-modified spiral phase in MnSi.

In Chapter 2, we have shown that the free energy (including quantum fluctuations) is a functional of the mean-field dispersion. In the previous section, we have seen that, if we neglect small $\tilde{D}$ terms (which do not affect the position of the phase boundaries significantly), the mean-field dispersion looks the same as that of a spiral ferromagnet without spin orbit coupling, with the wave vector shifted to $\tilde{Q} = Q - D$. We have already analysed such a phase diagram in Chapter 4.

In the region of the phase diagram where there was a uniform ferromagnet in the absence of a spin-orbit interaction, there will now be a helical ferromagnet with $Q = D$ ($\tilde{Q} = 0$). As fluctuations get stronger, they start favouring a state with non-zero $\tilde{Q}$. We associate this fluctuation-modified spiral state with the partially ordered phase. This provides an explanation for the experimentally observed small increase in the wave vector in the partially ordered phase. One would expect a dynamical order in a phase that is stabilized by quantum fluctuations. This is exactly what has been observed in the neutron scattering experiments and μSR. From these measurements, the time-scale on which the order fluctuates has also been estimated. However, we still lack the theory of such fluctuating spiral phases.

The nature of the phase transitions between different phases remains unchanged from our previous analysis for a system without a spin-orbit coupling. We predict (i) a Lifshitz line, along which $\tilde{Q} = Q - D = 0$, between the helimagnet and the partially ordered phase and (ii) a weakly first order transition between the partial order and the paramagnetic phase. This is inconsistent with the experiments, where (i) the helimagnet-to-partial order transition was found to be weakly first order, and where (ii) a crossover between the partially ordered phase and the paramagnet was observed. A possible resolution of the disagreement lies in including smaller $\tilde{D}$ terms in the analysis of the phase boundaries. They can drive the Lifshitz transition to become weakly first order in $\tilde{Q}$ (in a similar way to which they cause the discontinuous change in the direction of $\mathbf{Q}$).

6.3.2 Directional dependence of the wave vector

By examining the directional-dependent terms in the free energy (up to sixth order), we show that the wave-vector re-orients from the (111) direction in the helical phase to the (110) direction in the partially ordered phase.

One of the most puzzling features of the partially ordered phase is its neutron scattering pattern, characterized by the wave vector reorientation to the (110) direction. Previously, we have shown that mean-field terms pin the wave vector along the (111) direction. We expect fluctuations to favour the directions as far from the mean-field pinning as possible. Hence, the re-orientation of the wave vector in the fluctuation-driven partially ordered phase occurs. The outline of

the calculation is as follows:

1. We note that there are two directional-dependent terms in the dispersion: $\gamma_1 Q$ and $\gamma_2 Q^2$
2. To 6th order, they generate only two directional-dependent contributions to the free energy $\delta F_1 \sim Q^2 M^2$ and $\delta F_2 \sim Q^4 M^2$, which we evaluate explicitly.
3. The subtle balance of δF_1 and δF_2 will determine the directional dependence across the phase diagram.

6.3.2.1 Mean-field like directional dependent term δF_1

We begin by analysing the directional-dependent term δF_1. We already encountered it in Section 6.2.2.3 when we deduced the mean-field dependence of the wave vector. Now, if we include the fluctuation contributions to it we obtain

$$\begin{aligned} \delta F_1 &= \frac{15}{8}\tilde{D}^2\langle\gamma_1^2\rangle\alpha Q^2 M^2 \\ \langle\gamma_1^2\rangle &= \frac{1}{40}\left(\sum_\alpha \lambda_\alpha^4 - \frac{1}{3}\right), \end{aligned} \tag{6.16}$$

i.e. we have only replaced $\alpha_{MF} \to \alpha$ since, to leading order, the same proportionality as in mean-field theory holds for the fluctuation contribution to this coefficient (A similar line of arguments can be followed as in Section 3.3.3). This term is minimized for $\mathbf{Q}$ along the (111) direction – it is mean-field like.

6.3.2.2 Fluctuation-driven directional dependent term δF_2

We now consider the directional dependent $\delta F_2 \sim Q^4 M^2$ term in the free energy. We use the fact that the free energy (2.14) is a functional of the mean-field dispersion. Let us inspect the dispersion

$$\epsilon^{\pm}(\mathbf{k}) = k^2 - \tilde{D}\gamma_1(\mathbf{k},\mathbf{Q})Q \pm \sqrt{\left[k_z(Q-D) - \tilde{D}\gamma_2(\mathbf{k},\mathbf{Q})Q^2\right]^2 + (gM)^2}, \tag{6.17}$$

which enters the free energy (2.14). We see that there are in principle two terms that can contribute:

- $\sim \gamma\langle\gamma_1^4\rangle Q^4 M^2$ – this term arises when we bring down the γ_1 factor every time we differentiate the dispersion with respect to Q (four times in total). There are two derivatives arising from the differentiation with respect to M. Together, this results in a coefficient proportional to the already evaluated sixth order Ginzburg-Landau coefficient of the uniform ferromagnet

γ. However, the directional dependence of this term vanishes, as the $\langle\gamma_1^4\rangle$ average is independent of θ and ϕ.

- $\sim \beta\langle\gamma_2^2\rangle Q^4M^2$. From (6.17), we see that the $\gamma_2 Q^2$ term enters the dispersion in the same way as the $k_z\tilde{Q}$ term. From this it follows that the $\langle\gamma_2^2\rangle Q^4M^2$ term will come with the same pre-factor as the $\langle k_z^2\rangle\tilde{Q}^2M^2$ term (see Eq. (3.27)).

From this it follows that

$$\delta F_2 = 2\tilde{D}^2\beta\langle\gamma_2^2\rangle Q^4M^2. \tag{6.18}$$

Since $Q \sim D$ this term is suppressed by a factor of order D^2 compared to $\delta F_1 \sim Q^2M^2$. However, since it is proportional to $\beta \sim \ln T$ we nonetheless expect it to dominate at low enough temperatures. The fact that $\beta \sim \ln T$, indicates that this term is fluctuation driven and we expect it to dominate in the partially ordered phase. We define $g(\phi,\theta) = 192\langle\gamma_2^2\rangle$. The directional dependence enters δF_2 through

$$\begin{aligned} \delta F_2 &= \frac{1}{96}\tilde{D}^2\beta g(\phi,\theta)Q^4M^2 \\ g(\phi,\theta) &= \frac{1}{16}\sin(2\phi)^2\left[\sin(\theta) - 3\sin(3\theta)\right]^2 + \cos(2\phi)^2\sin(2\theta)^2. \end{aligned} \tag{6.19}$$

Since $\beta < 0$ in the partially ordered phase, δF_2 is minimized when $g(\phi,\theta)$ is at its maximum. This occurs for $\phi = \pi/4$ and $\theta = \pi/2$, that is along the (110) direction.

6.3.2.3 Change of the directional dependence

We have seen that δF_1 dominates in the helical phase and pins $\mathbf{Q}$ along the (111). Here, we show that the wave vector reorients to the (110) as we cross the helimagnet-to-partial order boundary.

The change of the direction occurs when $\delta F_{(111)} = \delta F_{(110)}$. To a first approximation, this leads to $\delta F_1 \approx \delta F_2$, which gives the condition $\alpha \sim \beta D^2$. Since the phase diagram was obtained to $\mathcal{O}(D)$, to this accuracy the line is equivalent to the $\alpha = 0$ line, which represents the helimagnet-to-partial order boundary.

We have shown how quantum fluctuations stabilize directions which are far away from the mean-field pinning and how the wave vector re-orientation in the partially ordered phase follows naturally from our approach.

In conclusion, we have explained the origin of the partially ordered phase in MnSi and the wave vector re-orientation. We used the Stoner Hamiltonian in

the presence of a spin-orbit coupling and applied the quantum order-by-disorder approach. We showed that the helical phase emerges as the mean-field solution of this model, while the partially ordered phase is stabilized by quantum fluctuations. By examining the directional dependent terms in the free energy arising from a small anisotropic spin-orbit interaction, we have shown that the wave vector re-orients from the (111) direction in the helical phase to the (110) direction in the partially ordered phase. This results in the shift of the neutron scattering peak to the (110) direction, and is consistent with the neutron scattering data. In the next Chapter, we explore this further and make quantitative predictions for the neutron scattering pattern.

Chapter 7

Comparison with Experiment and Other Related Theories

In the previous Chapter, we have seen how the quantum-order-by-disorder approach reproduces the correct topology of the phase diagram of MnSi. We proposed a possible explanation for the origin of the partially ordered phase – that it is stabilized by quantum fluctuations – and explained why the neutron scattering peak shifts from the (111) direction to the (110) direction.

We now wish to investigate the wave vector re-orientation further and make more quantitative predictions for the neutron scattering pattern. We calculate the distribution in angular directions and plot the neutron-scattering intensity. The agreement with the experiment is very good.

We discuss other related theories of MnSi – the blue fog scenario and skyrmions – and draw comparison with our approach. The blue fog scenario relies on the analogy with blue phases in liquid crystals. It claims that the partial order-to-paramagnet transition is a liquid-gas transition from the helical phase (chiral liquid) to paramagnet (chiral gas). Skyrmions develop a very similar magnetization pattern to that of blue phases. They are topologically stable structures, that can be realized in chiral magnets due to spin-orbit interactions. Roszler *et al.* proposed a ground state of randomly distributed skyrmion tubes with axes along the (111) directions as a candidate for the partially ordered phase. It has been argued that such arrangement leads to neutron scattering intensity distributed over a surface of a sphere, with peaks along the (110) direction. Our approach, in principle, does not exclude the possibility of skyrmions. However, we believe that the skyrmion scenario is not necessary to explain the phase diagram in the absence of a magnetic field or the wave vector re-orientation. We propose several experiments that would allow one to distinguish between spiral and a skyrmion ground state.

7.1 Phase diagram

We have seen how our phase diagram in the temperature versus inverse interaction plane qualitatively reproduces the experimental phase diagram of MnSi in the temperature-pressure plane. We explained the directional dependence of the wave vector in the helical phase and the partially ordered phase and a small increase in magnitude of Q in the partially ordered phase. The cross-over behaviour (rather than a first order transition) when going out of the partially ordered phase into the rest of the non-Fermi liquid phase, as well as the mysterious non-Fermi liquid behaviour, that extends over a wide range of the phase diagram, remain unaccounted for in our approach. It is suspected that the effects of disorder upon the partially ordered phase provide the key to understanding the unusual non-Fermi liquid resistivity [105]. The consequences of this within the order-by-disorder approach is an intriguing avenue for further study.

7.1.1 Distribution of magnetic moments in the partially ordered phase: comparison to experiment

We make a theoretical prediction for the neutron scattering pattern in the partially ordered phase and compare it to experiments.

Previously, we have shown that the free energy is minimized for $\mathbf{Q}$ along the (110) direction. In our picture, large domains in which $\mathbf{Q}$ wiggles along one of the principal (110) directions form, see Fig. 7.1. In order to make quantitative predictions for the neutron scattering, in particular to calculate the angular distribution, we need to include the terms in the free energy which explicitly account for small deviations in the direction of $\mathbf{Q}$ (which were previously left out).

Spatial modulations in Q. Terms which take into account the spatial dependence of $\mathbf{Q}$ can be deduced by looking at the phenomenological Ginzburg-Landau expansion of the free energy.

There are two types of terms in the phenomenological Ginzburg-Landau expansion, that can generate $(\nabla\hat{Q})^2$ terms (to sixth order in the expansion), that we previously left out from our analysis: (i) $\delta F_A \sim \sum_\alpha (\nabla M_\alpha)^2$ and (ii) $\delta F_B \sim \sum_\alpha (\nabla^2 M_\alpha)^2$.

(i) Let us first inspect the $\sum_\alpha (\nabla M_\alpha)^2$ term in the phenomenological Ginzburg-Landau expansion. After substituting the spiral magnetization (3.16), and allowing for spatial variations in the direction of $\mathbf{Q}$, we obtain

$$\sum_\alpha (\nabla M_\alpha)^2 = M^2 \tilde{Q}^2 + M^2 \sum_\alpha (\nabla \hat{Q}_\alpha)^2, \tag{7.1}$$

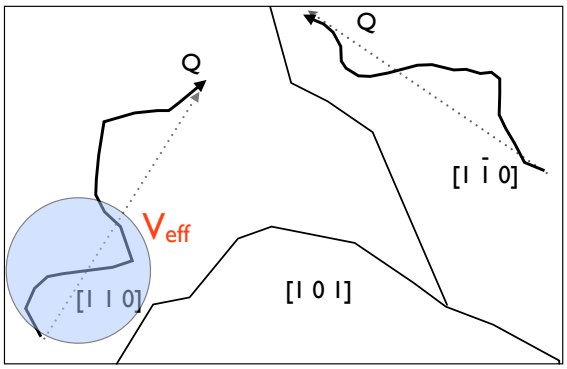

Figure 7.1: **Formation of domains in MnSi:** Domains of spirals with the wave vector **Q** pointing along one of the principle directions. Within every domain, there are small deviations in the direction of **Q**. This leads to the effective volume V_{eff}.

where $\hat{Q}$ represents the unit vector pointing along the direction of **Q**. It follows that the $M^2 \sum_\alpha (\nabla \hat{Q}_\alpha)^2$ term comes with the same coefficient as the $\tilde{Q}^2 M^2$ term. We have already determined the $M^2\tilde{Q}^2$ coefficient – it is equal to $\frac{2}{3}\beta$, see Eq. (3.27). Hence, we need to include and additional term of the form

$$\delta F_A = \frac{2}{3}\beta M^2 \sum_\alpha (\nabla \hat{Q}_\alpha)^2 \tag{7.2}$$

in the free energy.

(ii) We inspect the $\sum_\alpha (\nabla^2 M_\alpha)^2$ contribution. Similarly, we obtain

$$\sum_\alpha (\nabla^2 M_\alpha)^2 = M^2\tilde{Q}^4 + 4M^2\tilde{Q}^2 \sum_\alpha (\nabla \hat{Q}_\alpha)^2. \tag{7.3}$$

From this it follows that the coefficient of the $M^2\tilde{Q}^2 \sum_\alpha (\nabla \hat{Q}_\alpha)^2$ term in the free energy is four times bigger than the coefficient of the $M^2\tilde{Q}^4$ term. The coefficient of the $M^2\tilde{Q}^4$ term is equal to $\frac{3}{5}\gamma$, see Eq. (3.27). Hence,

$$\delta F_B = 4\frac{3}{5}\gamma M^2 \tilde{Q}^2 \sum_\alpha (\nabla Q_\alpha)^2. \tag{7.4}$$

Adding up the two contributions δF_A, given by (7.2), and δF_B, given by (7.4), we obtain

$$\delta F_{\nabla \hat{Q}} = -\frac{2}{3}\beta M^2 \sum_\alpha (\nabla Q_\alpha)^2, \tag{7.5}$$

where we have replaced $\tilde{Q}^2$ by $\tilde{Q}^2 \approx -\frac{5\beta}{9\gamma}$, from Eq. (4.1).

Taking the previously calculated anisotropy (6.18) into account, directional dependent terms in the free energy sum to give

$$\delta F \sim \tilde{D}^2 \beta g(\phi,\theta) Q^4 M^2 - \beta M^2 (\nabla \hat{Q})^2. \tag{7.6}$$

We consider fluctuations around $\theta_0 = \pi/2$; that is $\theta = \pi/2 + \psi$, where ψ is small. By replacing $g(\phi,\theta) \sim -\psi^2$ and $(\nabla\hat{Q})^2 = (\nabla\psi)^2$, we obtain

$$\delta F(\psi) \sim -\tilde{D}^2 \frac{\beta^3}{\gamma^2}\psi^2 - \beta M^2 (\nabla\psi)^2. \tag{7.7}$$

From this we calculate the expectation value of ψ^2 (i.e. angular spread):

$$\begin{aligned} \langle\psi^2\rangle &= \frac{\int d\psi \psi^2 e^{-\frac{-\delta F(\psi)}{T}}}{\int d\psi e^{-\frac{-\delta F(\psi)}{T}}}, \\ \langle\psi^2\rangle &\sim \left(\frac{T}{M^2\beta}\right)^{\frac{3}{2}} e^{-\frac{\tilde{D}^2 M^2 \beta^3}{\gamma^2}}. \end{aligned} \tag{7.8}$$

7.1.1.1 Calculation of the correlation volume

We can obtain the same distribution in angular directions by using the Boltzmann weight $V_{\text{eff}}\delta F_2$:

$$\langle\psi^2\rangle = \frac{\int d\psi \psi^2 e^{-V_{eff}\tilde{D}^2\frac{\beta^3}{\gamma^2 T}\psi^2}}{\int d\psi e^{-V_{eff}\tilde{D}^2\frac{\beta^3}{\gamma^2 T}\psi^2}}, \tag{7.9}$$

where we have used that $\delta F_2 \sim \tilde{D}^2\frac{\beta^3}{\gamma^2 T}\psi^2$, and with the V_{eff} given by

$$V_{\text{eff}}(T) \sim (M\gamma^2\tilde{D}^{-2}|\beta|^{-3/2}T^{-1/2}) \exp[\tilde{D}^2 M^2 |\gamma|^3/(\gamma^2 T)]. \tag{7.10}$$

Here, V_{eff} represents the effective volume associated with a spread in directions of $\mathbf{Q}$ ($\mathbf{Q}$ is now spatially varying), see Fig. 7.1. We assume that the magnetic structure factor is proportional to the Boltzmann weight $\exp[-V_{\text{eff}}\delta F_2/T]$, which is a function of θ and ϕ.

Our picture consists of domains of spirals pointing along one of the principal directions. Within every domain, we allow $\mathbf{Q}$ to wiggle around its direction, see Fig. 7.1. The effective volume V_{eff} is the correlation volume associated with this wiggling. At very low temperatures [$T < \tilde{D}^2 M^2 |\beta|^3/\gamma^2$], V_{eff} tends to infinity and thermal fluctuations in orientation become small.

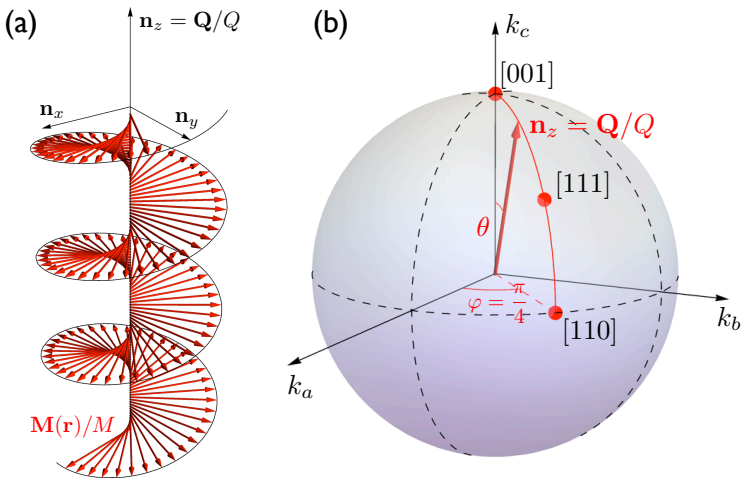

Figure 7.2: **Principal directions in MnSi:** (a) the spiral wave vector points along the local $\mathbf{n}_z$ axis. (b) high symmetry directions in MnSi. The wave vector will pick a certain direction in the crystal axes frame $(\mathbf{n}_a, \mathbf{n}_b, \mathbf{n}_c)$ in such a way that the free energy is minimized.

Neutron scattering intensity in the partially ordered phase. We plot the neutron scattering pattern along different angular directions along a sphere of radius Q, see Fig. 7.2 depicting high symmetry directions, such as (111) or (110). The distribution is proportional to the Boltzmann weight $I(\phi, \theta) = I_0 \exp[-V_{\text{eff}} \delta F_2 / T]$ arising from the dominant, fluctuation-driven, directional-dependent term $\delta F_2 = \frac{1}{96} \tilde{D}^2 \beta g(\phi, \theta) Q^4 M^2$ in the partially ordered phase. To compare the angular distribution with the experimental results, we set $I(\phi, \theta) = I_0 \exp[c g(\phi, \theta)]$, where $g(\phi, \theta)$ is given by (6.19), and find the best fit for $c = 4$. The theoretically predicted neutron scattering pattern is shown in Fig. 7.3 (a) and closely resembles the experimental one. We also perform the intensity scan along the $\phi = \pi/4$ direction (see Fig. 7.2), as it encompasses all the relevant directions. The agreement with the experimental data is very good, see Fig. 7.3 (b). We predict considerably smaller secondary maxima in the neutron scattering pattern, where no experimental data has yet been taken.

Sharp peaks in the neutron scattering data in the helical phase indicate the presence of a true long-range order. Smeared, but still present peaks are a characteristic of partial order that survives on intermediate time and length scales in the partially ordered phase. The question arises: How can our approach explain sharp neutron scattering peaks in the helical phase and diffuse peaks in the partially ordered phase? The Boltzmann weight entering the neutron scattering

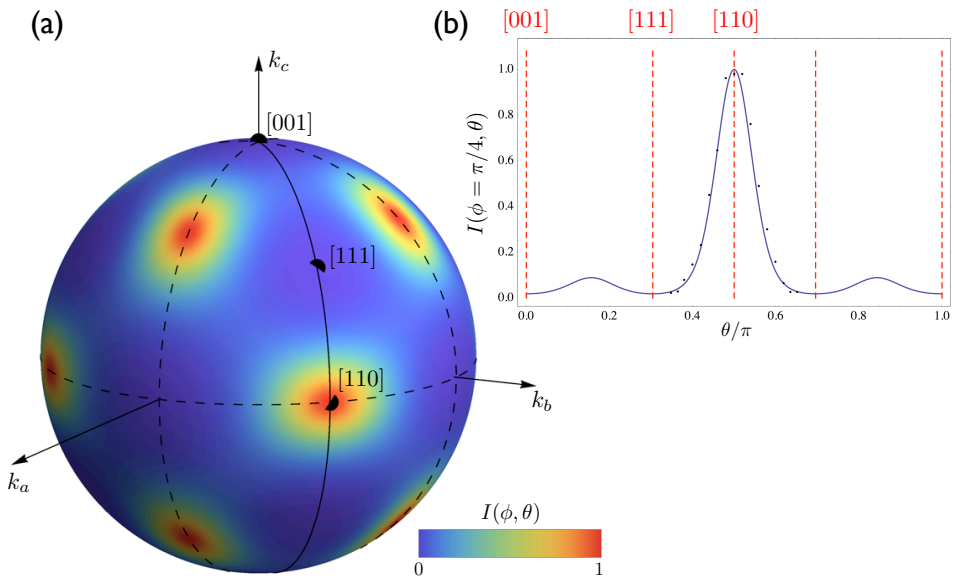

Figure 7.3: **Theoretically predicted neutron scattering pattern:** (a) plotted along the entire sphere. Fluctuations favour spirals along [110] and equivalent directions while almost no intensity is found along the [111] directions. (b) along a great circle connecting the high-symmetry directions in quantitative comparison with the experimental data [20].

intensity is proportional to M^3; a single factor of M arises from the effective volume (7.10), while $\delta F_2 \sim M^2$, from (6.18). Far inside the helical phase, the magnetization is large which leads to a sharp peak. As we approach the transition into the partially ordered phase, the magnetization gets smaller, which results in a broader neutron scattering peak (which also shifts in the direction, as we have already seen).

7.2 Other related theories

We move on to discuss other proposed theoretical scenarios that suggested various explanations for the partially ordered phase – the blue phase scenario [106; 107; 108] and skyrmion phases [109; 110] which are, in spirit, quite similar to blue phases. We begin by looking into the blue fog scenario proposed by Tewari *et al.* [108].

7.2.1 Magnetic analogue of blue phases and skyrmion structures in MnSi

Blue phases occur in liquid crystals [111]. They are characterized by partial order of directors (elongated liquid crystal molecules). It was postulated that similar phases can occur in chiral magnets without an inversion symmetry, analogous to the liquid crystal case. We begin with a theoretical outline of blue phases that occur in liquid crystals.

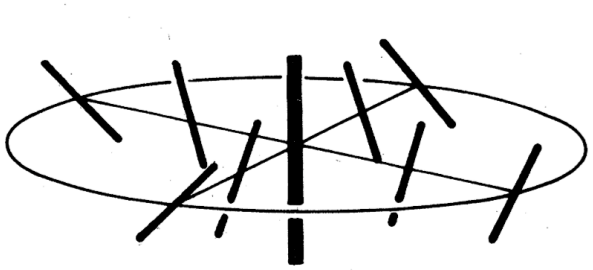

Figure 7.4: **Double-twist structure in liquid crystals:** Taken from [111]. The director field, $\mathbf{n}(\mathbf{r})$, twists along all directions perpendicular to itself; $\mathbf{n}(\mathbf{r}) = \hat{z}\cos(Qr) - \hat{\phi}\sin(Qr)$ in cylindrical coordinates.

Blue phases in liquid crystals. Liquid crystals consist of elongated molecules called directors, which are disordered in position but adopt a certain type of order in their orientation. Liquid crystals are well known to display a variety of helical phases. In a single spiral phase the director field $\mathbf{n}(\mathbf{r})$ twists about a single direction, the pitch axis, and is uniform in the plane perpendicular to the pitch axis: $\mathbf{n}(\mathbf{r}) = \hat{x}\cos(Qz) + \hat{y}\sin(Qz)$, for the pitch axis along the z-direction. At the transition out of this helical phase, the system enters a new phase with partial helical order [111]. The director field in this phase is given by $\mathbf{n}(\mathbf{r}) = \hat{z}\cos(Qr) - \hat{\phi}\sin(Qr)$ in cylindrical coordinates. From Fig. 7.4, we see that $\mathbf{n}(\mathbf{r})$ twists along all directions perpendicular to itself and, in particular, it rotates along both of a pair of orthogonal directions; hence this structure was named the double-twist. There are several different types of blue phases, the one that will interest us is so called "BPIII" – or the blue-fog phase [112].

Blue quantum fog scenario in MnSi. The free energy of a chiral magnet takes a similar form to that of a liquid crystal. It has been suggested that the partially ordered phase is a magnetic analogue of the blue fog phase in cholesteric liquid crystals, where magnetic moments form double-twist structures [108]. The theory interprets the partial order-to-paramagnet transition along $T_0(p)$ line (see

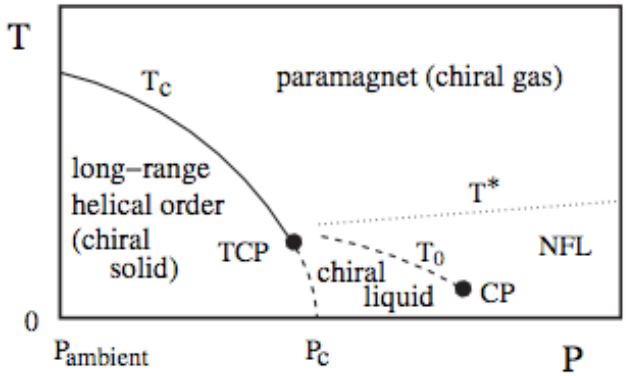

Figure 7.5: **Blue fog phase diagram of MnSi:** Taken from [108]. The partially ordered phase can be identified with the chiral liquid phase, and the partial order-to-paramagnet boundary ($T_0(p)$) as the condensation line when going from the chiral gas (paramagnet) to the chiral liquid (partially ordered phase).

Fig. 7.5) as a first order transition from a chiral liquid to a chiral gas as one crosses the condensation temperature. The phases that constitute the phase diagram of MnSi, shown in Fig. 7.5, can be interpreted as: i) a helical phase with true long-range helical order – a chiral solid, ii) partial order with short-ranged helical correlations – a chiral liquid, and iii) a paramagnet (disordered phase) – a chiral gas. The authors begin their analysis of the transition by defining a chiral order parameter $\psi = \mathbf{M}.(\nabla \times \mathbf{M})$. This is non-zero both in the chiral liquid and the chiral gas phase, as the two phases have the same symmetry (like the normal gas and the liquid). Crossing the $T_0(p)$ line results in a discontinuous change in the expectation value of ψ. Tewari *et al.* show that for certain values of the parameters (temperature and pressure), attractive interaction can arise between chiral fluctuations ψ and the gas-liquid condensation becomes possible. It was shown that the neutron scattering peak in the chiral gas phase is less pronounced than in the chiral liquid phase, which can lead to the disappearance of the neutron scattering signal above the $T_0(p)$ line. The theory did not address the issue of the wave vector re-orientation when going from the helical phase to the partially ordered phase.

Skyrmion-like crystals. Skyrmions [113] develop a very similar magnetization pattern to that of a blue fog phase. In a skyrmion, the magnetization vector twists smoothly moving away from the centre of the skyrmion, in such a way that it is antiparallel between the centre and the edge of the skyrmion, see Fig. 7.6. Skyrmions are topologically stable structures – they are robust against small perturbations. First, it was believed that they could not be spontaneously stabilized

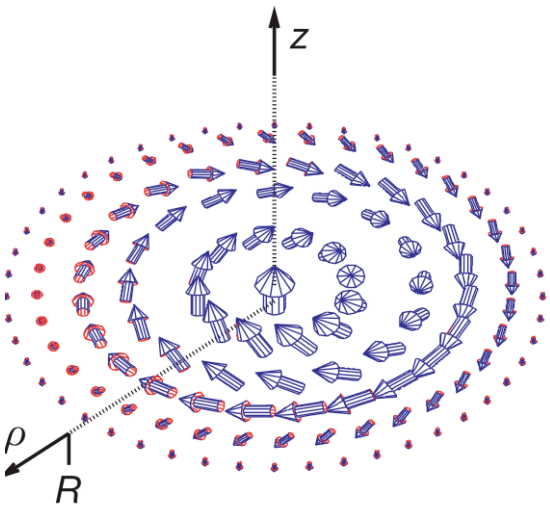

Figure 7.6: **The magnetization pattern of a skyrmion:** Taken from [113]. The magnetization vector twists smoothly when moving away from the centre of of the skyrmion. The skyrmion shown here has a soft magnetization amplitude which disappears at its edge.

in chiral ferromagnets. However, Rössler *et al.* [109] proved that skyrmion structures can form in condensed matter systems with chiral interactions, even without the presence of an external magnetic field. They considered a skyrmion with soft magnetization amplitude (which disappears on the edge of the skyrmion), and showed that the ground state of a chiral ferromagnet in three spatial dimensions, in a certain parameter regime, consists of randomly oriented two-dimensional skyrmion tubes.

In MnSi, the Dzyaloshinskii-Moriya interaction acts as a chiral interaction which stabilizes skyrmion solutions. It has been proposed that the partially ordered phase represents an amorphous texture of cylindrical skyrmion tubes (see Ref. [109], supplementary material). It was argued that if these tubes are oriented along the easy (111) axis, this will result in neutron scattering pattern spread over a surface of a sphere with peaks along the (110) directions.

The specific heat data [114], shows a pronounced spike at the transition out of helical phase, followed by a broad shoulder of width of $1K$. This is consistent with the amorphous skyrmion phase (as well as with the picture of randomly oriented helical domains).

The quantum order-by-disorder approach does not exclude the possibility of the existence of a skyrmion ground state. To verify if this is possible, we would need to substitute the dispersion of electrons in the presence of the skyrmion into the expression for the free energy and see if there is a region in the phase

diagram where the skyrmion configuration has the lowest free energy. We have demonstrated that skyrmions are not necessary to explain the phase diagram and the neutron scattering data of MnSi in the absence of an external magnetic field.

We propose several experiments that would allow one to distinguish between spirals and skyrmions. (i) In μSR different signals in spiral and skyrmion backgrounds would be observed, due to the modulation of the amplitude in the skyrmion background. (ii) Annealing in magnetic field applied along one of the principle directions would align the spiral domains. Neutron scattering would show an intensity imbalance of the scattering peaks – this effect is not expected for skyrmions. Annealed samples would also show anisotropic transport.

In summary, we have made theoretical predictions for the magnetic structure factor in the partially ordered phase, probed by neutron scattering. We have shown that it matches the experimental data very well.

In our picture, there are domains of spirals with wave vectors $\mathbf{Q}$ pointing along one of the principal directions. Inside every domain we allowed for small spatial modulations in the direction of $\mathbf{Q}$. The magnetic structure factor is then proportional to the Boltzmann weight $\exp[-V_{\text{eff}}\delta F_2/T]$, where V_{eff} is the correlation volume associated with the spatial modulation of $\mathbf{Q}$ and δF_2 is the dominant directional-dependent contribution to the free energy in the partially ordered phase.

We then discussed other related theories of MnSi: the blue fog scenario, and skyrmions. Our approach is, in principle, compatible with the existence of skyrmions or blue fog phases. However, we believe that these structures are not necessary to explain the phase diagram in the absence of an external magnetic field or the wave vector re-orientation.

Chapter 8

Conclusions

8.1 Summary

In summary, we have shown how fluctuations can lead to the formation of new phases. This mechanism is known as order-by-disorder. It is something that we encounter in everyday life – the formation of ripple patterns on sand dunes, or beautiful snowflakes of perfect geometric shapes are some examples.

In this thesis we investigated how quantum fluctuations, associated with the Heisenberg uncertainty principle, can lead to formation of new phases. Motivated by the experimental notion that one, in principle, never sees 'naked' quantum critical points (*i.e.* simply *two* different phases, separated by a phase transition), we investigated instabilities that can occur in the vicinity of itinerant ferromagnetic quantum critical points. We have demonstrated that itinerant ferromagnetic quantum critical points are intrinsically multi-critical – showing instabilities towards the formation of an inhomogeneous ferromagnetic state and a spin nematic. Fermi surface distortions, associated with the onset of a certain type of order, enhance the phase-space available for quantum fluctuations and in that way self-consistently lower the free energy. In an itinerant system, fluctuations can be thought of as virtual excitations of pairs of particle-hole pairs above the Fermi surface.

The quantum order-by-disorder approach at an itinerant ferromagnetic quantum critical point not only establishes the connection to deformations of the Fermi surface, which are accessible by various experimental probes, but also leads to relatively simple analytical calculations, based on self-consistent second order perturbation theory. As such, it is more accessible than technically involved diagrammatic techniques. The two approaches are formally equivalent; expanding self-consistently about a saddle point with the already established order re-sums a selected series of diagrams that give rise to non-analytic corrections to the free energy.

In familiar realizations of the quantum order-by-disorder approach in condensed matter systems, new ground states are stabilized by quantum fluctuations of a bosonic order parameter. In our approach, the underlying Fermi statistics and Pauli blocking of the phase space become evident. This 'fermionic' quantum order-by-disorder not only provides an intuitive physical picture for the emergence of new phases in the vicinity of itinerant quantum critical points, but identifies a general principle behind the phase reconstruction near such quantum-critical points.

The quantum order-by-disorder approach can be applied to a variety of systems and phases. Adding a small spin-orbit coupling to the Stoner model of magnetism has enabled us to explain the most important feature of the partially ordered phase of MnSi – its unusual neutron scattering pattern. In the partially ordered phase, the directrix of the helimagnetic ordering becomes unpinned from the lattice favoured (111) direction and instead re-orients to point along the (110) direction in order to open up and benefit energetically from extra phase space for low-energy particle-hole excitations.

There are several natural directions for extending and developing our approach. We discuss them next.

8.2 Suggestions for Further Work

8.2.1 Quantum order-by-disorder at an itinerant ferromagnetic quantum critical point in two spatial dimensions

It is a well-known fact that quantum fluctuations have more profound effects as the dimensionality of a system is reduced. The calculation of the phase diagram of an itinerant ferromagnet in two spatial dimensions, using the quantum order-by-disorder approach is currently work in progress of C. Pedder. Similarly to the three dimensional case, it has been found that the quartic coefficient in the free energy expansion diverges as the temperature is lowered. The form of divergence is, however, different: $\beta \sim \frac{1}{T}$. This is in accordance with the work of Belitz *et al* [115]. The divergence occurs due to the particle-hole pairs with momentum $2k_F$, as was the case in three spatial dimensions. Calculations of the phase diagram indicate instabilities towards a spiral ferromagnetic phase and a multi-critical spin nematic phase – the phase where spin nematic states with different order parameter symmetries (p and d-wave for example) all have the same free energy. The numerical phase diagram in two spatial dimensions, considering only uniform ferromagnetic state, has been obtained by means of Monte-Carlo techniques in Ref. [116].

8.2.2 Interplay between quantum fluctuations and lattice effects

There are two effects that can lead to the occurrence of a first order transition and a spiral instability in the vicinity of ferromagnetic quantum critical points – (i) quantum fluctuations, the role of which has been explored in this thesis, and (ii) lattice effects. It has been shown that, on the mean-field level, lattice effects [18; 95] can lead to the stabilization of a spiral phase in the vicinity of a ferromagnetic quantum critical point, due to certain features in the bandstructure (peaks in the density of states). It would be interesting to consider the interplay between lattice-driven magnetism and quantum fluctuations. The two effects could reinforce each other, which would lead to a higher tri-critical temperature. Alternatively, the effects could cancel each other to produce a continuous transition. Another possibility is that one of the effects dominates. This question represents an avenue for further study.

8.2.3 Fluctuation-driven spiral state with multiple wave vectors

Modulation of the ferromagnetic order does not necessarily occur at a single wave vector, as considered in this thesis. It would be interesting to investigate weather a multiple $\mathbf{Q}$ state – a superposition of several single spiral states – can be stabilized by the quantum order-by-disorder approach in the vicinity of an itinerant ferromagnetic quantum critical point. One would need to investigate if such a state can be favoured over a single spiral state and in which range of parameter space. This is quite similar to the FFLO states, where different multiple $\mathbf{Q}$ states can be realized [117]. This question is of relevance to MnSi, where proposed blue phases and skyrmion structures essentially represent multiple $\mathbf{Q}$ states (see Section 7.2.1). In their work, Binz, Vishwanath and Aji [106] suggested such a helical spin crystal ground state as a candidate for the partially ordered phase of MnSi.

8.2.4 Fluctuating spiral phase

In order to explain the partially ordered phase (and the fluctuation-driven spiral phase in an itinerant ferromagnet without spin-orbit coupling), we performed an expansion around **static** order. Partially ordered phase is a dynamical phase, characterized by temporal fluctuations of the magnetization, as well as spatial ones. Time-scales of these fluctuations have even been estimated to be of order 10^{-10}s [103]. In order to explain this feature of the partially ordered phase, one needs to construct the theory of the fluctuating spiral phase, which we currently

lack. Such theory could also shed some light onto the unusual non-Fermi liquid behaviour that occurs in the partially ordered phase (and beyond).

8.2.5 Superconductivity

Another type of instability that can occur in the vicinity of an itinerant ferromagnetic quantum critical point is the superconducting instability. Here, magnetic fluctuations serve as a superconducting glue [118; 119], rather than phonon-mediated attraction between electrons which occurs in conventional Bardeen-Cooper-Schrieffer (BCS) superconductors. Magnetic fluctuations are more likely to generate pairing in the spin-triplet channel, than in the conventional singlet channel. Intuitively, if such a pairing is stabilized (for example $\uparrow\uparrow$ pair) superconductivity does not need to compete with the ferromagnetic order. States with triplet pairing are known to occur in He^3 [93; 120] and Sr_2RuO_4. A similar mechanism of fluctuation mediated superconductivity is strongly believed to occur in high temperature superconductors.

Spin fluctuation theory [93; 94] addresses such questions as the coexistence of ferromagnetism and superconductivity. It has been shown [121] that two superconducting domes can be stabilized in the vicinity of the putative quantum critical point of an itinerant ferromagnet – one in the ferromagnetic phase with a larger critical temperature, and another in the paramagnetic phase with a considerably smaller critical temperature.

Recently, A. Green has worked out the theoretical underpinnings of including superconductivity in the quantum order-by-disorder picture. It has been shown that quantum fluctuations drive the formation of a p-wave spin-triplet superconducting state in the vicinity of a putative itinerant ferromagnetic quantum critical point through the quantum order-by-disorder approach. Green was able to demonstrate that the quantum order-by-disorder approach yields the same equations for the superconducting gap as the spin fluctuation theory, thus showing the formal equivalence between the two methods. What remains to be done is to determine the exact location of the superconducting state within the phase diagram shown in Fig. 4.4. Moreover, the nature of this superconducting phase where it overlaps with the spiral phase raises the exciting possibility of spontaneous, fluctuation-driven, spatially modulated superconductivity. It would be interesting to see if such FFLO state [122; 123] could be stabilized in the vicinity of the putative quantum critical point.

As we have already seen, non-analytic corrections to Hertz-Millis theory have successfully treated spiral and spin-nematic instabilities in the vicinity of itinerant ferromagnetic quantum critical points (as has the quantum order-by-disorder approach). Spin fluctuation theory has, so far, represented a complimentary approach that addresses the formation of superconducting instabilities. What one

might ask is: Do these two approaches reveal the same physics? Quantum order-by-disorder, as a unified approach that treats *all* instabilities on an equal footing, offers a clear answer to this question, providing an intuitive physical picture of the phase reconstruction in the vicinity of quantum critical points.

Appendix A: Modified Particle-Hole Densities of States and Their Derivatives

In Chapter 2, it was shown that the fluctuation corrections to the free energy can be written as an integral over modified particle-hole densities of states. Here, we calculate the modified particle-hole densities of states of the uniform ferromagnet, at finite temperature. By their explicit evaluation, a 9-dimensional integral in the fluctuation-corrected free energy (2.14) can be reduced to a 3-dimensional one. This enables us to evaluate the fluctuation corrections to the free energy, which is done in Chapter 3.

The fluctuation corrections to the free energy are given by a high dimensional integral over momenta $\mathbf{k}_1, \ldots, \mathbf{k}_4$ and correspond to excitations of virtual pairs of particle-hole pairs of opposite spin and equal and opposite momenta. It is therefore possible to rewrite the regularized fluctuation corrections $\mathcal{F}_{\text{fl}}$ (2.14) as a lower dimensional integral over modified particle-hole densities of states,

$$\mathcal{F}_{\text{fl}} = 2g^2 \sum_{\sigma=\pm 1} \int_{\mathbf{q},\epsilon_1,\epsilon_2} \frac{\Delta\rho^{\sigma}(\mathbf{q},\epsilon_1)\rho^{-\sigma}(-\mathbf{q},\epsilon_2)}{\epsilon_1+\epsilon_2}, \tag{1}$$

where we have defined $\int_{\mathbf{q}} := \int \frac{\mathrm{d}^3\mathbf{q}}{(2\pi)^3}$ and $\int_{\epsilon} := \int_{-\infty}^{\infty} \mathrm{d}\epsilon$. The modified particle-hole

densities of states as a function of momentum $\mathbf{q}$ and energy ϵ are given by

$$\begin{aligned}\rho^\sigma(q,\epsilon) &= \int_{\mathbf{k}} n(\epsilon^\sigma_{\mathbf{k}-\frac{\mathbf{q}}{2}})\delta(\epsilon-\epsilon^\sigma_{\mathbf{k}+\frac{\mathbf{q}}{2}}+\epsilon^\sigma_{\mathbf{k}-\frac{\mathbf{q}}{2}}),\\ \Delta\rho^\sigma(q,\epsilon) &= \int_{\mathbf{k}} n(\epsilon^\sigma_{\mathbf{k}-\frac{\mathbf{q}}{2}})n(\epsilon^\sigma_{\mathbf{k}+\frac{\mathbf{q}}{2}})\delta(\epsilon-\epsilon^\sigma_{\mathbf{k}+\frac{\mathbf{q}}{2}}+\epsilon^\sigma_{\mathbf{k}-\frac{\mathbf{q}}{2}}),\end{aligned} \tag{2}$$

and are related to the particle-hole density of states as $\rho^\sigma_{\rm ph} = \Delta\rho^\sigma - \rho^\sigma$. The modified particle-hole density of states of the uniform ferromagnet can be calculated analytically at finite temperature. This leads to a tremendous simplification of the fluctuation integral. The modified particle-hole densities of states are functions of the magnetization M, which enters through the dispersion $\epsilon^\sigma_{\mathbf{k}} = \epsilon_{\mathbf{k}} - \sigma g M$ of the uniform ferromagnet. In order to construct the Ginzburg-Landau expansion of the free energy, we require the derivatives of ρ^σ and $\Delta\rho^\sigma$ with respect to M. However, since in ρ^σ and $\Delta\rho^\sigma$ the dispersion only enters for either spin up or spin down (and not both) we can relate the derivatives with respect to M to derivatives with respect to the chemical potential μ,

$$\begin{aligned}\partial^i_M \Delta\rho^\sigma(q,\epsilon)\big|_{M=0} &= (\sigma g)^i \partial^i_\mu \Delta\rho^\sigma(q,\epsilon)\big|_{M=0}\\ &= (\sigma g)^i \partial^i_\mu \Delta\rho(q,\epsilon).\end{aligned} \tag{3}$$

Now let us derive explicit expressions for $\Delta\rho = \Delta\rho^\sigma|_{M=0}$ and $\rho = \rho^\sigma|_{M=0}$ and their derivatives.

Evaluation of $\Delta\rho(q,\epsilon)$ and $\rho(q,\epsilon)$

Starting from Eq. (2), we perform the angular integration

$$\begin{aligned}\Delta\rho(\mathbf{q},\epsilon) &= \frac{1}{(2\pi)^2}\int k^2\, dk\, dc\;\; \delta(\epsilon-kqc) n\left(\frac{k^2+q^2/4+kqc}{2}-\mu\right)\\ &\qquad\qquad \times n\left(\frac{k^2+q^2/4-kqc}{2}-\mu\right)\\ &= \frac{1}{(2\pi)^2 q}\int_{\epsilon/q}^{\infty} k\, dk\;\; n(\frac{k^2+q^2/4}{2}+\frac{\epsilon}{2}-\mu) n(\frac{k^2+q^2/4}{2}-\frac{\epsilon}{2}-\mu),\end{aligned} \tag{4}$$

where $c = \cos\theta$. Changing variables to $u = \frac{k^2}{2} - \mu$, we get

$$\Delta\rho(\mathbf{q},\epsilon) = \frac{1}{(2\pi)^2}\frac{1}{q}\int_{\epsilon^2/2q^2-\mu}^{\infty} du\; n\left(u+\frac{q^2}{8}+\frac{\epsilon}{2}\right) n\left(u+\frac{q^2}{8}-\frac{\epsilon}{2}\right). \quad (5)$$

To evaluate this integral, we make a further change of variables to $y = e^{\beta u}$ and rewrite it as

$$\Delta\rho(\mathbf{q},\epsilon) = \frac{1}{(2\pi)^2}\frac{T}{q}\int_{e^{\beta\left(\frac{\epsilon^2}{2q^2}-\mu\right)}}^{\infty} dy\;\; \frac{1}{y}\frac{1}{e^{\beta(\frac{q^2}{8}+\frac{\epsilon}{2})}y+1}\frac{1}{e^{\beta(\frac{q^2}{8}-\frac{\epsilon}{2})}y+1}. \quad (6)$$

This leads to

$$\Delta\rho(\mathbf{q},\epsilon) = \frac{1}{(2\pi)^2}\frac{T}{q}\left[\frac{1}{1-e^{\frac{\epsilon}{T}}}\ln\left(1+e^{-\frac{1}{T}\phi^-(\epsilon,q)}\right) + \frac{1}{1+e^{\frac{-\epsilon}{T}}}\ln\left(1-e^{-\frac{1}{T}\phi^+(\epsilon,q)}\right)\right], \quad (7)$$

where,

$$\phi^{\pm}(\epsilon,q) = \frac{1}{2}\left(\frac{\epsilon}{q}\pm\frac{q}{2}\right)^2 - \mu. \quad (8)$$

Following the same procedure, we find that

$$\rho(q,\epsilon) = \frac{1}{(2\pi)^2}\frac{T}{q}\ln\left(1+e^{-\frac{1}{T}\phi^+(\epsilon,q)}\right). \quad (9)$$

Evaluation of derivatives of $\Delta\rho(q,\epsilon)$ and $\rho(q,\epsilon)$ with respect to the chemical potential μ

Next, we evaluate the derivatives of the modified particle-hole densities of states with respect to the chemical potential μ; $\Delta\rho^{(i)}(q,\epsilon) := \partial_\mu^{(i)}\Delta\rho(q,\epsilon)$. From Eq. (5) we see that the only μ dependence appears in the lower limit of the integral.

Hence, if we differentiate with respect to μ i times we obtain

$$\begin{aligned} \Delta\rho^{(i)}(q,\epsilon) &= \frac{1}{(2\pi)^2}\frac{1}{q}\partial^{(i-1)}\left\{n\left[\phi^-(\epsilon,q)\right]\ n\left[\phi^+(\epsilon,q)\right]\right\}, \\ \rho^{(i)}(q,\epsilon) &= \frac{1}{(2\pi)^2}\frac{1}{q}\partial^{(i-1)}n\left[\phi^+(\epsilon,q)\right], \end{aligned} \tag{10}$$

for $i \geq 1$.

Appendix 2: Leading temperature dependence of α_{fl} and β_{fl}

In this Appendix, we derive leading temperature dependencies of α_{fl} and β_{fl}.

Analytical calculation of zero temperature asymptotics of α_{fl}

We begin by evaluating α_{fl}. In Chapter 2, we have shown that

$$\alpha_{\text{fl}} = 2g^4 \sum_{i=0}^{2} (-1)^i \begin{pmatrix} 2 \\ i \end{pmatrix} J_{i,2-i}, \tag{11}$$

where $J_{i,j}$ are given by

$$J_{i,j} = \int_{\mathbf{q},\epsilon_1,\epsilon_2} \frac{\partial_\mu^i \Delta\rho(q,\epsilon_1) \partial_\mu^j \rho(q,\epsilon_2)}{\epsilon_1 + \epsilon_2}. \tag{12}$$

We rescale energies and momenta entering the Fermi functions in modified particle-hole densities of states (evaluated in the Appendix 1) by the Fermi energy and the Fermi momentum, respectively: $x = \frac{q}{k_F}$, $y = \frac{\epsilon_1}{\mu}$ and $z = \frac{\epsilon_2}{\mu}$. The density of

states at the Fermi surface is denoted by ρ_F. In what follows, we evaluate each of the three terms that contribute to α_{fl} individually:

$$
\begin{aligned}
J_{0,2} &= -\frac{\rho_F^3}{8}\int_0^2 dx \int_0^{2x-x^2} dy \int_{-\infty}^{\infty} dz \frac{1}{y+z}\left[1-\left(\frac{y}{2x}+\frac{x}{2}\right)^2\right]\delta\left(\left(\frac{z}{2x}+\frac{x}{2}\right)^2-1\right) \\
&\quad -\frac{\rho_F^3}{8}\int_0^2 dx \int_{-2x+x^2}^{0} dy \int_{-\infty}^{\infty} dz \frac{1}{y+z}\left[1-\left(\frac{y}{2x}-\frac{x}{2}\right)\right]\delta\left(\left(\frac{z}{2x}+\frac{x}{2}\right)^2-1\right) \\
&= -\frac{\rho_F^3}{8}\int_0^2 dx \int_0^{2x-x^2} dy \left[1-\left(\frac{y}{2x}+\frac{x}{2}\right)^2\right] x\left[\frac{1}{y+2x-x^2}+\frac{1}{y-2x-x^2}\right] \\
&\quad -\frac{\rho_F^3}{8}\int_0^2 dx \int_{-2x+x^2}^{0} dy \left[1-\left(\frac{y}{2x}-\frac{x}{2}\right)^2\right] \frac{x}{2}\left[\frac{1}{y+2x-x^2}+\frac{1}{y-2x-x^2}\right] \\
&= -\frac{\rho_F^3}{8}\int_0^2 dx \left[2x^2(1-x/2)\ln[2]-x(1-x/2)(1+5x/2)-2x^2(1+x/2)\ln\left[\frac{x}{1+x/2}\right]\right] \\
&\quad -\frac{\rho_F^3}{8}\int_0^2 dx \int_{-2x+x^2}^{0} dy \frac{1}{4x}\left[-2y+x^2\right] \\
&= -\frac{\rho_F^3}{8}\left[-\frac{2}{3}+\frac{8}{3}\ln[2]\right].
\end{aligned}
$$

$$
\begin{aligned}
J_{2,0} &= -\frac{\rho_F^3}{8}\int_0^2 dx \int_{-2x-x^2}^{2x-x^2} dy \int_{-2x-x^2}^{2x-x^2} dz \frac{1}{y+z}\,\delta\left(1-\left(\frac{y}{2x}-\frac{x}{2}\right)^2\right)\left[1-\left(\frac{z}{2x}+\frac{x}{2}\right)^2\right] \\
&\quad -\frac{\rho_F^3}{8}\int_0^2 dx \int_{-2x+x^2}^{2x+x^2} dy \int_{-2x-x^2}^{2x-x^2} dz \frac{1}{y+z}\,\delta\left(1-\left(\frac{y}{2x}+\frac{x}{2}\right)^2\right)\left[1-\left(\frac{z}{2x}+\frac{x}{2}\right)^2\right] \\
&= -\frac{\rho_F^3}{8}\int_0^2 dx \int_{-2x-x^2}^{2x-x^2} dz \frac{1}{x^2-2x+z}\, x\left[1-\left(\frac{z}{2x}+\frac{x}{2}\right)^2\right] \\
&\quad -\frac{\rho_F^3}{8}\int_0^2 dx \int_{-2x-x^2}^{2x-x^2} dz \frac{1}{2x-x^2+z}\, x\left[1-\left(\frac{z}{2x}+\frac{x}{2}\right)^2\right] \\
&= \frac{\rho_F^3}{8}\int_0^2 \frac{dx}{4x}\int_{-2x-x^2}^{2x-x^2} dz(2x+z+x^2) \\
&\quad -\frac{\rho_F^3}{8}\int_0^2 \frac{dx}{4x}\int_{-2x-x^2}^{2x-x^2} dz \frac{(2x-z-x^2)(2x+z+x^2)}{2x-x^2+z} \\
&= \frac{\rho_F^3}{2}-\frac{\rho_F^3}{8}\int_0^4 dv \frac{1}{4}(4-v)v\int_0^2 dx \frac{x}{v-2x}
\end{aligned}
$$

$$
\begin{aligned}
&= \frac{\rho_F^3}{2} + \frac{\rho_F^3}{8}\int_0^2 dv \frac{1}{4}(4-v)(v)\left[1+\frac{v}{4}\ln\left[\frac{4-v}{v}\right]\right] \\
&= \frac{3\rho_F^3}{4}.
\end{aligned}
$$

$$
\begin{aligned}
2J_{1,1} &= 2\frac{\rho_F^3}{8}\int_0^2 dx \int_{-2x+x^2}^{2x-x^2} dy \int_{-2x-x^2}^{2x-x^2} dz \frac{1}{y+z} \\
&= 2\frac{\rho_F^3}{8}\int_0^2 dx \int_0^{2x-x^2} dy \int_0^{2x-x^2} dz \left(\frac{1}{y+z}-\frac{1}{y-z}\right) \\
&\quad -2\frac{\rho_F^3}{8}\int_0^2 dx \int_0^{2x-x^2} dy \int_0^{2x+x^2} dz \left(\frac{1}{y+z}-\frac{1}{y-z}\right) \\
&= -2\frac{\rho_F^3}{8}\int_0^2 dx \int_0^{2x-x^2} dy \int_{2x-x^2}^{2x+x^2} dz \left(\frac{1}{y+z}-\frac{1}{y-z}\right) \\
&= -2\frac{\rho_F^3}{8}\int_0^2 dx \int_0^{2x-x^2} dy \left[\ln\left(\frac{2x+x^2+y}{2x-x^2+y}\right)+\ln\left(\frac{2x+x^2-y}{2x-x^2-y}\right)\right] \\
&= -\rho_F^3.
\end{aligned}
$$

After setting $\mu = 1$, and adding the three terms calculated above, we obtain

$$\alpha_{\text{fl}} \simeq -\lambda(1+2\ln 2)g^4, \tag{13}$$

where $\lambda = \frac{16\sqrt{2}}{3(2\pi)^6}$.

Analytical calculation of zero temperature asymptotics of β_{fl}

We deduce the leading temperature dependence of β_{fl}, which arises from the $J_{2,2}$ term in (3.9). Here, we explicitly show that $J_{2,2} \sim \ln T$.

In terms of modified particle-hole densities of states $J_{2,2}$ can be written as

$$J_{2,2} = \int_{\mathbf{q},\epsilon_1,\epsilon_2} \frac{\partial_\mu^2 \Delta\rho(q,\epsilon_1)\partial_\mu^2 \rho(q,\epsilon_2)}{\epsilon_1+\epsilon_2}. \tag{14}$$

The divergent part of $J_{2,2}$ arises from the following term

$$J_{2,2}^{div} = \int \frac{d\mathbf{q}}{(2\pi)^3} \frac{d\epsilon_1\, d\epsilon_2}{\epsilon_1+\epsilon_2} n\left[\phi^-(\epsilon_1,q)\right] n^{(1)}\left[\phi^+(\epsilon_1,q)\right] n^{(1)}\left[\phi^+(\epsilon_2,q)\right], \tag{15}$$

where we have substituted for the derivatives of particle-hole densities of states, Eq. (10) in Appendix 1, and where $\phi^{\pm}(\epsilon,q) = \frac{1}{2}\left(\frac{\epsilon}{q} \pm \frac{q}{2}\right)^2 - \mu$. Replacing derivatives of the Fermi functions by appropriate delta functions (the ones that give the divergence near $2k_F$) and keeping an explicit temperature dependence in $n\left[\phi^-(\epsilon_1,q)\right]$, we obtain

$$J_{2,2}^{div} = \frac{1}{(2\pi)^6} \int q^2\, dq\, d\epsilon_1\, d\epsilon_2 \frac{1}{\epsilon_1+\epsilon_2} \delta\left(\epsilon_2 - qk_F + \frac{q^2}{2}\right) \delta\left(\epsilon_1 - qk_F + \frac{q^2}{2}\right) n(-\epsilon_1). \tag{16}$$

Performing the energy integrals and changing the variables to $x = q - 2k_F$, the integral reduces to

$$\begin{aligned} J_{2,2}^{div} &= -\frac{2\sqrt{2}}{(2\pi)^6} \int_{-2k_F}^{\infty} \frac{dx}{x} n\left[\frac{x}{2}(x+2k_F)\right] \\ &\approx \frac{2\sqrt{2}}{(2\pi)^6} \ln T. \end{aligned} \tag{17}$$

In the last line, we used the fact that the Fermi function cuts off the divergence.

References

[1] Landau, L. and Lifshitz, E. *Statistical Physics Part 1.* Butterworth Heinemann, Oxford. 4, 36

[2] Sachdev, S. *Quantum Phase Transitions.* Cambridge University Press, Cambridge, (1999). 4, 6

[3] Bitko, D., Rosenbaum, T. F., and Aeppli, G. *Phys. Rev. Lett.* **77**, 940–943 (1996). 5

[4] Vojta, T. *ArXiv e-prints* , cond–mat/0010285. 7

[5] Löhneysen, H. v., Rosch, A., Vojta, M., and Wölfle, P. *Rev. Mod. Phys.* **79**, 1015–1075 (2007). 8, 69

[6] Stoner, E. *Reports on Progress in Physics* **11**, 43 (1947). 9

[7] Hertz, J. A. *Phys. Rev. B* **14**, 1165–1184 (1976). 11, 14, 30

[8] Millis, A. J. *Phys. Rev. B* **48**, 7183–7196 (1993). 11, 30

[9] Huxley, A., Sheikin, I., Ressouche, E., Kernavanois, N., Braithwaite, D., Calemczuk, R., and Flouquet, J. *Phys. Rev. B* **63**, 144519 (2001). 14

[10] Pfleiderer, C. and Huxley, A. D. *Phys. Rev. Lett.* **89**, 147005 (2002). 14

[11] Graf, T., Thompson, J. D., Hundley, M. F., Movshovich, R., Fisk, Z., Mandrus, D., Fisher, R. A., and Phillips, N. E. *Phys. Rev. Lett.* **78**, 3769–3772 (1997). 14

[12] Movshovich, R., Graf, T., Mandrus, D., Thompson, J. D., Smith, J. L., and Fisk, Z. *Phys. Rev. B* **53**, 8241–8244 (1996). 14

[13] Kawasaki, S., Yashima, M., Kitaoka, Y., Takeda, K., Shimizu, K., Oishi, Y., Takata, M., Kobayashi, T. C., Harima, H., Araki, S., Shishido, H., Settai, R., and Ōnuki, Y. *Phys. Rev. B* **77**, 064508 (2008). 14

[14] Moriya, T. *Spin Fluctuations in Itinerant Electron Magnetism.* Springer-Verlag, Berlin, New York, (1985). 14

[15] Otero-Leal, M., Rivadulla, F., Saxena, S. S., Ahilan, K., and Rivas, J. *Phys. Rev. B* **79**, 060401 (2009). 14, 55

[16] Uhlarz, M., Pfleiderer, C., and Hayden, S. M. *Phys. Rev. Lett.* **93**, 256404 (2004). 14, 55

[17] Borzi, R. A., Grigera, S. A., Farrell, J., Perry, R. S., Lister, S. J. S., Lee, S. L., Tennant, D. A., Maeno, Y., and Mackenzie, A. P. *Science* **315**, 214–217 (2007). 14

[18] Berridge, A. M., Green, A. G., Grigera, S. A., and Simons, B. D. *Phys. Rev. Lett.* **102**, 136404 (2009). 15, 61, 100

[19] Saxena, S. S., Agarwal, P., Ahilan, K., Grosche, F. M., Haselwimmer, R. K. W., Steiner, M. J., Pugh, E., Walker, I. R., Julian, S. R., Monthoux, P., Lonzarich, G. G., Huxley, A., Sheikin, I., Braithwaite, D., and Flouquet, J. *Nature* **406**, 587–592 (2000). 14, 15

[20] Pfleiderer, C., Reznik, D., Pintschovius, L., Lohneysen, H. v., Garst, M., and Rosch, A. *Nature* **427**, 227 (2004). 14, 15, 70, 93

[21] Baumberger, F., Ingle, N. J. C., Kikugawa, N., Hossain, M. A., Meevasana, W., Perry, R. S., Shen, K. M., Lu, D. H., Damascelli, A., Rost, A., Mackenzie, A. P., Hussain, Z., and Shen, Z.-X. *Phys. Rev. Lett.* **96**, 107601 (2006). 14

[22] Brando, M., Moroni-Klementowicz, D., Albrecht, C., and Grosche, F. M. *Physica B: Condensed Matter* **378**, 111 – 112 (2006). 14

[23] Rost, A. W., Perry, R. S., Mercure, J.-F., Mackenzie, A. P., and Grigera, S. A. *Science* **325**, 1360–1363 (2009). 14

[24] Mathur, N., Grosche, F. M., Julian, S. R., Walker, I. R., Freye, D. M., Haselwimmer, R. K. W., and Lonzarich, G. G. *Nature* **394**, 39–43 (1998). 14

[25] Stewart, G. R. *Rev. Mod. Phys.* **73**, 797–855 (2001). 14

[26] Gegenwart, P., Si, Q., and Steglich, F. *Nat. Phys.* **4**, 186 (2008). 14

[27] Laughlin, R. B., Lonzarich, G. G., Monthoux, P., and Pines, D. *Advances in Physics* **50**, 361–365 (2001). 15

[28] She, J.-H., Zaanen, J., Bishop, A. R., and Balatsky, A. V. *Phys. Rev. B* **82**, 165128 (2010). 15, 18

[29] Maldacena, J. *Adv. Theor. Math. Phys.* **2**, 231 (1998). 15

[30] Witten, E. *Adv. Theor. Math. Phys.* **2**, 253 (1998). 15

[31] Gubser, S., Klebanov, I. R., and Polyakov, A. M. *Physics Letters B* **428**, 105 – 114 (1998). 15

[32] Hartnoll, S. A., Herzog, C. P., and Horowitz, G. T. *Journal of High Energy Physics* **0812**, 015 (2008). 15

[33] Sachdev, S. *Phys. Rev. Lett.* **105**, 151602 (2010). 15

[34] Chubukov, A. V., Pépin, C., and Rech, J. *Phys. Rev. Lett.* **92**, 147003 (2004). 16, 17, 20

[35] Rech, J., Pépin, C., and Chubukov, A. V. *Phys. Rev. B* **74**, 195126 (2006). 16, 19

[36] Belitz, D. and Kirkpatrick, T. R. *Phys. Rev. Lett.* **89**, 247202 (2002). 16

[37] Chubukov, A. V., Maslov, D. L., and Millis, A. J. *Phys. Rev. B* **73**, 045128 (2006). 16

[38] Chubukov, A. V. and Maslov, D. L. *Phys. Rev. B* **68**, 155113 (2003). 16

[39] Maslov, D. L. and Chubukov, A. V. *Phys. Rev. B* **79**, 075112 (2009). 16

[40] Efremov, D. V., Betouras, J. J., and Chubukov, A. *Phys. Rev. B* **77**, 220401 (2008). 16

[41] Belitz, D., Kirkpatrick, T. R., and Vojta, T. *Rev. Mod. Phys.* **77**, 579–632 (2005). 16

[42] Maslov, D. L. and Chubukov, A. V. *Phys. Rev. B* **79**, 075112 (2009). 16

[43] Betouras, J., Efremov, D., and Chubukov, A. *Phys. Rev. B* **72**, 115112 (2005). 16, 19

[44] Maslov, D. L., Chubukov, A. V., and Saha, R. *Phys. Rev. B* **74**, 220402 (2006). 16

[45] Vojta, T., Belitz, D., Naryanan, R., and Kirkpatrick, T. R. *Z. Phys. B* **103**, 451 (1997). 16, 19, 20

[46] Vojta, T., Belitz, D., Kirkpatrick, T., and Narayanan, R. *Annalen der Physik* **8**, 593–602 (1999). 16, 41

[47] Belitz, D., Kirkpatrick, T. R., and Vojta, T. *Phys. Rev. B* **55**, 9452–9462 (1997). 16, 17

[48] Kirkpatrick, T. R. and Belitz, D. *Phys. Rev. B* **67**, 024419 (2003). 16

[49] Vojta, T., Belitz, D., Narayanan, R., and Kirkpatrick, T. R. *Europhys. Lett* **36**, 191 (1996). 17

[50] Chubukov, A. V. and Maslov, D. L. *Phys. Rev. Lett.* **103**, 216401 (2009). 17, 18, 19, 30, 45, 48, 60

[51] Coleman, S. and Weinberg, E. *Phys. Rev. D* **7**, 1888–1910 (1973). 18, 24

[52] Larkin, A. I. and Pikin, S. A. *Zh. Eksp. Teor. Fiz.* **56**, 1664 (1969). 18

[53] Karahasanovic, U., Krüger, F., and Green, A. G. *Phys. Rev. B* **85**, 165111 (2012). 20

[54] Zaanen, J. *Phys. Rev. Lett.* **84**, 753–756 (2000). 22

[55] Feinery, L. F., Olesz, A. M., and Zaanen, J. *J. Phys.: Condens. Matter* **10**, 555–561 (1998). 22

[56] Shannon, N. and Chubukov, A. V. *Phys. Rev. B* **65**, 104418 (2002). 22

[57] Chubukov, A. V. and Jolicoeur, T. *Phys. Rev. B* **46**, 11137 (1992). 22

[58] Mulder, A., Ganesh, R., Capriotti, L., and Paramekanti, A. *Phys. Rev. B* **81**, 214419 (2010). 22

[59] Khaliullin, G. *Phys. Rev. B* **64**, 212405 (2001). 22

[60] Chubukov, A. *Phys. Rev. Lett.* **69**, 832–835 (1992). 22

[61] Chandra, P., Coleman, P., and Larkin, A. I. *Phys. Rev. Lett.* **64**, 88–91 (1990). 22, 25

[62] Mila, F., Poilblanc, D., and Bruder, C. *Phys. Rev. B* **43**, 7891–7898 (1991). 22

[63] Krüger, F. and Scheidl, S. *EPL* **74**, 896 (2006). 22

[64] Bergman, D., Alicea, J., Gull, E., Trebst, S., and Balents, L. *Nat. Phys.* **3**, 487 – 491 (2007). 23, 24

[65] Pathria, R. K. *Statistical Mechanics.* Heinemann, Oxford, Boston, (1996). 29

[66] Conduit, G. J., Green, A. G., and Simons, B. D. *Phys. Rev. Lett.* **103**, 207201 (2009). 29, 30, 32, 54, 58, 59

[67] Conduit, G. J. and Simons, B. D. *Phys. Rev. A* **79**, 053606 (2009). 29

[68] Mohling, F. *Phys. Rev.* **122**, 1062–1090 (1961). 29

[69] Abrikosov, A. A. and Khalatnikov, I. M. *Sov. Phys. JETP* **6**, 888 (1958). 29, 32, 39

[70] Duine, R. A. and MacDonald, A. H. *Phys. Rev. Lett.* **95**, 230403 (2005). 29, 32

[71] DeGennes, P. and Prost, J. *The Physics of Liquid Crystals.* Clarendon, Oxford, (1993). 44

[72] Fradkin, E., Kivelson, S. A., and Oganesyan, V. *Science* **315**, 196–197 (2007). 45

[73] Fradkin, E., Kivelson, S. A., Lawler, M. J., Eisenstein, J. P., and MacKenzie, A. P. *Annual Review of Condensed Matter Physics* **1**, 153–178 (2010). 45

[74] Fradkin, E., Kivelson, S. A., Manousakis, E., and Nho, K. *Phys. Rev. Lett.* **84**, 1982–1985 (2000). 45

[75] Halboth, C. J. and Metzner, W. *Phys. Rev. Lett.* **85**, 5162–5165 (2000). 45

[76] Cooper, K. B., Lilly, M. P., Eisenstein, J. P., Pfeiffer, L. N., and West, K. W. *Phys. Rev. B* **65**, 241313 (2002). 45

[77] Dell'Anna, L. and Metzner, W. *Phys. Rev. Lett.* **98**, 136402 (2007). 45

[78] Dell'Anna, L. and Metzner, W. *Phys. Rev. B* **73**, 045127 (2006). 45

[79] Kee, H.-Y. and Kim, Y. B. *Phys. Rev. B* **71**, 184402 (2005). 45

[80] Oganesyan, V., Kivelson, S. A., and Fradkin, E. *Phys. Rev. B* **64**, 195109 (2001). 45

[81] Wu, C., Sun, K., Fradkin, E., and Zhang, S.-C. *Phys. Rev. B* **75**, 115103 (2007). 45, 48

[82] Xu, C., Müller, M., and Sachdev, S. *Phys. Rev. B* **78**, 020501 (2008). 45

[83] Fernandes, R. M., Chubukov, A. V., Knolle, J., Eremin, I., and Schmalian, J. *Phys. Rev. B* **85**, 024534 (2012). 45

[84] Fernandes, R. M., Vanbebber, L. H., Bhattacharya, S., Chandra, P., Keppens, V., Mandrus, D., McGuire, M. A., Sales, B. C., Sefat, A. S., and Schmalian, J. *Phys. Rev. Lett.* **105**, 157003 (2010). 45

[85] Kirkpatrick, T. R. and Belitz, D. *Phys. Rev. Lett.* **106**, 105701 (2011). 45, 48, 59

[86] Hirsch, J. E. *Phys. Rev. B* **41**, 6820–6827 (1990). 48

[87] Millis, A. J. *Phys. Rev. B* **81**, 035117 (2010). 55

[88] Halperin, B. I., Lubensky, T. C., and Ma, S.-k. *Phys. Rev. Lett.* **32**, 292–295 (1974). 55

[89] Pfleiderer, C., McMullan, G. J., Julian, S. R., and Lonzarich, G. G. *Phys. Rev. B* **55**, 8330–8338 (1997). 55, 69

[90] Huxley, A., Sheikin, I., and Braithwaite, D. *Physica B: Condensed Matter* **284**, 1277 – 1278 (2000). 55

[91] Yu, W., Zamborszky, F., Thompson, J. D., Sarrao, J. L., Torelli, M. E., Fisk, Z., and Brown, S. E. *Phys. Rev. Lett.* **92**, 086403 (2004). 55, 70

[92] Senthil, T., Sachdev, S., and Vojta, M. *Phys. Rev. Lett.* **90**, 216403 (2003). 60

[93] Anderson, P. W. and Brinkman, W. F. *Phys. Rev. Lett.* **30**, 1108–1111 (1973). 60, 101

[94] Fay, D. and Appel, J. *Phys. Rev. B* **22**, 3173–3182 (1980). 60, 101

[95] Berridge, A. M., Grigera, S. A., Simons, B. D., and Green, A. G. *Phys. Rev. B* **81**, 054429 (2010). 61, 100

[96] Ishikawa, Y., Tajima, K., Bloch, D., and Roth, M. *Solid State Communications* **19**, 525 – 528 (1976). 68

[97] Bak, P. and Jensen, H. M. *Journal of Physics C: Solid State Physics* **13**, L881 (1980). 69

[98] Nakanishi, O., Yanase, A., Hasegawa, A., and Kataoka, M. *Solid State Communications* **35**, 995 – 998 (1980). 69

[99] Pfleiderer, C., Julian, S., and Lonzarich, G. *Nature* **414**, 427 (2001). 69

[100] Doiron-Leyraud, N., Walker, I. R., Taillefer, L., Steiner, M. J., Julian, S. R., and Lonzarich, G. G. *Nature* **425**, 595 (2003). 69

[101] Grosche, F. *Physica B Condensed Matter* **206**, 20 (1995). 69

[102] Arsenijevic, S., Petrovic, C., Forro, L., and Akrap, A. *unpublished* (2012). 71, 72

[103] Uemura, Y. J., Goko, T., Gat-Malureanu, I. M., Carlo, J. P., Russo, P. L., Savici, A. T., Aczel, A., MacDougall, G. J., Rodriguez, J. A., Luke, G. M., Dunsiger, S. R., McCollam, A., Arai, J., Pfleiderer, C., Böni, P., Yoshimura, K., Baggio-Saitovitch, E., Fontes, M. B., Larrea, J., Sushko, Y. V., and Sereni, J. *Nature Physics* **3**, 29–35 (2007). 71, 100

[104] Krüger, F., Karahasanovic, U., and Green, A. G. *Phys. Rev. Lett.* **108**, 067003 (2012). 74

[105] Kirkpatrick, T. R. and Belitz, D. *Phys. Rev. Lett.* **104**, 256404 (2010). 89

[106] Binz, B., Vishwanath, A., and Aji, V. *Phys. Rev. Lett.* **96**, 207202 (2006). 93, 100

[107] Hamann, A., Lamago, D., Wolf, T., v. Löhneysen, H., and Reznik, D. *Phys. Rev. Lett.* **107**, 037207 (2011). 93

[108] Tewari, S., Belitz, D., and Kirkpatrick, T. R. *Phys. Rev. Lett.* **96**, 047207 (2006). 93, 94, 95

[109] Rössler, U. K., Bogdanov, A. N., and Pfleiderer, C. *Nature* **442**, 797 (2006). 93, 96

[110] Fischer, I., Shah, N., and Rosch, A. *Phys. Rev. B* **77**, 024415 (2008). 93

[111] Wright, D. C. and Mermin, N. D. *Rev. Mod. Phys.* **61**, 385–432 (1989). 94

[112] Anisimov, M. A., Agayan, V. A., and Collings, P. J. *Phys. Rev. E* **57**, 582–595 (1998). 94

[113] Pfleiderer, C. and Rosch, A. *Nature* **465**, 880–881 (2010). 95, 96

[114] Pfleiderer, C. *J. Magn. Magn. Mater.* **23**, 226–230 (2001). 96

[115] Kirkpatrick, T. R. and Belitz, D. *ArXiv e-prints* , 1203.3826 (2012). 99

[116] Conduit, G. J. *Phys. Rev. A* **82**, 043604 (2010). 99

[117] Casalbuoni, R. and Nardulli, G. *Rev. Mod. Phys.* **76**, 263 (2004). 100

[118] Pfleiderer, C. *Rev. Mod. Phys.* **81**, 1551–1624 (2009). 101

[119] Roussev, R. and Millis, A. J. *Phys. Rev. B* **63**, 140504 (2001). 101

[120] Brinkman, W. F., Serene, J. W., and Anderson, P. W. *Phys. Rev. A* **10**, 2386–2394 (1974). 101

[121] Kirkpatrick, T. R., Belitz, D., Vojta, T., and Narayanan, R. *Phys. Rev. Lett.* **87**, 127003 (2001). 101

[122] Fulde, P. and Ferrell, R. A. *Phys. Rev.* **135**, A550–A563 (1964). 101

[123] Larkin, A. I. and Ovchinnikov, Y. N. *Zh. Eksp. Teor. Fiz.* **47**, 1136 (1964). 101